Institut für Wärmetechnik

TU Graz
Graz University of Technology

Robert Pratter, B.Sc.

VALIDATION OF A SOLAR-ICE STORAGE-HEAT PUMP SYSTEM AND DEFINITION OF A DESIGN GUIDELINE

MASTERARBEIT

zur Erlangung des akademischen Grades

Diplom-Ingenieur

Masterstudium Wirtschaftsingenieurwesen-Maschinenbau

eingereicht an der

Technischen Universität Graz

Betreuer

Dipl.-Ing. Werner Lerch
Dipl.-Ing. Dr.techn. Richard Heimrath

Beurteiler

Ao. Univ.-Prof. Dipl.-Ing. Dr. techn. René Rieberer
Institut für Wärmetechnik

Graz, Mai 2017

EIDESSTATTLICHE ERKLÄRUNG

AFFIDAVIT

Ich erkläre an Eides statt, dass ich die vorliegende Arbeit selbstständig verfasst, andere als die angegebenen Quellen/Hilfsmittel nicht benutzt, und die den benutzten Quellen wörtlich und inhaltlich entnommenen Stellen als solche kenntlich gemacht habe. Das in TUGRAZonline hochgeladene Textdokument ist mit der vorliegenden Masterarbeit identisch.

I declare that I have authored this thesis independently, that I have not used other than the declared sources/resources, and that I have explicitly indicated all material which has been quoted either literally or by content from the sources used. The text document uploaded to TUGRAZonline is identical to the present master's thesis.

_____ _____

Datum / Date Unterschrift / Signature

KURZFASSUNG

Titel: Validierung eines Solarkollektor-Eisspeicher-Wärmepumpensystems und Erstellen einer Dimensionierungsrichtlinie

Autor: Robert Pratter

1. Stichwort: Wärmebereitstellung
2. Stichwort: Mehrfamilienhaus
3. Stichwort: Simulation

Der Aspekt des Umweltschutzes sowie die Tatsache, dass die fossilen Brennstoffe früher oder später zu Ende gehen werden, macht den Bereich der innovativen, energieeffizienten und umweltschonenden Heizsysteme zu einem sehr interessanten Forschungsgebiet der heutigen Zeit. Ein solches Heizsystem wurde unter dem Projektnamen „Hot Ice Weiz“ mit dem Solarkollektor-Eisspeicher-Wärmepumpensystem für ein Mehrfamilienhaus in Weiz realisiert.

Im ersten Teil dieser Arbeit wurde die Funktionsweise dieses Systems anhand der Messdaten des ersten Betriebsjahres analysiert. Außerdem wurden diese Messdaten genutzt, um ein weitgehend bereits vorhandenes TRNSYS Simulationsmodell zu validieren. Es konnte gezeigt werden, dass sich die tatsächliche Funktionsweise dieses Systems damit sehr gut wiedergeben lässt. Dieses Simulationsmodell diente außerdem als Basis für die Erstellung einer Dimensionierungsrichtlinie für solche Systeme. Hier wurde eine Grundlage geschaffen, mit der anhand des Heizwärmebedarfs die benötigte Solarkollektorfläche sowie das benötigte Eisspeichervolumen für verschieden große Anteile an elektrischer Nachheizung relativ einfach und unkompliziert ermittelt werden kann. Dafür stehen unterschiedliche Varianten mit verschieden großen Anteilen an elektrischer Nachheizung sowie Varianten für verschiedene Klimadaten zur Verfügung, um in jedem Fall individuell entscheiden zu können, nach welchen Gesichtspunkten das Heizsystem für ein bestimmtes Gebäude dimensioniert werden soll.

ABSTRACT

Title: Validation of a solar-ice storage-heat pump system and definition of a design guideline

Author: Robert Pratter

1st keyword: heat supply
2nd keyword: multifamily building
3rd keyword: simulation

The aspect of environmental protection as well as the fact that fossil fuels will run out some day, makes the topic of renewable, energy-efficient and environmentally friendly heating systems an extremely interesting topic for today's research. Such a system was realised under the name "Hot Ice Weiz" as a solar-ice storage-heat pump system for a multifamily building in Weiz (Austria).

In the first part of this thesis, the operation mode of this system was analysed by using the measurement data of the first year. In addition, these measurement data were used to validate a, in large parts already existing, TRNSYS simulation model. It could be shown that the actual functionality of this system can be reproduced very well. Moreover, this simulation model served as a basis for the elaboration of a design guideline for such systems. A possibility was provided to determine the required solar collector area as well as the required ice storage volume for a different share of auxiliary heating in a simple and uncomplicated way, based on the heat demand. This heat demand based on the energy performance certificate is a further reason why this value is particularly suitable. For the dimensioning, different design guidelines with a varying share of auxiliary heating as well as various climatic data are available. An individual decision, which design should be used for which building, can thereby be made separately for each case.

PREFACE

This master thesis was developed during my Master's Degree Program Mechanical Engineering and Business Economics at the Technical University of Graz at the Institute of Thermal Engineering in the period from September 2016 to May 2017. The work was supported by the Werner Hochegger Forschungsstiftung and the findings serve as an input to the IEA HPT Annex 50.

I would really like to thank Werner Lerch for the great support in any regard during this work. Furthermore, I like to thank Richard Heimrath for his guidance and technical assistance in many points.

Most of all I like to thank my parents for their support throughout my entire studies. Without them this theses would not exist!

Thanks to all!

Graz, 12.04.2017

Robert Pratter

CONTENTS

1 INTRODUCTION

1.1 Motivation

The topic of the “best” heating system has been much discussed, not only among customers but also among experts in the field. Depending on the chosen literature, many completely different opinions can be found. That no one can say with certainty which one is the most favourable heating system for the next 20 years, can be seen from the multitude of alternatives on the market. Of course, the choice strongly depends on the type of building to be heated (e.g., new building, old building, passive house, etc.) as well as other factors (e.g., district heating connection available), but even if all of this is known, opinions tend to differ. So, what can one say with certainty? Most people agree that fossil fuels will run out some day, and that renewable, energy-efficient and environmentally friendly heating systems will play a significant part in the future.

One example off such systems are heat pump heating systems. These systems have already played an important role in form of ground- or air source heat pumps in the heating of passive or low energy houses. Many different variants exist for this purpose. For example, brine heat pumps can be operated with flat collectors or deep drilling. An essential factor in the installation of these systems is the partly necessary approval by the Bezirkshauptmannschaft. While air heat pumps are exempt from that, this is not the case for brine heat pumps. In Germany, for example, the conditions have been tightened over the last few years. As a result, no systems with deep drilling have been permitted in water protection areas any more. (Müllers, 2008)

This is where the heat pump system in combination with ice storages scores. Normally, no authorization is required for this kind of system. In addition, it allows the use of three different heat sources: the solar heat from direct radiation, the heat from the air and the ground heat. With an optimum design, it is possible to achieve a similar system performance as with geothermal systems. Since this is a relatively new technology, it is necessary to gain further insights into the operation of such systems by building pilot projects as the one in Weiz. With this gained experience, further improvements can be made to the system.

1.2 State of the art

This chapter is mainly based on the study “Eisspeicher-Wärmepumpen-Anlagen mit Sonnen-kollektoren“ from Energy Schweiz. (Minder et al., 2014)

Ice storages have been used for decades as components in cooling systems. In these systems, the ice storage is used as an energy store to smooth load peaks. The use of ice storages as heat source for heat pumps, on the other hand, is a comparatively new field of application. Untill this day, only a few hundred of such plants have been in operation in Europe. Currently, there are only three suppliers of complete ice storage heat pump systems on the market. The approaches of the suppliers differ mainly in the type of collector used, the construction, the hydraulic integration of the ice storage, the ice storage capacity and the integration of the collector heat:

- The complete system from Viessmann/Isocal (Viessmann, 2017), which is used in Weiz, with a heating range between 6 kW and 17 kW (different systems) uses a simple, uncovered plastic absorber. The capacity of one or two ice storages, buried in the ground, each with a capacity of 9600 litres water, corresponds to about one week running time of the heat pumps. The absorber heat is used for the ice storage regeneration and as a direct source for the heat pump.

- The Solaera complete system from Consolar (Consolar, 2017) with 6.9 kW heating capacity uses selectively coated glazed flat collectors, which are actively ventilated with a fan to use the ambient heat. The small 320 litre ice storage unit is integrated in the system package together with the heat pump, the hydraulics and the controller in a cabinet and can be placed in the building. The storage capacity corresponds to approximately 7 hours running time of the heat pump. When the temperatures are high enough the solar heat can be used directly for the heating support and for DHW heating in parallel.

- Energie Solaire (Energie Solaire, 2017) uses the Consolar Solaera system (heat pump, ice storage, hydraulics and controller) with an uncovered, non-actively ventilated but selectively coated collector.

In addition to these standard systems, several large-scale systems have already been implemented, as for example the La Cigale in Genf with two 30 m^3 ice storages and a 1680 m^2 solar collector. According to Energy Solaire (2017), this system is used for two multifamily buildings with 273 apartments with a heating requirement of approximately 644 MWh/a, or a plant in Monheim with an 1800 m^3 ice storage and a 550 m^2 collector (22000 m^2 heated area, 1.2 MW heating power).

Furthermore, various research activities concerning this topic take place, such as the IEA SHC Task 44 (IAE SHC, 2017), which examines various aspects of the combination of solar systems and heat pumps.

Detailed simulation studies show that ice storage heat pump systems should achieve a similar Seasonal Performance Factor (SPF) as geothermal heat pumps if the system is operating correctly. Typical values are between 3.5 and 4. If the solar heat is additionally used in parallel, higher SPF up to more than 5 are possible. Even a SPF of 6 was achieved in the simulation of a specially designed system.

Several measuring campaigns on field installations have been completed or still run. The previous operating experience and measurement results basically confirm that the seasonal performance factor of correctly designed and operated ice storage heat pumps can compete with geothermal probe heat pumps. However, with some monitored systems, it was noticeable that the expected SPF could only be reached after longer optimization periods, as for example in Weiz, where the system has been monitored and optimized since about two years. Therefore, it is recommended, with the current state of the art, to use technology from only one manufacturer so that all

components are perfectly matched to each other. Furthermore, an optimization phase should also be designated. Under these conditions, the use of ice storage heat pumps as an alternative to geothermal heat pumps can be recommended from a technological viewpoint if there is sufficient space for the ice storage and a suitable area for the collectors / absorbers. The solution is particularly attractive where no geothermal probes can be drilled.

With today's state of the art, there is still potential for a further increase of the SPF by developments of the ice storage, the control and the optimal dimensioning and combination of components. Independent analysis of plants and neutral simulation studies are still necessary and valuable. The success in the market will ultimately depend on pricing, cost-effectiveness (also compared to geothermal heat pumps), the promotion policy, the reliability of the plants and the dissemination of know-how among planners and system providers. (Minder et al., 2014)

1.3 Procedural method

To gain an insight into the current operation mode of the “Hot Ice Weiz” system, a lot of research was done. The measuring data of more than 200 sensors were available for the first year of operation. Since some changes have been made in the system and some problems with the measurement equipment have been occurred during this year, these data had to be prepared first. The prepared data served as a base for various analysis; for example, the ice storage temperature profile was analysed precisely to show when the phase transition had started and why a relatively deep subcooling of the ice storages had occurred. Moreover, different energy balances were created to show how the energy fluxes behave in the system and in which magnitude they move. Furthermore, characteristic numbers, like the system seasonal performance factor (SPF) or the specific heat demand, were determined to classify the system in comparison to other systems.

The second part of this thesis was to validate an, in large parts, already existing simulation model of this system. For this purpose, the main components were first validated isolated from the overall system, which means that an own TRNSYS project was created for them. For the required inputs, characteristic ranges of the measured data were selected. Next, the unknown parameters, as for example the characteristic line of the solar collector, were varied with an optimizer tool, until the outputs of the simulation module fit best with the measured data. After all individual components had been validated, they were integrated into the overall system. Finally, the overall system was validated as well, to ensure that the functionality of the simulation model matched as effectively as possible with the real system.

The last section of this thesis was to elaborate a design guideline for such systems on the basis of the validation result. For this purpose, buildings with a different heat demand were defined and the optimal dimensioning of the ice storage volume and solar collector area was determined. Since the heat requirement is known on account of the energy performance certificate in the construction of a building, a simple dimensioning of such systems is thereby possible. The design guideline was created by focusing on achieving the best efficiency with the lowest expenditure.

In addition, it should be noted that the validated model also serves as basis for a doctoral thesis (Lerch, 2017), where possible improvements of the system are investigated. Moreover, Richard Hackl (Hackl, 2016) wrote a Bachelor thesis on this topic and programmed a Microsoft Excel-Tool, which made the data evaluation significantly easier.

2 BASIC INFORMATION

This chapter is intended to provide an insight into the theoretical foundations of the main components of the system. In order not to exceed the framework of this study and since the system in Weiz already exists in this form anyway, the theoretical consideration is strongly based on the actually installed components. Therefore the contemplation of possible alternatives is largely dispensed.

2.1 Heat pumps

The heat pump is an aggregate which absorbs a heat flow at a low temperature level (cold side, heat source) and delivers it again at a higher temperature level (hot side, heat use), by using exergetically higher energy. The necessary driving power can be supplied, depending on the functional principle, whether as mechanical or as thermal energy. According to this, a distinction is made between compression and sorption heat pumps. (Leven et al., 2001) In this thesis, the explanations will be restricted to the compression heat pumps. Their function principle is shown in Figure 2-1.

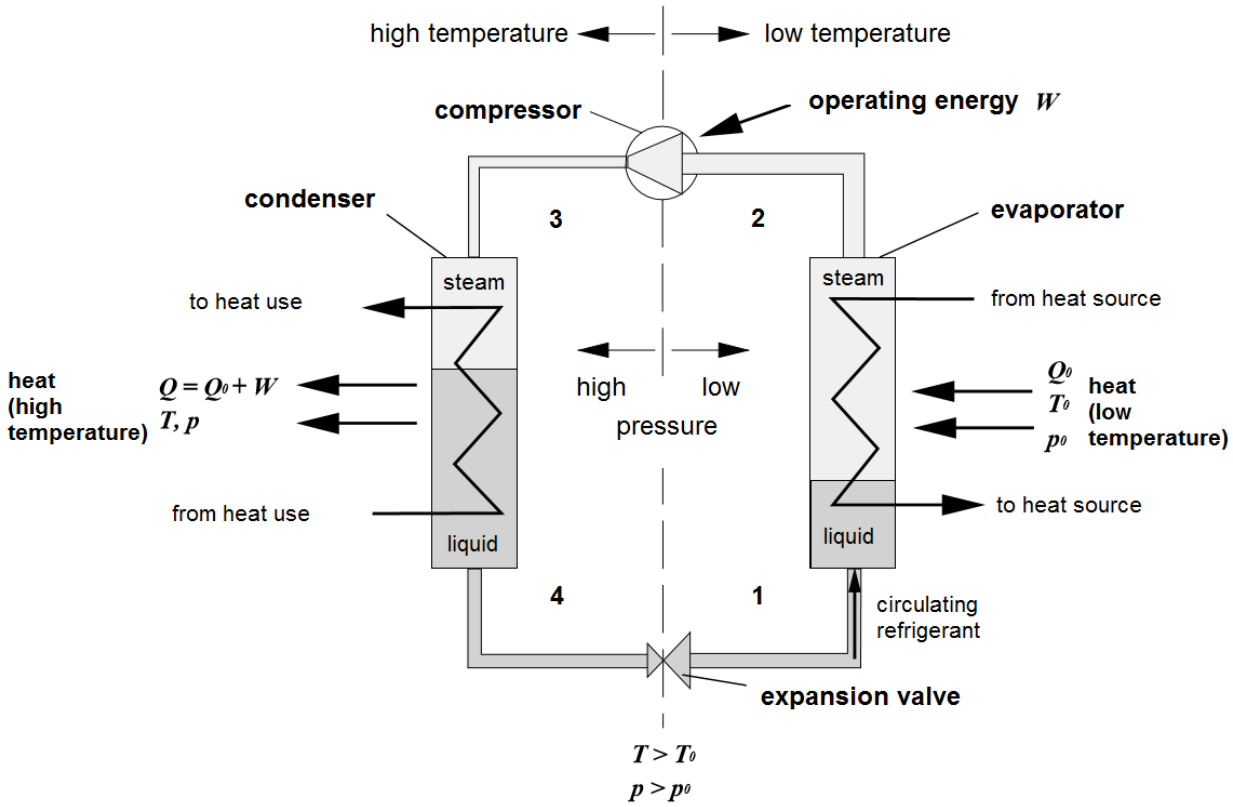

Figure 2-1: Function principle of an electric driven heat pump (Halozan & Holzapfel, 1987)

In the evaporator, the refrigerant is supplied with enough energy that the refrigerant is evaporated (1→2). The resulting refrigerant steam is “pumped” through the working circuit with a compressor. Because of the compressor, the pressure is rising (2→3). As the pressure and temperature of the refrigerant are connected, the condensation temperature also rises with the

pressure. In this way, the energy content of the vapour coming from the evaporator is increased by the energy from the compressor. (Wenzel et al., 2006)

In the next step, the refrigerant is condensed (3→4), this means that the refrigerant is liquid again in point 4. In order to condense, the refrigerant must reject the absorbed energy to a "heat sink", as for example to the domestic hot water storage. In the next step, the refrigerant flows through an expansion valve and is throttled there from the high pressure in the condenser to the low one in the evaporator (4→1). The refrigerant is now returned to its initial state, and the process begins anew. (Wenzel et al., 2006)

For better illustration, this process can also be illustrated in a log p/h diagram as shown in Figure 2-2.

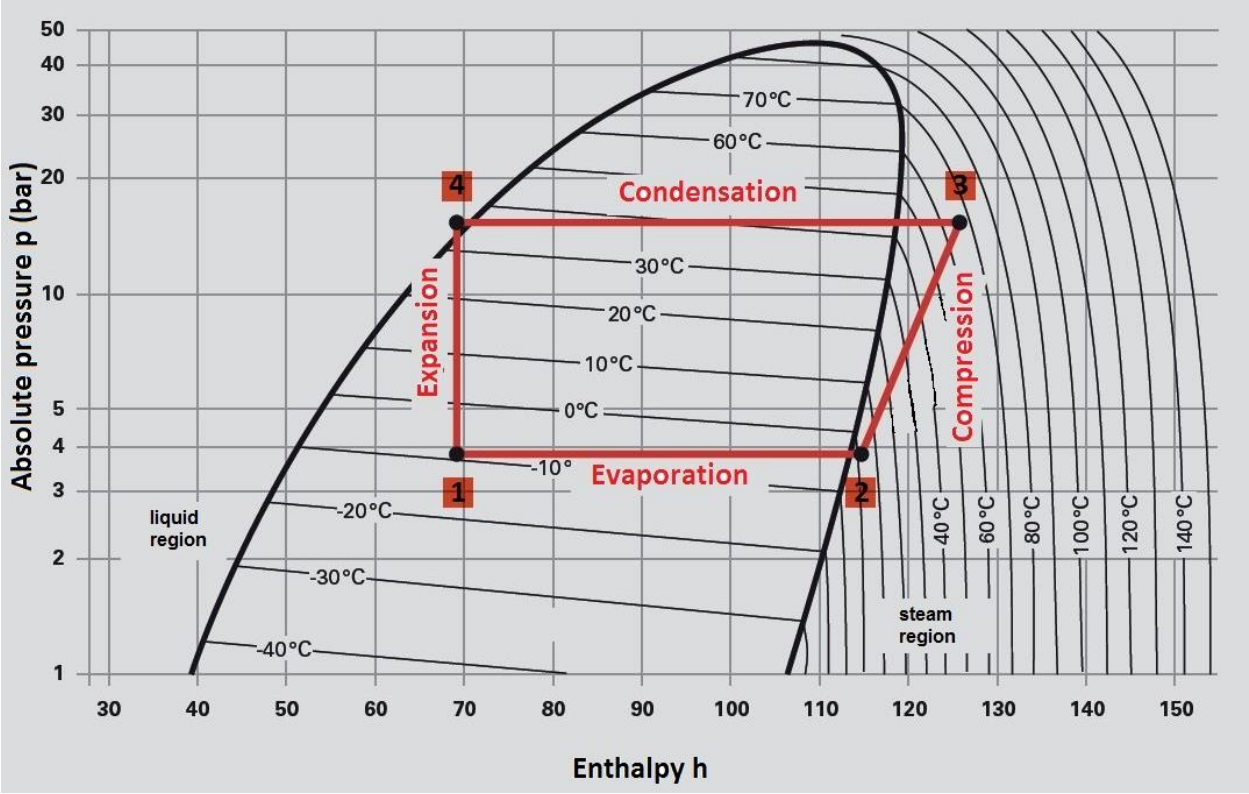

Figure 2-2: log p/h diagram of a heat pump with R 407C (Viessmann, 2011)

2.2 Function of solar collectors

Solar collectors absorb the (shortwave) solar radiation with an absorber and transfer the energy to a heat exchanger. Figure 2-3 shows the basic structure and the energy fluxes of such a solar collector. This subchapter is based on the script for the lecture “Sonnenenergienutzung” (Streicher et al., 2015)

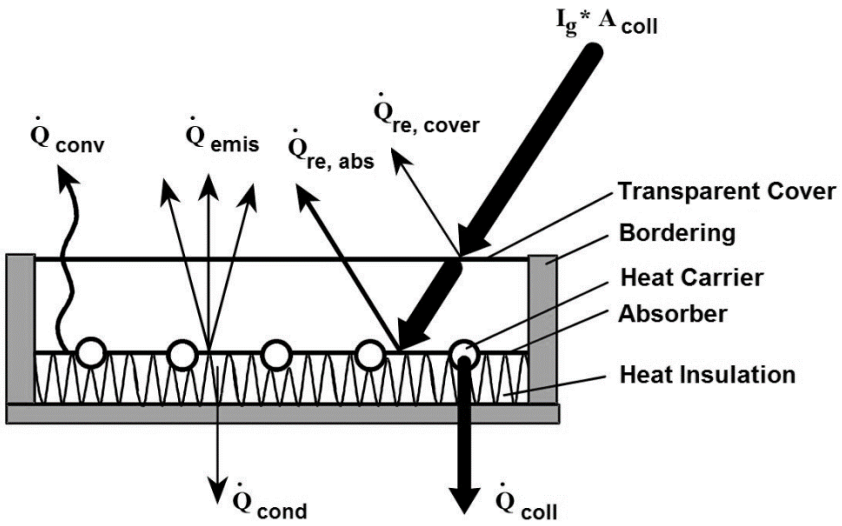

Figure 2-3: Basic structure and the energy fluxes of a solar collector (Streicher et al., 2015)

In the case of covered absorbers, a part of the radiation ($\dot{Q}_{re,cover}$) is already reflected on the transparent cover and never enters into the collector. Another small part is reflected by the absorber and leaves the collector again through the cover ($\dot{Q}_{re,abs}$). These are considered together as $\dot{Q}_{re}$. The remaining radiation is absorbed by the absorber, which however does not mean that this entire radiation energy can be used. The hot absorber emits a part of this energy as long-wave radiation ($\dot{Q}_{emis}$). In case of a non-selective absorber, the emission rate for long-wave solar radiation is the same as the absorption rate for short-wave solar radiation. In contrast, the emission level for long-wave radiation is significantly lower than the absorption rate for short-wave radiation in case of a selective absorber. Selective absorbers, therefore, have lower radiation losses than non-selective ones, which have a particular effect at higher temperatures.

Besides the radiation losses, the hot absorber also has a convective heat loss ($\dot{Q}_{conv}$) from the collector to the outside air. Finally, the collector should be well insulated on the back side, so that the energy losses due to heat conduction ($\dot{Q}_{cond}$) are small. The two losses $\dot{Q}_{conv}$ and $\dot{Q}_{cond}$ are described together by the heat loss coefficient U^*_{coll}, since they can usually not be measured separately. Therefore, the balance of energy for a collector with an area A_{coll} and a solar irradiation I_G is:

$$\dot{Q}_{coll} = I_G * A_{coll} - \dot{Q}_{re} - \dot{Q}_{emis} - \dot{Q}_{conv} - \dot{Q}_{cond} \quad (2\text{-}1)$$

The individual losses consist as follows:

$$\dot{Q}_{re} = I_G * A_{coll} * (1 - \tau_{cov} * \alpha_{abs}) \quad (2\text{-}2)$$

$$\dot{Q}_{emis} = A_{coll} * \varepsilon_{abs} * \sigma * \left(\bar{T}^4_{abs} - \acute{T}^4_a\right) \quad (2\text{-}3)$$

$$\dot{Q}_{conv} + \dot{Q}_{cond} = A_{coll} * U^*_{coll} * (\bar{T}_{abs} - T_a) \quad (2\text{-}4)$$

τ_{conv} is the transmission coefficient of the cover for high frequency solar radiation and α_{abs} the absorption coefficient of the absorber. In addition, ε_{abs} stands for the emission of the absorber as well as σ is the Stefan-Boltzmann-Constant with 5.67 * 10^{-8} W/m²K⁴. Moreover, the required temperatures are divided into the outside air temperature (T_a), the average collector temperature ($\overline{T}_{abs}$) and the sky temperature ($\acute{T}_a$). Further explanations can be found in the cited literature.

The efficiency of a collector results from the useful energy ($\dot{Q}_{coll}$) divided by the irradiance (I_G * A_{coll}):

$$\eta_{coll} = \frac{\dot{Q}_{coll}}{I_G * A_{coll}} \tag{2-5}$$

$$\eta_{coll} = \tau_{cov} * \alpha_{abs} - \frac{U^*_{coll}}{I_G} * (\bar{T}_{abs} - T_a) - \frac{\varepsilon_{abs} * \sigma}{I_G} * (\bar{T}^4_{abs} - \acute{T}^4_a) \tag{2-6}$$

For practical use, the radiation element is considered as a square element with the ambient temperature. Instead of the average absorber temperature ($\overline{T}_{abs}$), which is hardly measurable, all values are related to the mean liquid temperature in the absorber $T_{abs,li}$ because this temperature is easy to measure.

$$\bar{T}_{abs} = \frac{\bar{T}_{abs,in} + \bar{T}_{abs,out}}{2} \tag{2-7}$$

Moreover, the transmission, the absorption and the emission coefficient as well as the heat loss coefficient are often summarized to absolute terms. The equation can then be described as follows:

$$\eta_{coll} = c_0 - c_1 * \frac{(\bar{T}_{abs} - T_a)}{I_G} - c_2 \frac{(\bar{T}^4_{abs} - \acute{T}^4_a)^2}{I_G} \tag{2-8}$$

c_0 is called conversion factor and stands for the maximum possible efficiency, reached at the same temperature of the collector und the ambient.

c_1 is the heat loss coefficient of the collector based on the temperature difference between the absorber and the ambient. Usually it is given for still air and sometimes additionally for a wind speed of 4 m/s.

c_2 is an approximation of the real radiation losses and the variability of the heat loss coefficient at different temperature differences.

Figure 2-4 shows the characteristic line of different collector types for radiation on the absorber area related to the relative value $(\overline{T}_{abs} - T_a)/I_G$. If the temperature difference is zero, the efficiency is equal to the conversion factor. It can be seen that, in this case, the swimming pool

absorber has the highest efficiency, which is due to the fact that it is uncovered and, therefore, no reflection losses occur on the cover. However, as the temperature difference increases, its efficiency decreases rapidly.

Moreover, at the intersection with the x-axis, the downtime temperature, i.e. the maximum achievable temperature difference, can be calculated for a given radiance intensity.

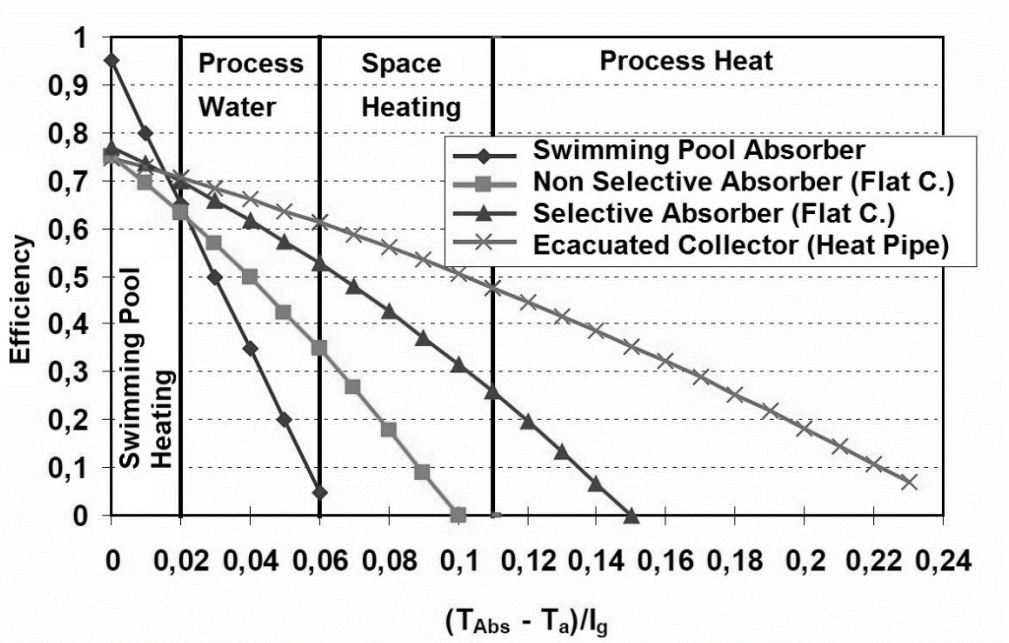

Figure 2-4: Characteristic curve of different types of solar collectors (Streicher et al., 2015)

Furthermore, Figure 2-5 shows the classification of the losses as well as the useful heat. The line between the thermal losses and the useful heat represents a possible characteristic line of a solar collector.

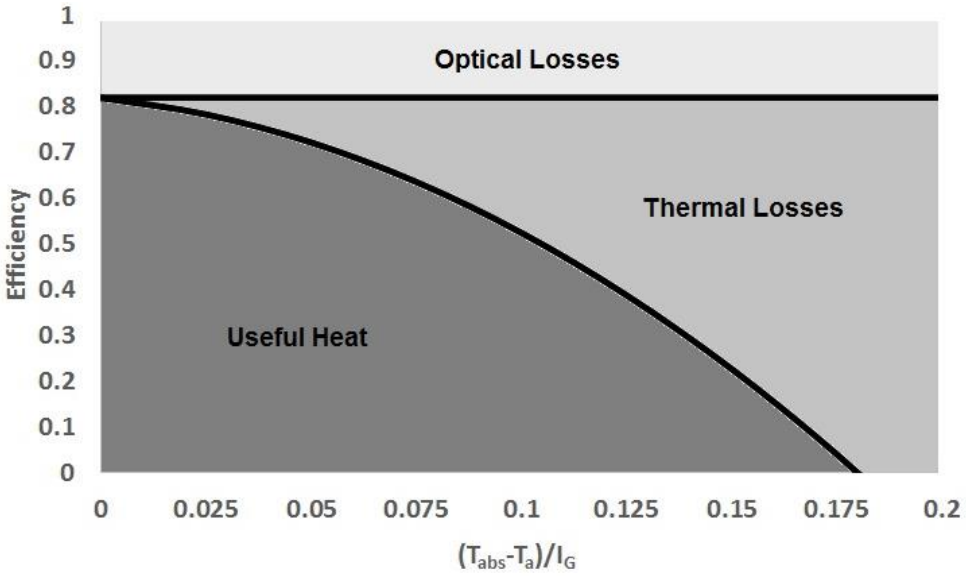

Figure 2-5: Classification of losses (Streicher et al., 2015)

2.3 Ice storage

The term "ice storage" in connection with ice storage heat pumps is a popular name for a latent heat store with water as storage medium. "Latent heat storage" means that the change of the energy during the phase transition from ice to water and delivered from water to ice is used as storage. This allows to store a large amount of heat at a small temperature difference. In the case of the ice storage, the phase change takes place at 0 °C. The complete melting of 1 kg of water requires at constant temperature the same amount of heat as the heating of 1 kg water from 0 °C to 80 °C. This so-called fusion enthalpy or fusion heat is 335 kJ/kg or 93 Wh/kg for water. (Minder et al., 2014)

Figure 2-6 shows the relationships discussed in a Temperature/Enthalpy-Diagram. In addition to that, the specific heat capacities of the different aggregate states are also indicated.

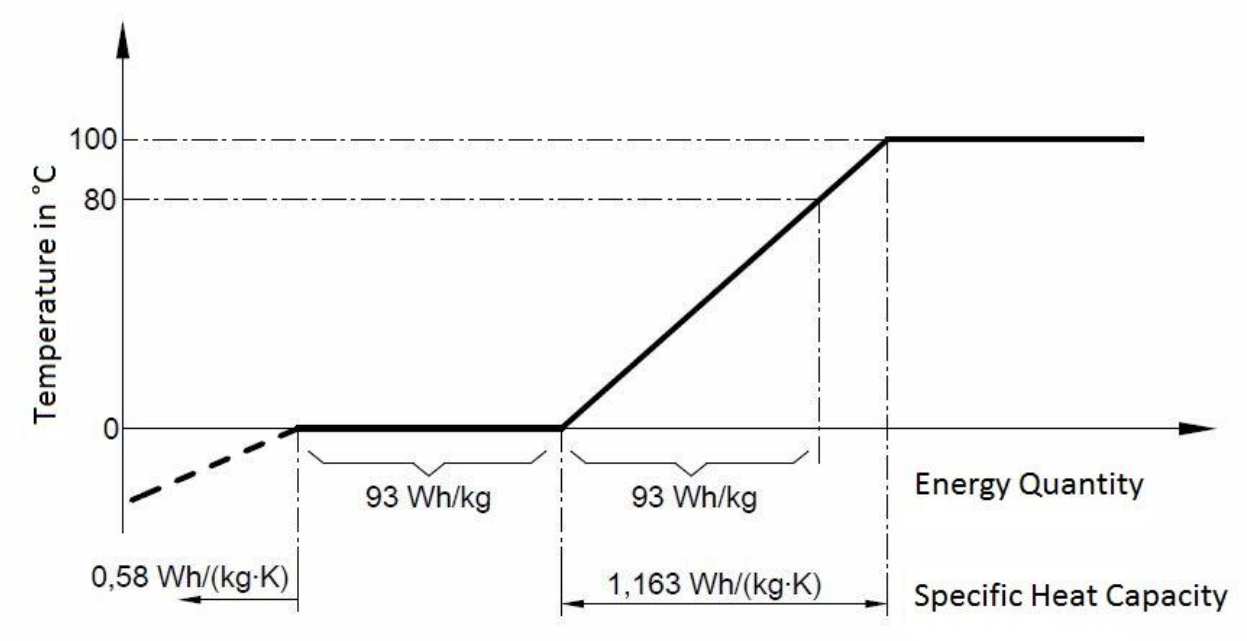

Figure 2-6 Temperature/Enthalpy-Diagram of water (Viessmann, 2014)

Ice storages are not only latent storages. When they are installed in connection with heat pumps they can also be used as sensitive heat storages in the temperature range above 0 °C. When heat is available at the solar collector, the storage is warmed up further after the complete melting to a maximum temperature, which can still be used by the heat pump. Depending on the design and mode of operation, this sensitive part of the heat storage can represent a significant percentage of the total storage capacity. (Minder et al., 2014)

Figure 2-7 shows an illustration of a common method for a construction of an ice storage. It is common for the heat exchanger to be made of spiralled plastic pipes on several planes. This has the positive effect that the extraction performance remains nearly constant. On the one hand, the ice which forms around the heat exchanger tubes acts as an insulation layer, which would reduce the abstraction performance. On the other hand, the ice generation also increases the heat exchanger surface, which again has a positive effect on the performance. (Gutensohn, 2012)

However, such heat exchangers have a much lower overall heat transfer coefficients compared with copper tube heat exchangers and plate heat exchangers. (Minder et al., 2014)

Figure 2-7: Illustration of an ice storage (Müllers, 2008)

2.4 Water storage

To guarantee that hot water for the heating system (SH) or domestic hot water preparation (DHW) is available when it is just needed, storages with the right capacity and temperature are necessary. The most frequently used ones are short time hot water storages. Water has the advantage that it is available “everywhere”. It is cheap in its purchase and disposal as well as non-toxic and ecologically harmless. Moreover, it is storage and heat transfer medium in the heating system at the same time. Beyond that, it has a high storage capacity, a low thermal conductivity and a, at higher temperatures, decreasing density. These are all desirable properties.

Figure 2-8 shows a common construction of a storage for a combined system with a solar collector and a second heating system. In the case of a pure solar heating, with or without a heat pump, the second (upper) heat exchanger would be omitted, for example. Furthermore, in such a case it makes sense to position the auxiliary heater slightly lower to ensure that there is always enough warm water available. (Heinz, 2015)

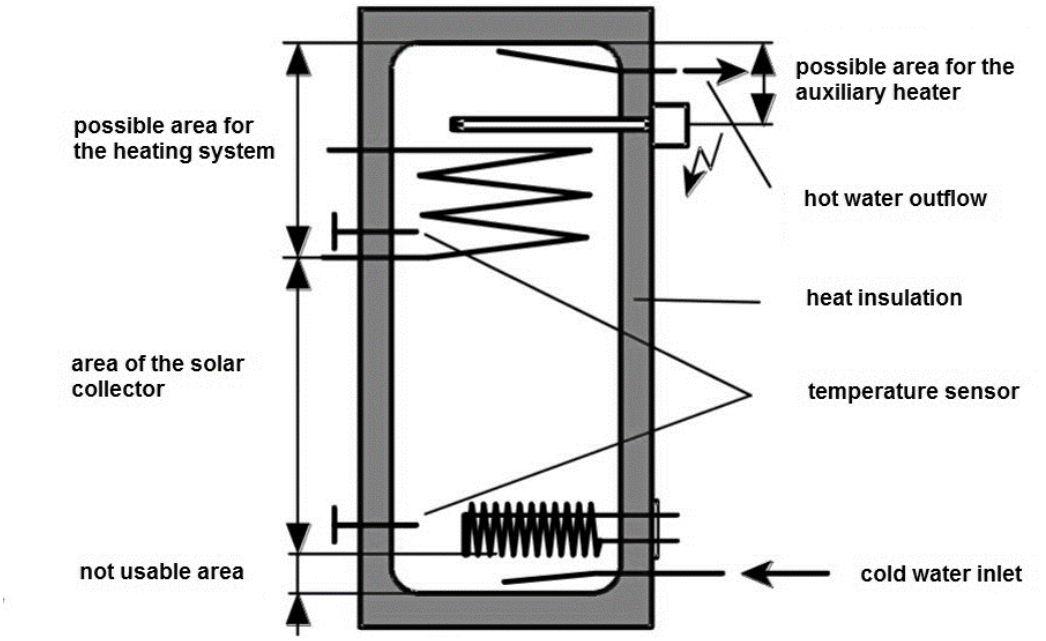

Figure 2-8: Common construction of a water storage (Heinz, 2015)

In addition, storages differ in their temperature distribution of the storage medium. Basically, stratified and non-stratified ones are distinguished, as shown in Figure 2-9. Both storages have the same energy content (the same mean temperature) but a different exergy. The advantages of a stratified storage are, for example, a better operating point of the solar collector or of the heat pump, and the better use of the hot water during discharging. However, this kind of storage has higher construction costs, which is resulting in higher acquisition costs. Therefore, it is reasonable to decide for each application separately, which storage suits best. In general, it can be said that stratified storages are particularly useful when there are small inflows and outflows compared to the storage size, or when the energy should be stored for a long period of time. (Heinz, 2015)

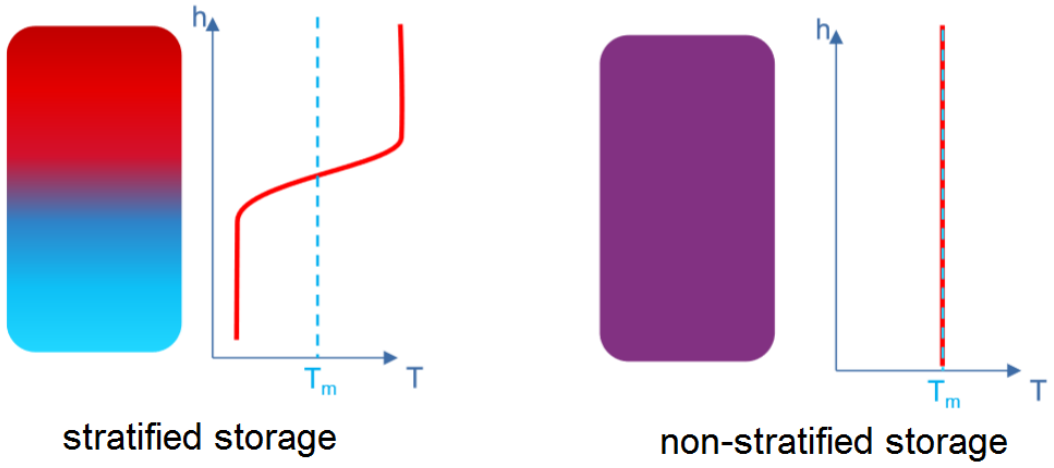

Figure 2-9: Temperature distribution of storages (Heinz, 2015)

3 THE SOLAR–ICE STORAGE–HEAT PUMP SYSTEM IN WEIZ

The project “Hot Ice Weiz” is focused on the use of latent heat with two ice storages and two heat pumps in combination with unglazed solar collectors and a PV system. It is designed as a pilot project for local heat supply.

The construction of the MFB (multi-family building) which is located at Bärentalweg 6 in 8160 Weiz was finished in April 2015. The building, shown in Figure 3-1, is a wood frame construction which accommodates ten different apartments on three floors. The total area adds up to 1477 m^2, whereof an area of 957 m^2 is heated. It fulfils the passive house standard and has a calculated thermal heat demand of 9.91 kWh/(m^2a).

Figure 3-1 Building in Weiz (Hutter, 2016)

Figure 3-2 shows the hydraulic scheme of the heating system which is used in this building. A more detailed description of the most important components can be found in the subchapter *3.1 Used technology.*

As shown in Figure 3-2, the heat provided from the solar collector can either be put into the ice storage by a heat exchanger or fed to the heat pumps. It is impossible to use the heat from the solar collector directly to heat the domestic hot water (DHW) or the space heating (SH) storage because the temperature is to low and must be brought to a higher level by the heat pumps before. Depending on the current energy requirement, one or two heat pumps work. The always work in one mode (DHW or SH storage) and ensure that the temperature in the storages remains within the desired range. Instead of the solar collector, the heat pump can also be fed from the ice storage. If both heat sources are not sufficient, there is the further possibility to heat the two storages with an auxiliary heater. During the summer, this system can also be used for cooling. For this, the ice storage is used directly as heat sink (“cold source"), so that no additional chiller is needed.

Furthermore, the building has a controlled ventilation system with heat recovery. With this ventilation system, it is possible to heat the supplied air. A more detailed scheme of the heating system including the sensor positions for the measurement as well as the ventilation system can be found in the appendix in Figure A- 14 and Figure A- 15 (TB Bierbauer GmbH, 2015).

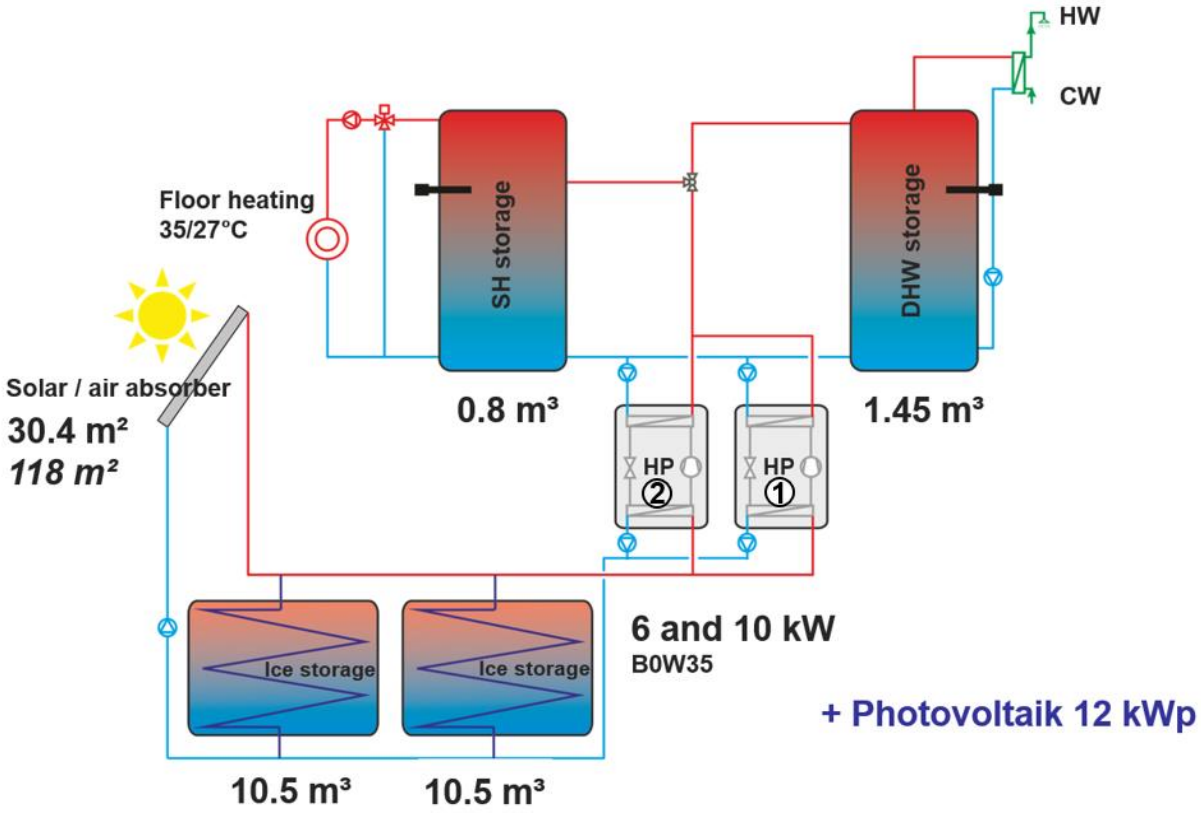

Figure 3-2: Hydraulic scheme (Lerch, 2017)

There are a huge number of sensors installed, which allows a detailed analysis of the functioning of the system. Some of the most important sensors are the heat meters, which measure the inlet and return temperature as well as the mass flow. In addition, they also provide the power and the heat quantity, which are calculated from the measured values and the fluid data: two for each heat pump (one for DHW and one for SH), one for the solar collector, one for cooling and one for the ventilation system. Furthermore, there are, for example sensors to measure the collector temperature, the global radiation, the ambient temperature, the electric power of the heat pumps and the electric heating elements to mention only some of them. Moreover, several sensors are installed to measure the ice storage and the surrounding soil temperatures.

The data of these sensors are not only recorded for later analysis, but can also be viewed using the HMI App (HMI-Master GmbH, 2017). This app visualizes the current system status. It is, therefore, possible to observe at any time in which operating mode the system is currently working, how high the storage temperatures are, or whether a problem occurs somewhere. In addition, all electrical and all heat quantity meters as well as the current weather data are displayed. Furthermore, the temperatures, CO2 concentrations and relative humidity of each apartment are also shown. This makes the app a valuable tool for monitoring and better understanding the functioning of the system.

3.1 Used technology

This section is intended to provide a brief overview of the main components, such as the solar collector, the heat pumps, the SH storage, the DHW storage and, of course, the ice storages.

3.1.1 Solar collector

A solar collector of the type SLK F, shown in Figure 3-3, from the company "Isocal HeizKühlsysteme GmbH" is used to provide the thermal energy. It is a low temperature collector with two overlapping layers for installations on flat roofs. The whole unglazed collector is made of polyethylene (PE) without any welded or bonded joints. Further important technical data is summarized in Table 3-1.

Figure 3-3: Picture and scheme of the installed solar collector; left (Projekt HOT ICE, 2017) right (Viessmann, 2017)

Table 3-1: Technical data of one solar collector module (Viessmann, 2014)

Type		**SLK-F**
Gross area	m^2	2.61
Absorber area	m^2	2.34
Heat exchanger surface	m^2	9.1
Dimensions	mm	2120x1225x50
Weight (empty/full)	kg	38/81
Used fluid		35 % Ethylenglykol / Water
Nominal flow rate	m^3/h	0.25
Maximum operating pressure	bar	3
Downtime temperature	°C	60
Hydraulic connection		Tichelmann

There are 13 of these modules installed, resulting in a total absorber area of 30.42 m^2 and a total heat exchanger surface of 118.3 m^2. The collector is able to use direct and diffuse radiation as well as energy from convection, precipitation and condensation.

The characteristic curve of the solar collector was not disclosed and had to be determined during the validation with TRNSYS shown in chapter *5.2.2 The solar collector.*

3.1.2 Heat pumps

To lift the heat to the required temperature level, provided by the solar collector or the ice storage, two heat pumps (managed in parallel) are used. Both are of the same type but with a different capacity. Depending on the current heat demand, the heat pumps can operate together or alone but they always work in the same operating mode (SH or DHW storage). If, for example, heat pump one provides heat for the DHW storage, heat pump two can either provide heat for the same storage or stands still; i.e., it is not possible that one heat pump provides heat for the DHW storage and the other one provides heat for the SH storage at the same time.

In the further work, the 10 kW heat pump is designated as "heat pump 1" and the 6 kW one as "heat pump 2". Both are operating with a temperature spread of 5 Kelvin on the heat sink side (design point). For this case, the technical data are listed in Table 3-2.

Table 3-2: Technical Data of the heat pump (Viessmann, 2015)

Type BW 301.A.		**06**	**10**
		Heat Pump 2	**Heat Pump 1**
Performance data (5K spread) B0W35			
Nominal heat output	kW	5.94	10.06
Cooling capacity	kW	4.71	8.08
Electric power consumption	kW	1.32	2.13
Coefficient of performance (COP)	-	4.51	4.72
Refrigerant	-	R410A	R410A
Brine (primary circuit)			
Contents	l	3.0	4.0
Min. volume flow (5K spread)	l/h	860	1470
Max. inlet temperature	°C	25	25
Min. inlet temperature	°C	-5	-5
Medium	-	35 % Ethylenglykol / Water	
Water (secondary circuit)			
Contents	l	2.4	3.4
Min. volume flow (5K spread)	l/h	520	880
Max. inlet temperature	°C	60	60

3.1.3 Space heating storage

One storage with a capacity of 0.8 m^3 is installed to ensure the required amount of hot water for the Space heating (SH). The temperature of this storage is hold between 30 °C and 35 °C. The energy, therefore, is provided from the heat pumps. In addition, an auxiliary heater with an electric power of 2.5 kW is integrated for the case that the heat pumps could not provide enough energy to hold the temperature level.

3.1.4 Domestic hot water storage

The domestic hot water (DHW) storage, with a capacity of 1.45 m^3 is similar to the SH storage, however, higher temperatures of 55-60 °C are required. Moreover an auxiliary heater with an electric power of 10 kW is integrated in this storage.

3.1.5 Ice storage

The heart of the whole system is the ice storage or better the two ice storages shown in Figure 3-4. Both are identical with the small difference that ice storage one is monitored more extensively because the controller uses ice storage one as input for the control and expects that the other one has the same state. They are non-insulated water filled steel-reinforced concrete containers, which are buried in the soil. To obtain an optimal heat output from the soil, care must be taken to ensure certain minimum distances between the reservoirs and the building of at least 3 m. In this case, the storages are placed with a distance of 3 m to each other and with 4 m to the cellar.

Figure 3-4: Pictures of the ice storage in Weiz (Projekt HOT ICE, 2017)

The freezing of the storage, indicated in Figure 3-5 by “Einfrieren”, takes place from the inside outwards and from the bottom upwards, to allow an expansion of the ice without destruction. The water filling of the reservoir is about 90% of the total volume. It is also important that the design of the cistern allows the utilization of heat from the surrounding soil. (Minder et al., 2014)

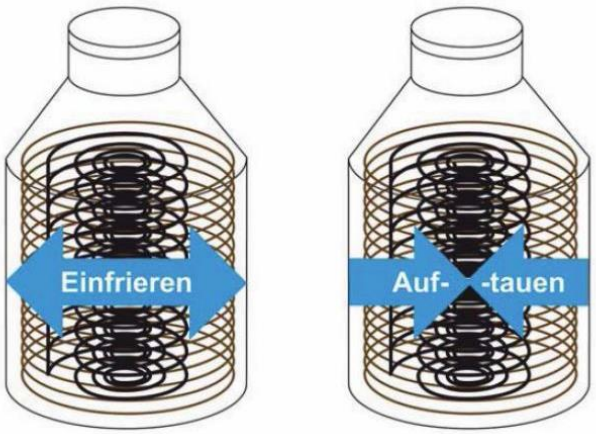

Figure 3-5: Freezing and unfreezing of the ice storage (Viessmann, 2017)

The basic characteristics are shown in Table 3-3:

Table 3-3: Technical data of the ice storage (Viessmann, 2014)

Type		**SE 12_10 B**
Intern volume	m^3	10.5
Dimensions	m	Ø 2.7 x 3.375
Weight (empty)	kg	ca. 9000
Used fluid storage		Water
Heat transfer fluid		35 % Ethylenglykol / Water
PE Dimension extraction		PE32
PE Dimension regeneration		PE25

In addition, Figure 3-6 shows the positioning of the sensors in and around the ice storages. As already mentioned, ice storage one is better monitored because it is used for the control. The sensors T_soil_1/1, T_soil_1/5 and T_soil_2/2 are positioned in a distance of one metre to the ice storages, while the others are placed without a gap. All sensors except of sensor T_soil_1/3 are installed with a thermowell. Except of that the sensor T_soil_1/3 is from the same type. Moreover all these soil temperature sensors are in the middle of the ice storage.

Furthermore, there are some sensors which are installed directly in the ice storages. The sensor T_{ice} is the one which is used for controlling, the others are only for visualisation.

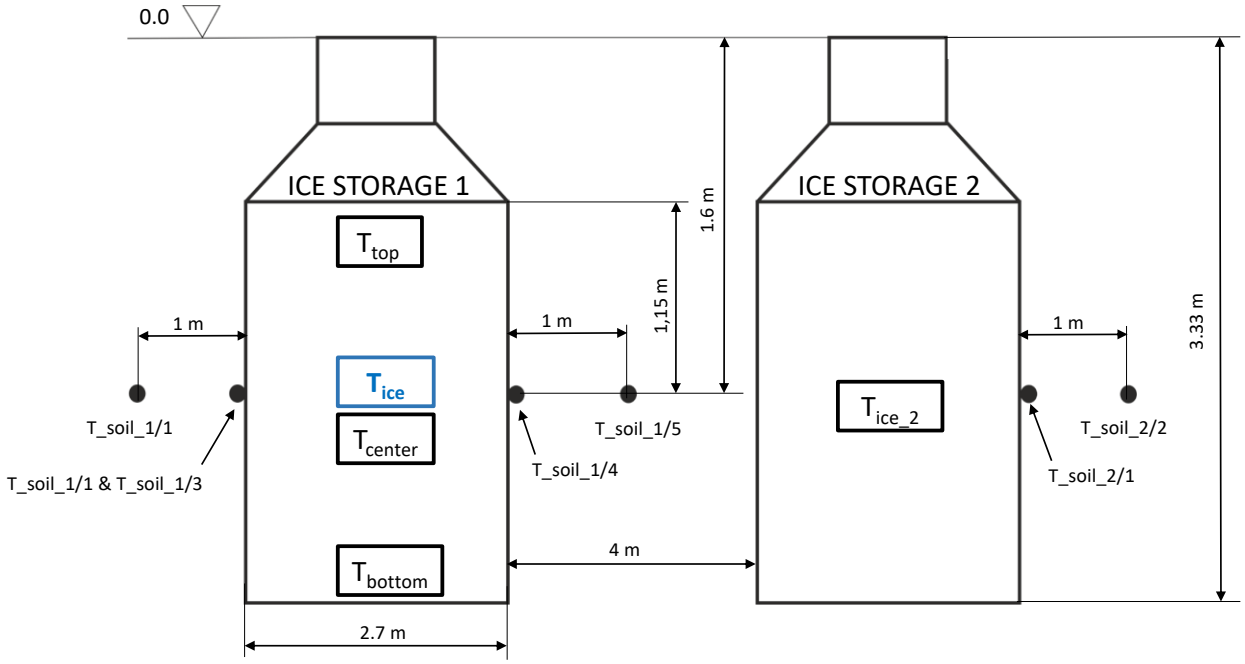

Figure 3-6: Ice storage (Viessmann, 2017)

3.1.6 Used measurement technique

As mentioned above, in addition to the already discussed sensors of the ice storage, a significant number of other sensors has been installed to analyse the functioning of the system. The measurement data are recorded using a KNX network that transfers the measured values to an HMI interface. This HMI App visualizes the current system status. It is, therefore, possible to access the current measured values at any time. Furthermore, all recorded data are automatically transferred to a database and can be exported as csv-file. (Hackl, 2016)

All sensor data were taken from the Bachelor thesis "Analyse einer realen Eisspeicher Wärmepumpenanlage mit Solar Luftkollektoren" (Hackl, 2016), which has already dealt with this topic. A detailed scheme of the sensors for the measurement can be found in the appendix in Figure A- 14 (TB Bierbauer GmbH, 2015).

Apartments:
In each of the ten apartments are KNX AQS/TH indoor sensors (Elsner Elektronik, 2017c) installed, which are used for the controlling of heating and ventilation. These measure:

- CO_2 concentration: Measurement range 0 . . . 2000 ppm, Accuracy ±50 ppm
- Temperature: Measurement range -10 . . . +50 °C, Accuracy ±0.4 °C
- Air humidity: Measurement range 0 . . . 95 %, Accuracy ±5 %

Additionally, in every room a KNX TH-UP Thermo–Hygrometer (Elsner Elektronik, 2017b) is installed, which measures the temperature and the relative humidity.

- Temperature: Measurement range 0 . . . +50 °C, Accuracy ±0.5 °C

- Air humidity: Measurement range 0 . . . 100 %, Accuracy ±5 %

Temperature:
For the measurement of the temperatures at the energy counters, PT500 temperature sensors are used according to EN 60751.

Electrical power:
The energy module EM/S 3.16.1 of ABB i-bus® KNX (ABB i-bus®, 2017) is used for the measurement of electrical power.

- Effective power: Measurement range 5.7 . . . 4600 W, Accuracy ±6 %

The measurement power values are summed with the energy counter EMU Professional 3/75 to the meter reading.

Weather conditions:
On the roof of the building the weather station P03/3 - RS485 (Elsner Elektronik, 2017d) basic from Elsner Electronik GmbH provides the values for:

- Brightness: Measurement range 0 . . .99000 Lux, Accuracy ±35 %
- Wind velocity: Measurement range 0 . . . 70 m/s, Accuracy ±25 %
- Temperature Measurement range -40 . . . +80 °C, Accuracy ±1.5 °C

To measure the global radiation, the KNX PY Pyranometer (Elsner Electronic, 2017a), also from Elsner Elektronik GmbH, is used.

- Global radiation: Measurement range 0 . . . 2500 W/m^2, Accuracy ±15 %

Heat quantity
There are three different types of heat quantity meters installed. At the heat pumps and for the ventilation in total, five heat quantity meters of the type UH50_1,5_OEM (Siemens AG, 2017) are used (“Zähler” 1, 2, 3, 4 and 6 in the measurement scheme in the appendix).

- Heat quantity meter: Measurement range 0 . . . 150 °C, Accuracy 2 %

For cooling the type, Ultraschall Sharky Heat 775 (Diehl Metering, 2017) with the same measurement range and accuracy is used (“Zähler 5” in the measurement scheme in the appendix). For the solar circuit, a new heat quantity meter (“Zähler Solar” in the measurement scheme) has been installed since November 2016. According to an email request, this should be of the type T550 Ultraheat (Landis+Gyr, 2017). Since this heat meter has only a measurement range above 0 °C, but temperatures below 0 °C have also to be measured, this information is possibly not true.

3.2 Operating modes

At the moment, the system works in four (five) different operating modes. In this subchapter, it will be clarified when which mode is used and how they work. It is also possible that the “Heat pump with ice storage mode” and the “Ice storage regeneration” work at the same time. This can be considered as a fifth operating mode.

3.2.1 Heat pump with solar collector mode

This mode is used when the collector temperature is higher than the ambient temperature, which is normally the case when the sun shines. Moreover, an energy demand for the SH or the DHW storage must be needed. In addition, the collector temperature must be between -4 °C and 25 °C, or if it is under -4 °C, it must be higher than the ice storage temperature. If all the requirements are fulfilled, the system works in the “Heat pump with solar collector mode”, which is illustrated in Figure 3-7.

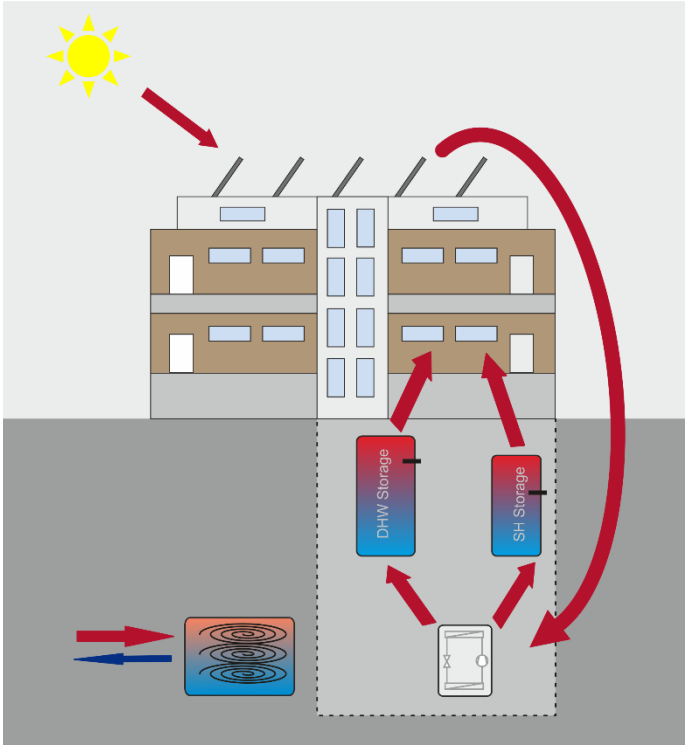

Figure 3-7: Heat pump with solar collector mode

This means that the energy is delivered directly from the solar collector to the heat pump. The ice storage is not used in this mode. However, in case of a lower ice storage than soil temperature, the ice storage is regenerating in the meantime.

Figure 3-8 represents typical data for this mode, measured on the February 4, 2016. The diagram shows that all conditions are fulfilled. Most of the time heat pump one (10 kW) works alone and provides energy for the SH storage, which can be seen by the fact that this storage temperature rises while the DHW storage temperature falls continuously. After the DHW storage drops below the desired temperature range of 55-60 °C (at 13:32 h), the system starts to provide energy for the DHW storage, since this one has the higher priority in the controlling system. This is also the

time, when the second heat pump is additionally turned on in Figure 3-8. Now the DHW temperature rises while the SH storage temperature remains constant.

Moreover, it is apparent that in the "heat pump with solar collector mode" the primary temperatures follow the collector temperature, while the secondary temperatures follow the respective storage temperature. The primary side is the side at the evaporator (heat source side of the HP) and the secondary side is the one at the condenser (heat sink side of the HP). On the primary side, the flow side is defined as the one which delivers the heat from the source to the HP. On the secondary side, it is the one which delivers the heat from the HP for the water storages.

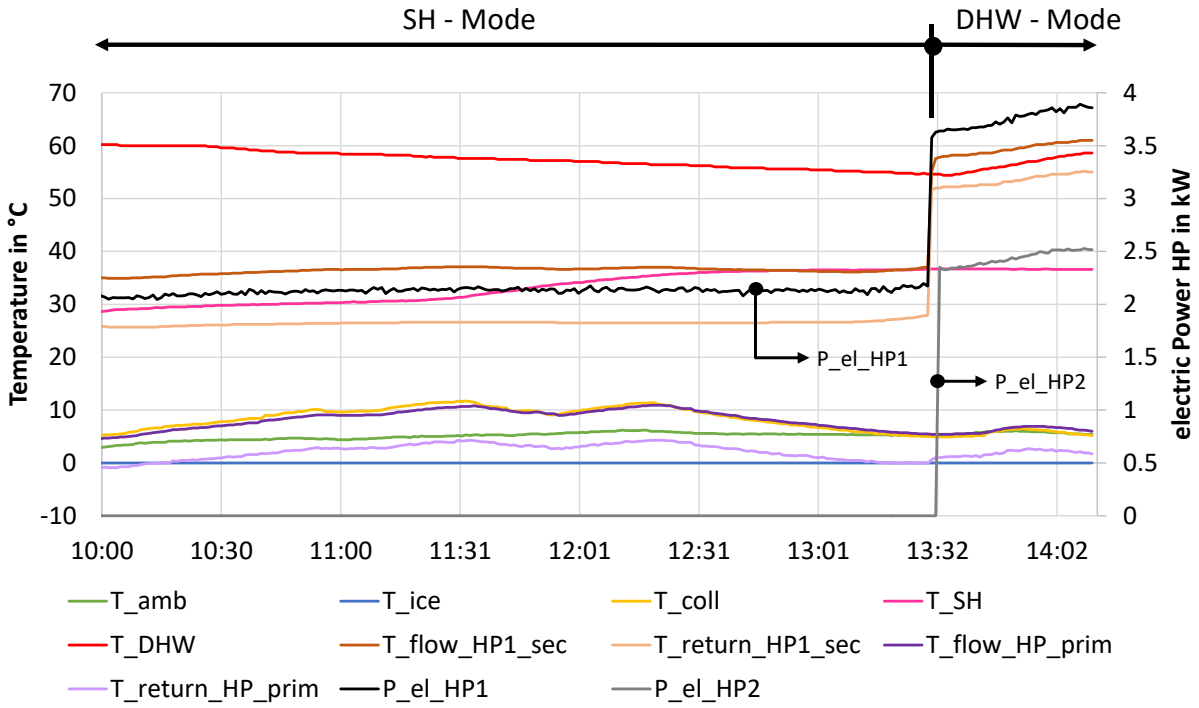

Figure 3-8: Measurement data of the heat pump with solar collector mode

3.2.2 Heat pump with air absorber mode

This operation mode, shown in Figure 3-9, is similar to the "Heat pump with solar collector mode" with the difference that the ambient temperature is higher than the collector temperature, which is usually the case, when no sun shines. As already described, the installed collector is able to use diffuse radiation as well as the energy from convection, precipitation and condensation. Therefore, energy from the collector can be provided even without direct solar radiation.

For the controller, it makes no difference which of the two modes occur, however, in chapter *5.2 Validation of the single components* these two cases must be analysed separately. For this reason, the differentiation is also made here.

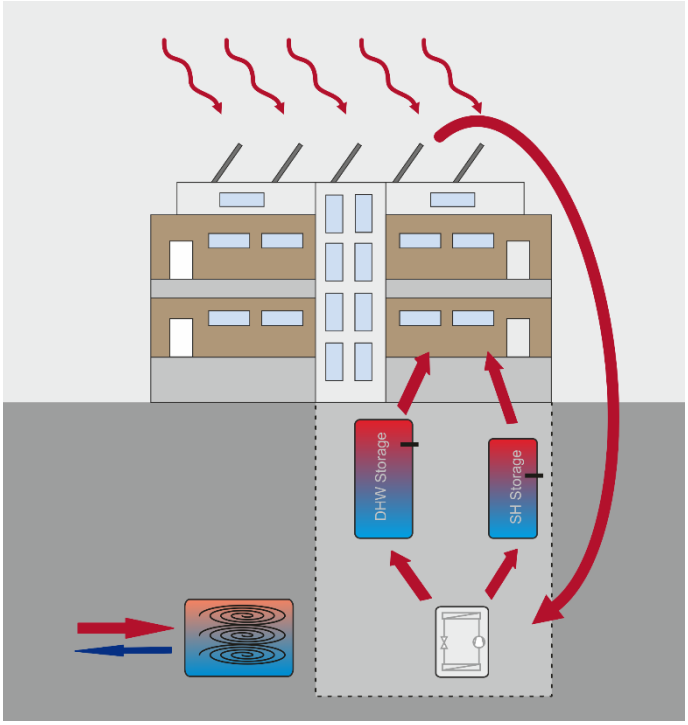

Figure 3-9: Heat pump with air absorber mode

Figure 3-10 shows an example of this operation mode. First, both heat pumps provide energy for the DHW storage. Since the SH temperature drops off in the meantime, the system switches over (at 05:11 h) and first one (until 06:11 h) and then both heat pumps provide energy for the SH storage. The temperature profiles of the primary and secondary side discussed in the operation mode before, can also be observed here.

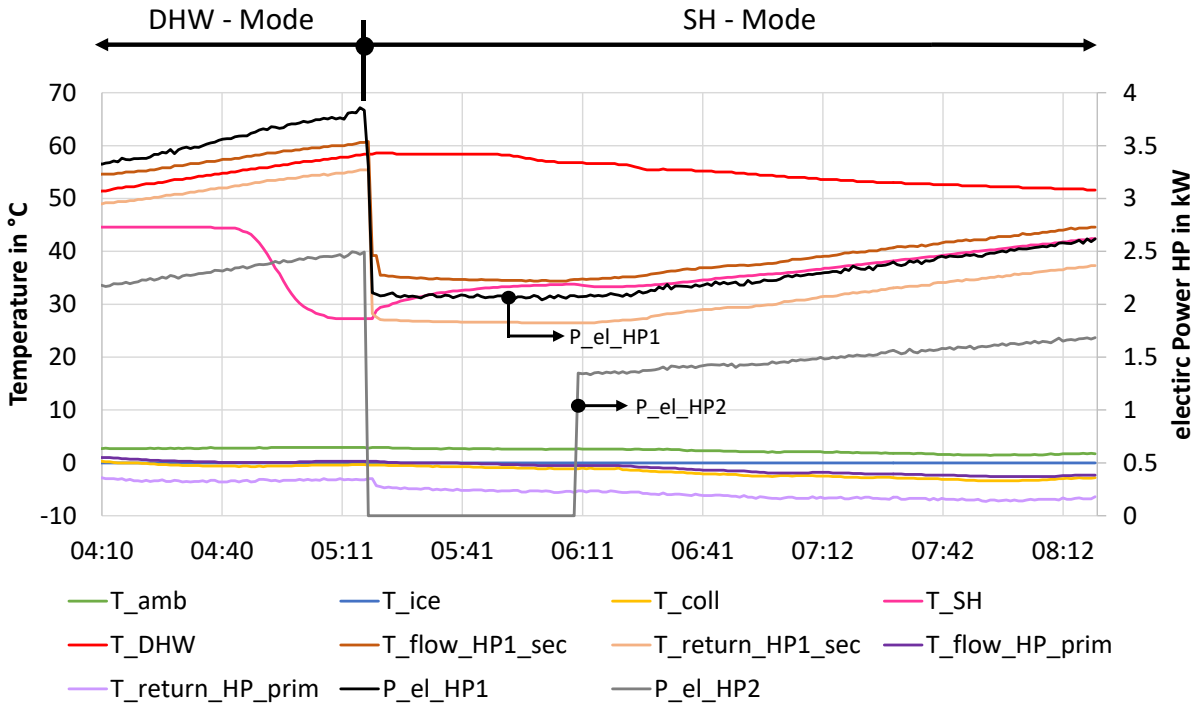

Figure 3-10: Measurement data of the heat pump with air absorber mode

3.2.3 Heat pump with ice storage mode

In contrast to the two previous described operating modes, the ice storage is used as the source for the HP instead of the solar collector. This is the case when the collector temperature drops below -4 °C, and the ice storage temperature is higher than the collector temperature, and if the collector temperature is higher than 25 °C. Moreover, an energy demand for the SH or the DHW storage must exist. The functionality of this operating mode is visualized in Figure 3-11.

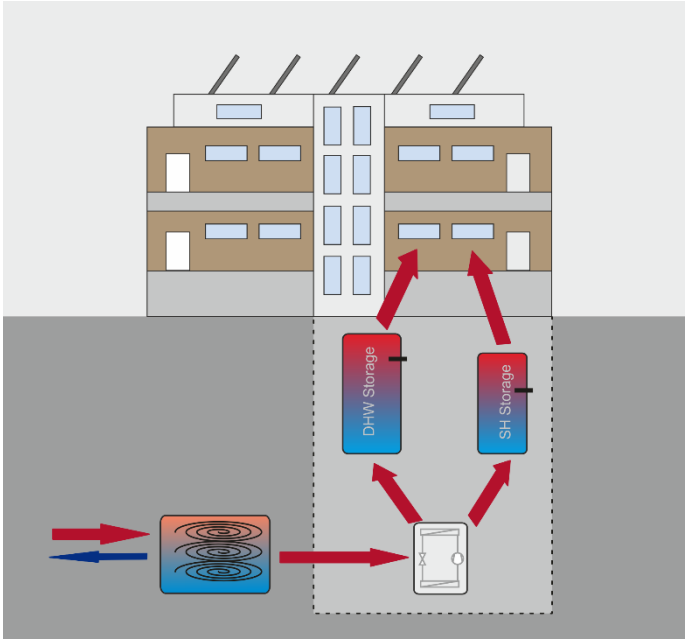

Figure 3-11: Heat pump with ice storage mode

In addition, Figure 3-12 shows typical data for this operation mode. The collector temperature is below -4 °C and the ice storage temperature is higher. For the temperatures on the secondary side applies the same as before. They follow either the DHW storage or the SH storage temperature. In this case, the storage for which the heat is provided is changed two times (at 18:45 h & at 20:45 h). The flow temperature on the primary side follows the ice storage temperature instead of the solar collector temperature in this mode.

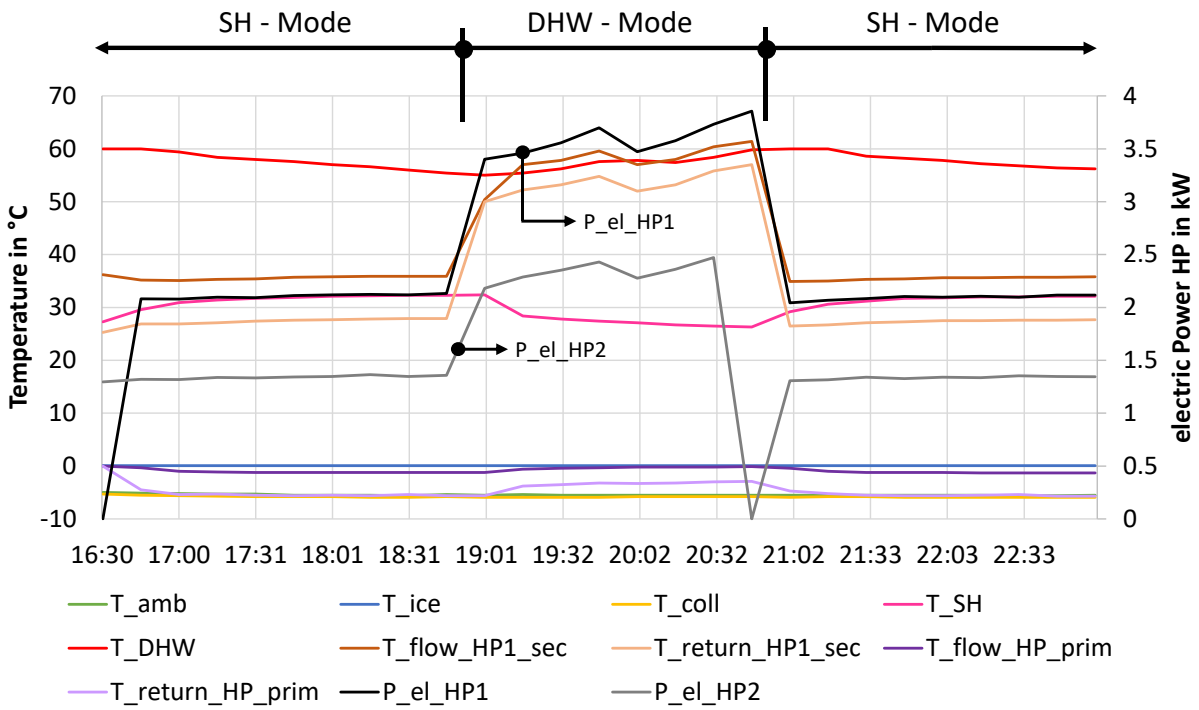

Figure 3-12: Measurement data of the heat pump with ice storage mode

3.2.4 Ice Storage Regeneration

The used operation mode, shown in Figure 3-13, is the ice storage regeneration. Neither an energy demand for the SH- nor for the DHW storage exist. In addition, the collector temperature must be higher than the ice storage temperature because the regeneration works directly without the use of the heat pumps. Moreover, the regeneration stops when the ice storage temperature exceeds 15 °C or the collector is used as source for the heat pumps.

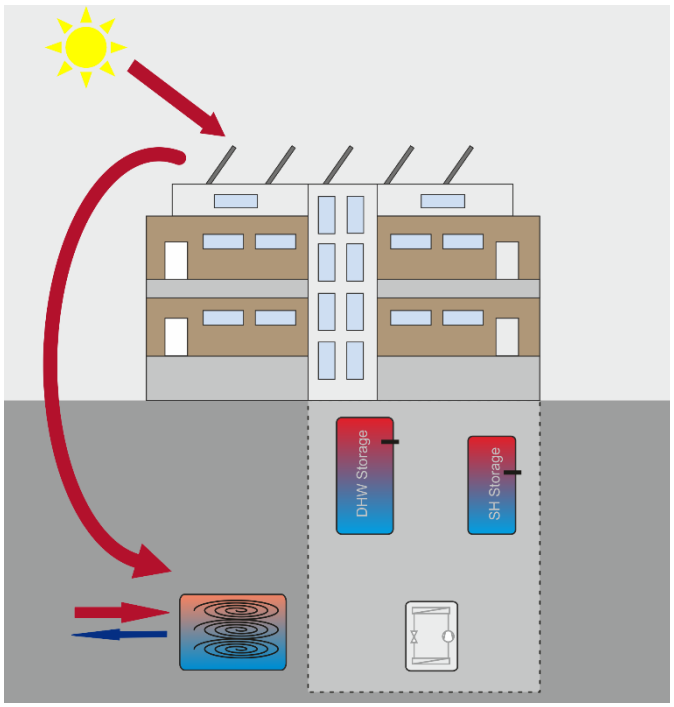

Figure 3-13: Ice storage regeneration

A typical case of this operation mode is shown in Figure 3-14. None of the heat pumps work, which can be seen by the electric power consumption. This is also confirmed by the fact that the SH storage and the DHW storage temperature remain the same or drop down. This conclusion is certainly only possible if none of the auxiliary heaters works, which is the case here. The solar collector temperature often cools down during the regeneration and the ice storage temperature rises or stays constant if it is in the phase change, as in this example. Here, the ice storage temperature remains constant although energy is supplied.

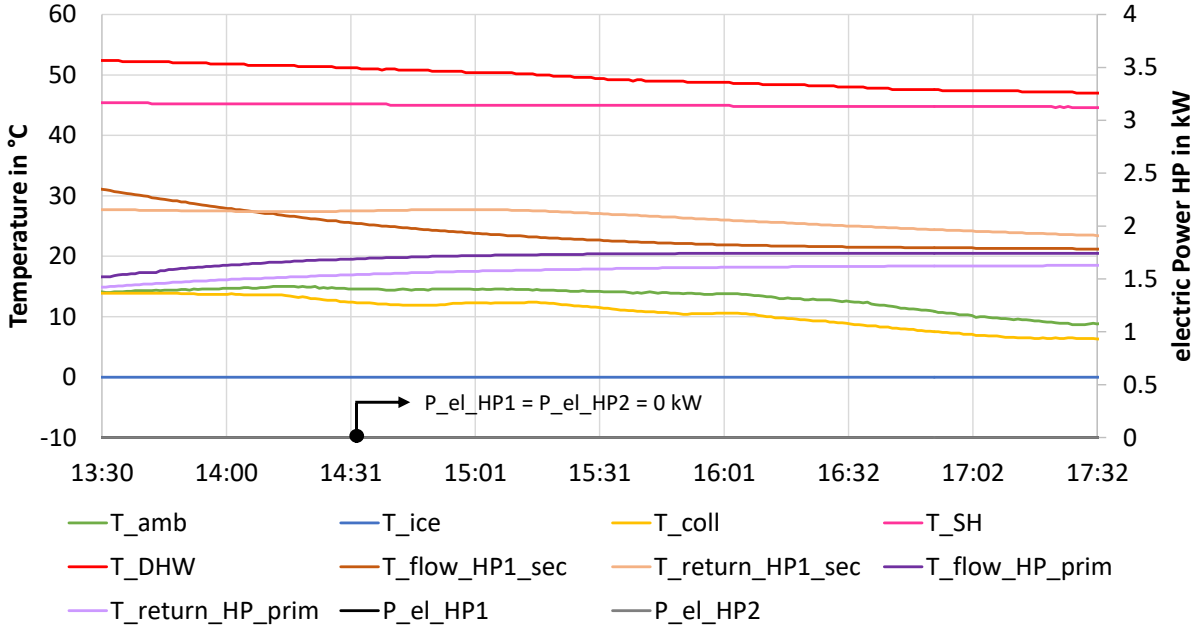

Figure 3-14: Measurement data of the ice storage regeneration

3.2.5 Combination of the “Heat pump with ice storage mode” with the regeneration

The combination of these two modes is only used when the collector temperature exceeds the maximum permissible temperature of 25° C. Moreover, there must be an energy demand for the SH or the DHW storage and the maximum temperature of the ice storage of 15 °C must not be exceeded. If this is the case, the solar collector regenerates the ice storage while the ice storage is used as source for the HP at the same time. According to these prerequisites, this operating mode occurs mainly during the summer. Figure 3-15 shows the energy flows for this case.

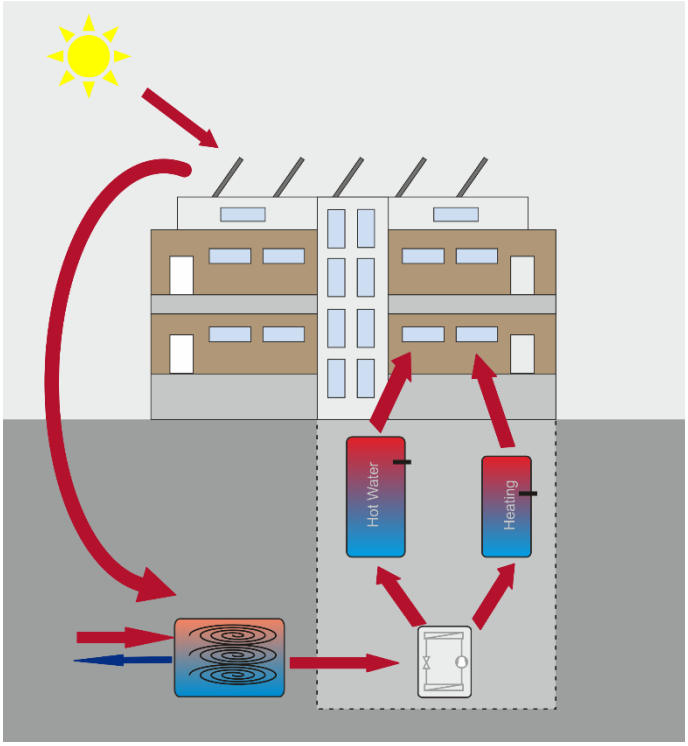

Figure 3-15: Combined mode

This operation mode is shown in Figure 3-16. The collector temperature is too high for the heat pump but, drops down during the measurement period because the collector is regenerates the ice storage. At the same time the ice storage is used as source for the heat pumps. The shown period was measured in the summer (07.06.2016). The reason why the SH storage is hold at such a high temperature is because of a control failure.

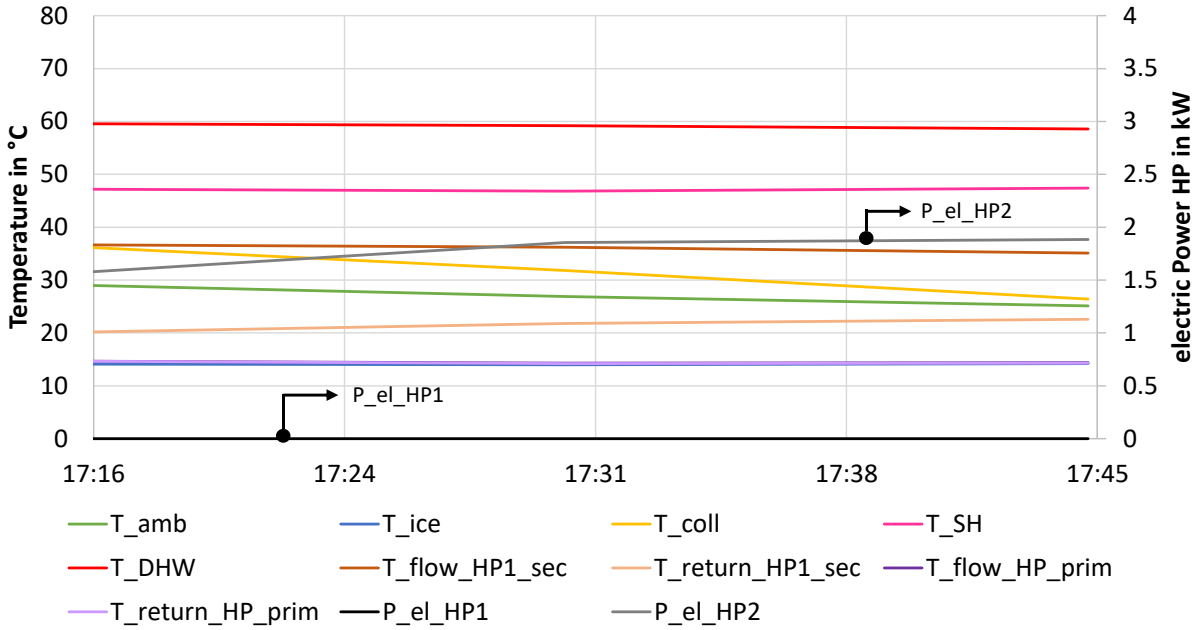

Figure 3-16: Measurement data of the combined mode

4 DATA ANALYSIS

For the assessment of the actual state of the system, the measured data of the installed sensors have been available since July 20, 2015. This data is collected in a Microsoft Excel file, which is updated at short intervals. Most of the time the data is measured in 15 min steps but there are some measuring periods with a lower step width of 1 min. The lower step width was necessary for the validation of some TRNSYS models. This chapter deals with the findings on the behavior of the system, which can be obtained from this data. In addition, it is intended to illustrate the procedure leading up to these findings as well as possible limitations and problems occurred.

4.1 Limitations of the measured data

Due to data losses, system modifications and defect sensors, the data must be treated and analyzed with caution. The most important of these limitations and their effects are described here.

4.1.1 Data losses

During the analyzed measurement period from 01.01.2016 until 31.01.2017, some longer data failures have occurred. They happened at:

- 07.02-10.02.2016: Data losses of the whole system
- 03.05-13.05.2016: Data losses of the whole system
- 26.07-13.09.2016: Data losses of the solar heat meter
- 19.10-24.10.2016: Data losses of the whole system
- 11.11-23.11.2016: Data losses of the solar heat meter
- 10.12-13.12.2016: Data losses of the whole system

The data losses of the whole system are caused by problems with the data transmission. That means that the sensors worked correctly during this time. This differentiation is particularly important for the heat quantities of the heat meters. The fact that the sensors worked correctly during this time means that the heat quantities are known without losses for the (monthly) energy balances. An exception of this is the solar heat meter, which is explained in chapter *4.1.2 The solar heat meter* and the electric meters of the heat pumps, which is explained in chapter *4.1.4 The electric meters.*

In addition, it happens sometimes that single measured values are missing. In the Excel file, this is indicated by the use of blank lines in the corresponding data record. These short data losses, however, are in a range that it has no substantial influence on the further data evaluation.

4.1.2 The solar heat meter

The solar heat meter is one of the most important data suppliers for the system analysis, unfortunately, however, it is one of the components that has created the biggest problems. Firstly, the solar heat meter was installed later than the other measurement devices. Therefore, these measured values have only been available since 14.12.2015. In the first time of the measurement, however, the problem occurred that the heat meter could not measure temperatures below 0 °C. As soon as negative temperatures occured, it came to an overflow. Since the flow and the return flow temperatures in winter are often below 0 °C (collector used as source for the heat pump), the measurement data cannot be used for the preparation of the energy balance until the problem was solved on 18.01.2016. Moreover, since 10.02.2016 the measurement of the inlet und return temperature has been converted to integer values. In addition, the temperature difference with a resolution of two decimals has been recorded from this time onwards.

A further problem occurred in the measurement of the power delivered by the collector. Apart from the fact that no reasonable values were measured till 18.01.2016, the problem with temperatures below 0 °C still remains here. As shown in Figure 4-1, the values of the solar collector power are not plausible in case of negative temperature values.

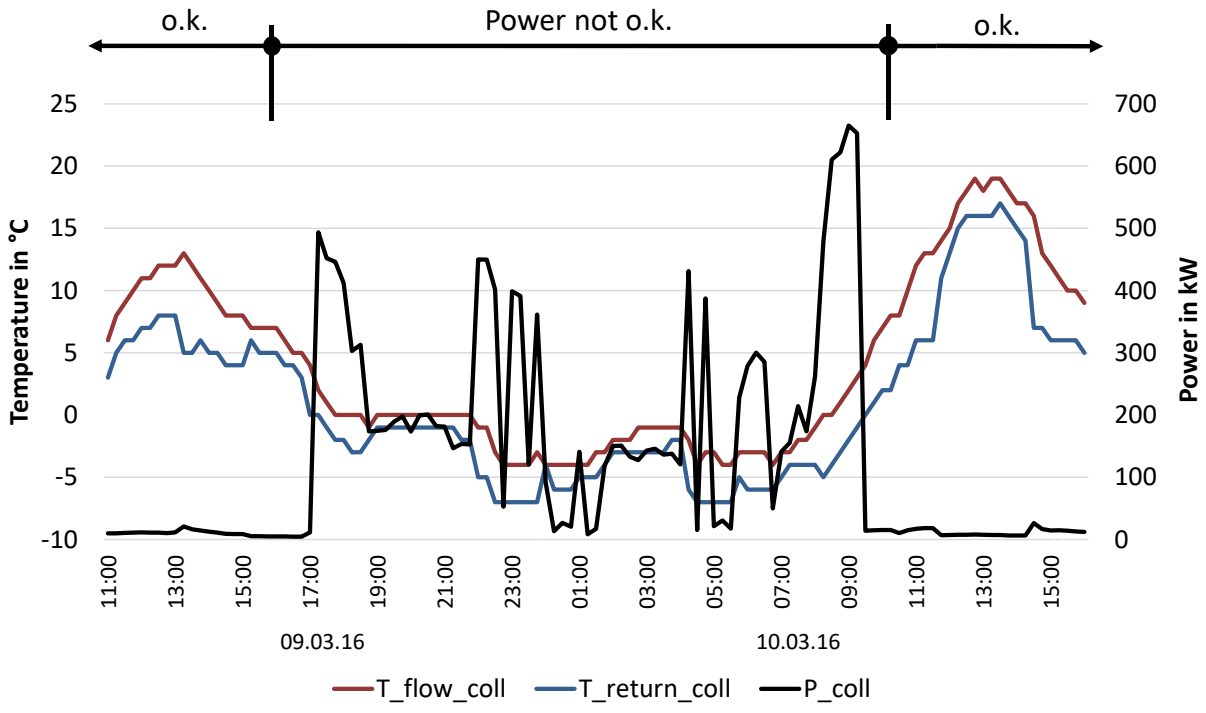

Figure 4-1: Solar collector heat meter

Due the fact that the heat meter calculates the heat quantity using a wrong power, the heat quantity is also wrong and cannot be used for the system evaluation.

In November 2016, after some unsuccessful attempts to solve the problem, the solar heat meter was replaced by a new one. Since then, all measured values have been recorded correctly.

4.1.3 Soil and ice storage temperatures

Between 08.10. and 30.10.2015 the connection boxes of the soil and ice storage temperature sensors became wet. They were installed in the ice storage at the top where normally no water should be. During this period, the measured temperatures were not correct and hence the range shown in Figure 4-2 has to be excluded from the analysis.

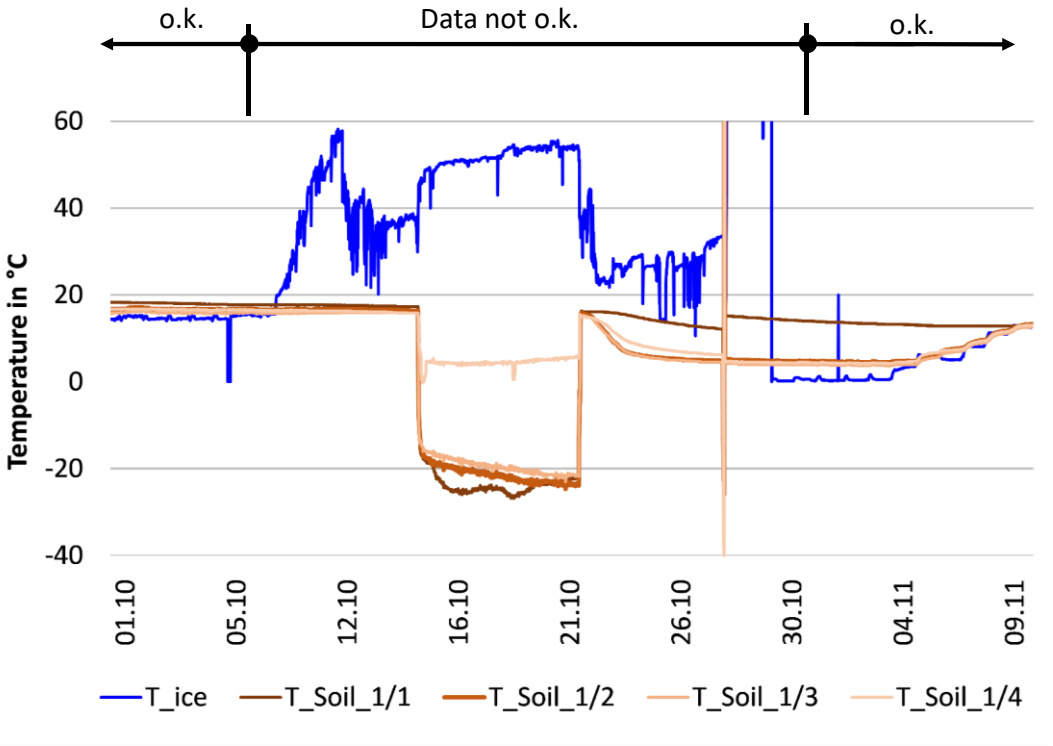

Figure 4-2: Soil and ice storage temperatures 2015

4.1.4 The electric meters

At first, the electric meters of the heat pumps and of the electric heating elements worked in such a way that the values were only updated when the data were retrieved manually. These are the jumps in Figure 4-3. Moreover, it is shown that the electric meter of the heat pump 2 did not work at all for a long period (until December 2016). It is certainly possible to calculate the values manually from the electric power, however, one should keep in mind that in this case the electric energy during the data losses cannot be considered. This is especially important in the monthly energy balances, when the different energies are partly calculated from the electric power and partly provided by the heat quantity meters.

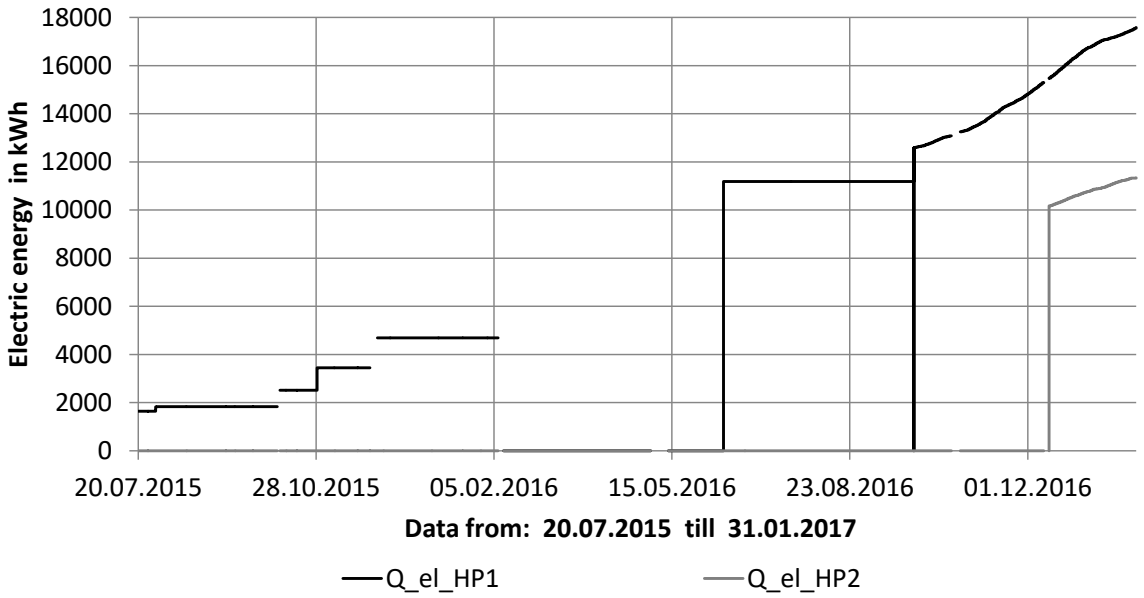

Figure 4-3: Electric energy consumption of the heat pumps

Since October 2016, the electric meter of the heat pump 1 has been updated and has been working correctly now. The heat meter of heat pump 2 was not working until the middle of December 2016.

4.1.5 Conclusion

As seen from the described problems, care must be taken in using the right data for the system analysis. In addition, it has to be mentioned that at the beginning of the measurements further errors at other sensors occurred. Therefore, and especially because of the solar heat meter, a reasonable monthly energy balance can only be created from February 2016 onwards. And even from this point on, some restrictions must be made, as the measurement data failures in February and May 2016, or the intermediate removal of the solar heat meter shows.

4.2 Ice storage and soil temperature profile

A look at the ice storage temperature profile, shown in Figure 4-4, is a good way to get a first overview of the functioning of the system. After a settling time, the ice storage temperature was nearly constant at the adjusted maximum temperature of 15 °C (09.2015). The data recorded in October (08.10. until 30.10.2015) were incorrect due to problems described in chapter 4.1.3. This data was removed to avoid misunderstandings.

At the end of November 2015, the ice storage temperature finally dropped down and started to fluctuate in a greater extent. The ice storage was used as source for the heat pumps but in contrast to the summer months, there was not enough energy to heat it again immediately after use. Furthermore, energy was needed for SH as well because of the start of the heating period. This can be seen in the fact that the temperature dropped relatively steeply. When the temperature increased again, the system was in regeneration mode and the ice storage was reheated by the solar collector.

However, in this period the ice storage is not yet used as a latent heat storage because the temperature is always higher than 0 °C. This happened for the first time in the beginning of January 2015. In Figure 4-5, this is shown in more detail. Two cold periods occurred with ambient air temperatures down to -10 °C. During the first cold period (30.12 until 06.01.2016), the ice storage temperature dropped down to 0 °C degrees for the first time and the water in the ice storage started with the phase change. For several days the storage worked as a latent heat storage. This corresponds to the planned/desired operating behaviour. At the beginning of the following second cold period (13.01.2016), however, the entire storage was already frozen. This can be seen in the fact that the storage temperature began to fall below 0 °C. In this section, the storage temperature dropped down till -12 °C until the storage slowly began to regenerate at the end of the cold period. The subsidence of the temperature into such a low range has the effect that the desired temperature level for the heat pump can no longer be provided. The result is that the auxiliary heater must be used until the ice storage warms up again. After this period (28.01.2016), the ice storage temperature remained in the range around 0 °C so that the storage operated as latent storage again. At the end of the heating season, it finally rose to the maximum storage temperature of 15 °C which was retained during the summer.

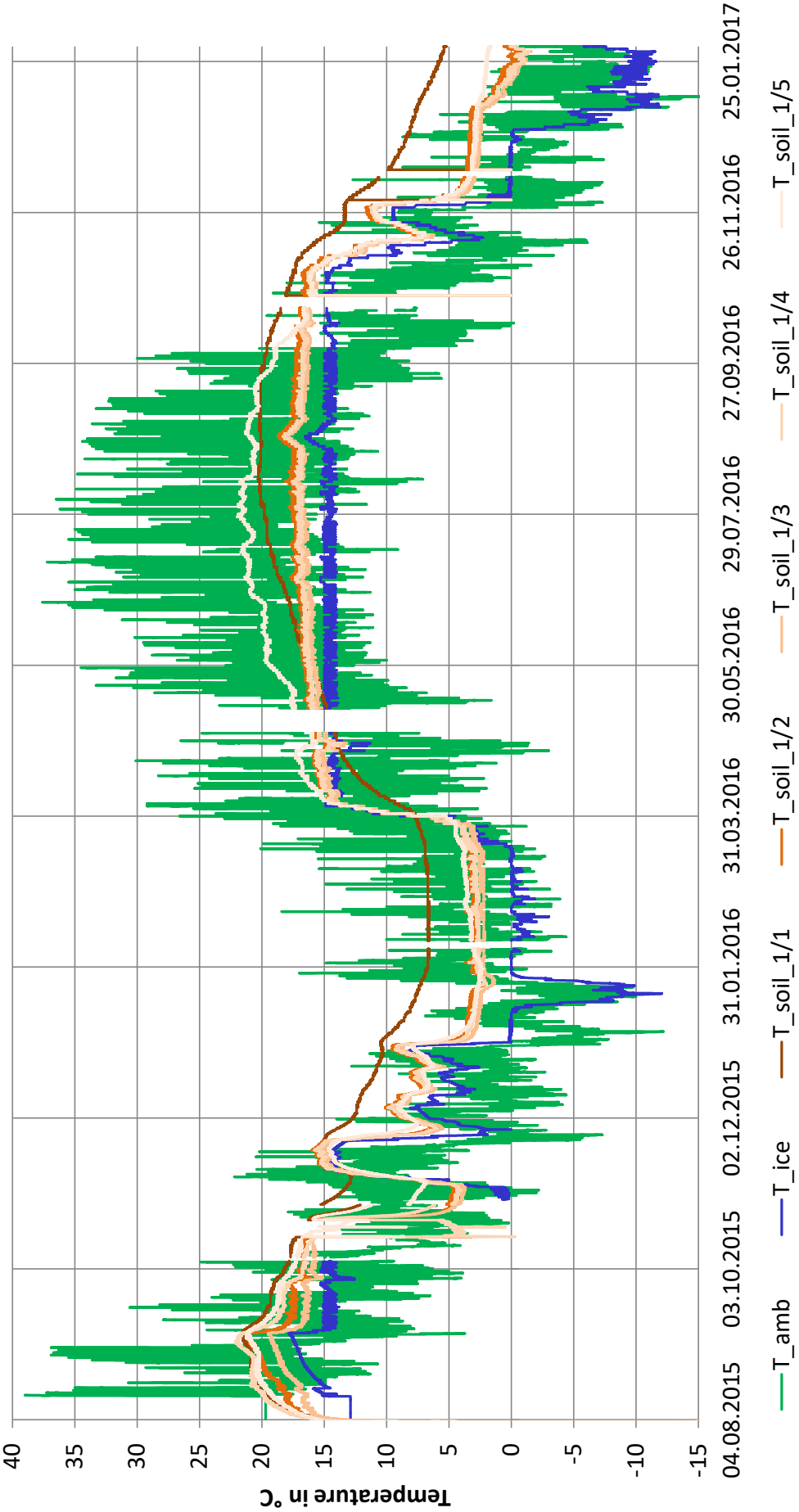

Figure 4-4: Ice storage and soil temperatures

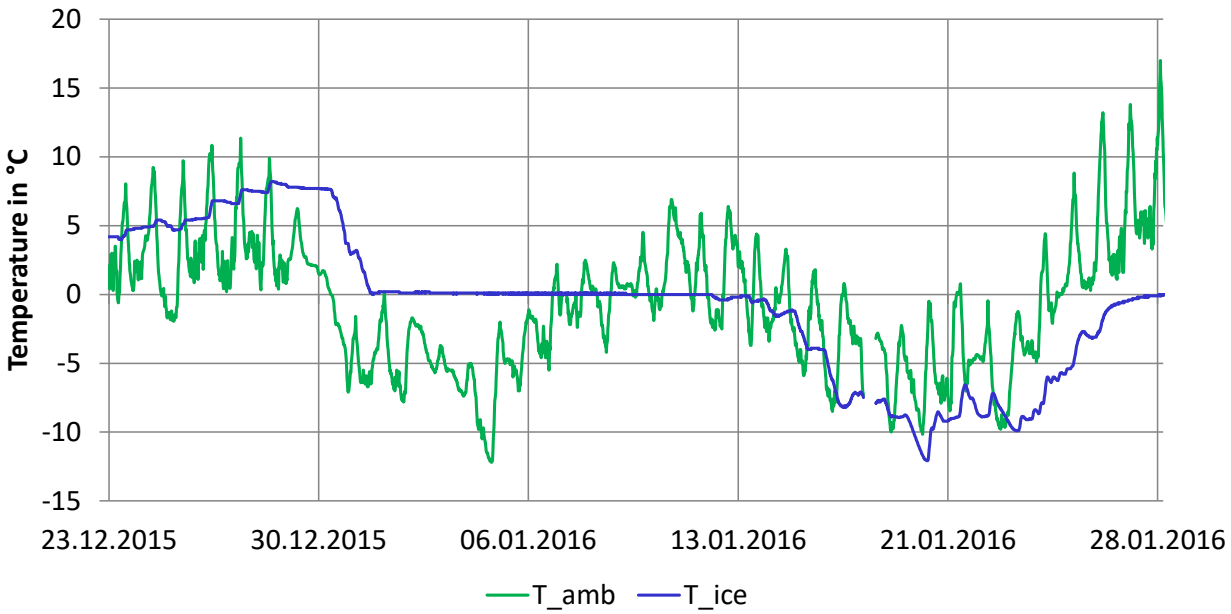

Figure 4-5: Temperature profile of the ambient air and the ice storage

After this, the cycle just described repeated itself, since no significant changes were made at the system in the meantime. However, the freezing of the ice storage in the second winter started earlier (28.12.2016) than in the first one. This is mainly because the winter in 2016/17 was colder. The reason that the soil around such systems is often a bit colder from the second year on, can have an influence on that though.

In addition, Figure 4-4 shows the soil temperatures around the ice storage 1. The soil temperatures are almost always higher than the ice storage temperature. This means that most of the time the ice storage gains energy from the environment instead of losing it, as most other kinds of storages do. This one of the essential advantages of this storages, and confirms the usefulness of burying them in the ground.

A look at the individual temperatures shows that, maybe except of temperature T_Soil_1/1, although they follow the same trend they deviate from each other in their absolute values. On the one hand, this is because there are different kinds of sensors in use and on the other hand the positioning plays an important role. These facts are shown in Figure 3-6. It is noticeable that especially sensor 1/1 deviates from the others. This one is positioned with a distance of 1 m to the ice storage on the side directed to the free soil. Particularly during the winter, the data of this sensor shows that the soil, almost unaffected by the ice storage, is much warmer than the storage. In general, it can be said that the soil temperature at a depth of about 10 m is constant at about 10 °C all year round. (Benkert et al., 2000) In this case, the temperature fluctuates between 7 and 20 degrees over the year and is not constant, because the storage is not so deeply buried and the ground temperature at a distance of one meter is influenced by the ice storage. Nevertheless, it can be seen that this temperature has the lowest fluctuation of all measured values and reacts more slowly to changes of both, the ice storage and the ambient temperature.

It is interesting to compare soil temperature 1/1 with soil temperature 1/5. Both are thermowell sensors placed with a distance of 1 m to the storage but with the difference that sensor 1/5 is on the side directed to the second ice storage. While in the summer the difference is not so big, the two temperatures differ clearly in the winter. In winter the soil temperature is much lower than on the other side and reacts to changes in the storage temperature much faster. On this side, it is almost equal to the soil temperature 1/4, which measures the temperature directly on the outside of the storage. The entire soil between the two reservoirs is, therefore, significantly colder than the soil on the other sides that is only influenced by one storage.

The other three soil sensors (1/2, 1/3, 1/4) show a similar characteristic. All of them are placed directly on the outside of the storage. As expected the temperatures are much more influenced by the ice storage. However, the temperature 1/4 on the side facing the other store is only slightly colder than that one on the other side (in comparison to the temperature 1/2). The comparison with the temperature 1/2 is regarded as more meaningful, since this one is measured by the same type of sensor. Therefore, despite the different soil temperatures at a greater distance from the reservoir, the temperature measured on the outside of the reservoir can be regarded as approximately constant around the circumference.

4.3 Energy balance

This sub-chapter is intended to show the energy quantities as well as the energy flows of the system. As already mentioned, the data have only been suitable for a meaningful analysis since February 2016, which is why the previously measured data are not considered here.

4.3.1 System energy balance

Figure 4-7 shows the heat quantity of the main system's in- and outputs per month as well as per annum. The system boundaries are selected in such a way that the energy obtained from the solar collector and the electrical energy of the heat pumps are counted as input. These are shown in the left bars. The electric energy consumption of the circulation pumps is not measured which is why they must be excluded from this analysis. The losses as well as the possible profits of the ice storage are also not considered here. The heat quantity from the solar collector is separated in the heat quantity, which is directly delivered to the heat pump and the one which is used to regenerate the ice storage. The electrical energy of the heat pumps is also divided. In this case, a distinction between the two heat pumps is made to analyse each of them individually. The heat quantities which are fed to the two storages, the SH storage and the DHW storage, are considered as output. Here again, a distinction between the two heat pumps is done. These energy flows are shown in Figure 4-6. The arrow "Solar heat to HP" and the arrow from the ice storage to the heat pumps are to be understood as meaning that both heat pumps can use the solar collector and the ice storage as source. In addition, a more detailed scheme of the overall system including the sensor positions for the measurement can be found in the appendix in Figure A- 14 (TB Bierbauer GmbH, 2015).

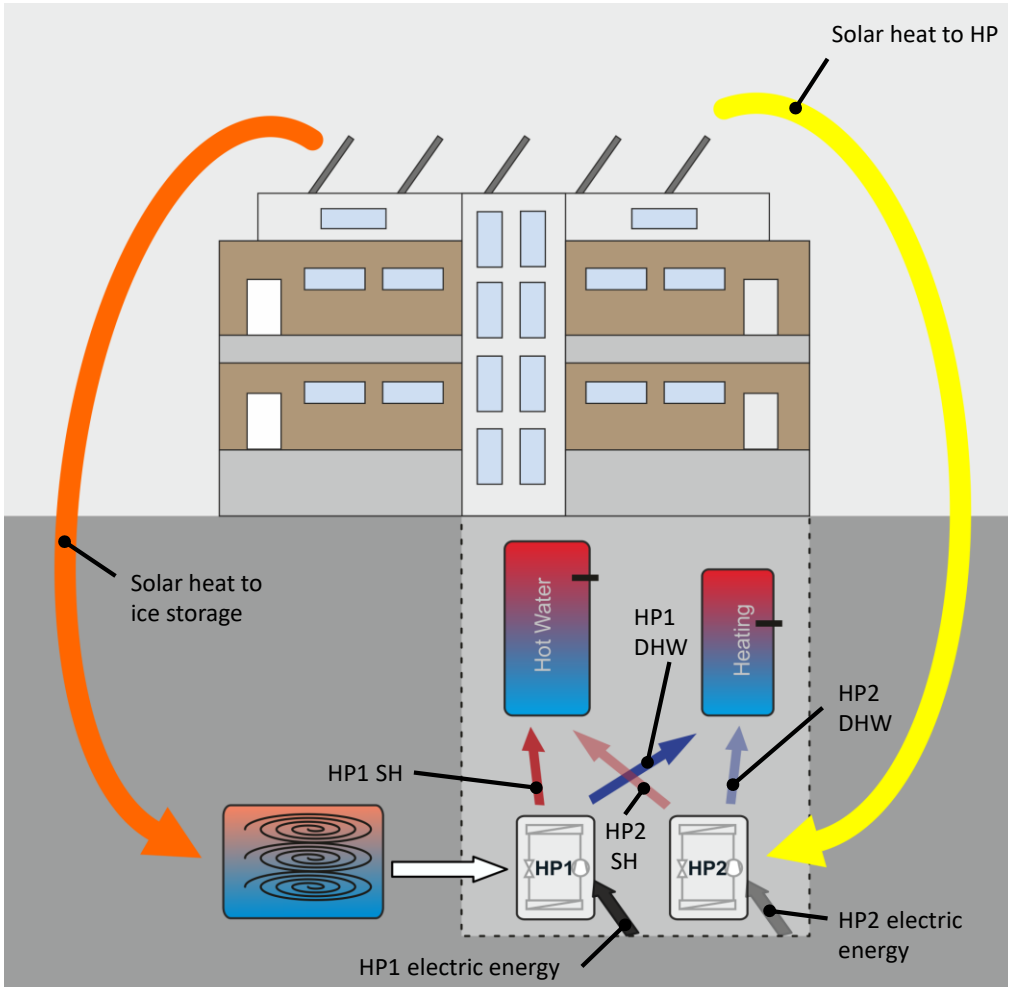

Figure 4-6: Considered energy flows in the system energy balance

The heat quantity of the solar collector was calculated with the measured mass flow and the measured temperature difference of the solar heat meter because of the problems described in chapter *4.1.2 The solar heat meter*. In addition, the electrical energy consumption of the heat pumps is also calculated (from the electric power) because of the in chapter *4.1.4 The electric meters* described reasons. The heat quantities supplied to the storages are known from the heat meters of the heat pumps. That means, that in case of problems with the measurement data transfer, the data from the heat meters for the heat quantities supplied to the storages is not lost, in contrast to the calculated heat quantity of the solar heat meter and the electric power consumption of the heat pumps. In Figure 4-7 only the data of the solar collector ("Solar heat to HP" and "Solar heat to ice storage") and the electric power consumption (“HP1 electric energy” and “HP2 electric energy”) is missing during the periods stated in chapter *4.1.1 Data losses*.

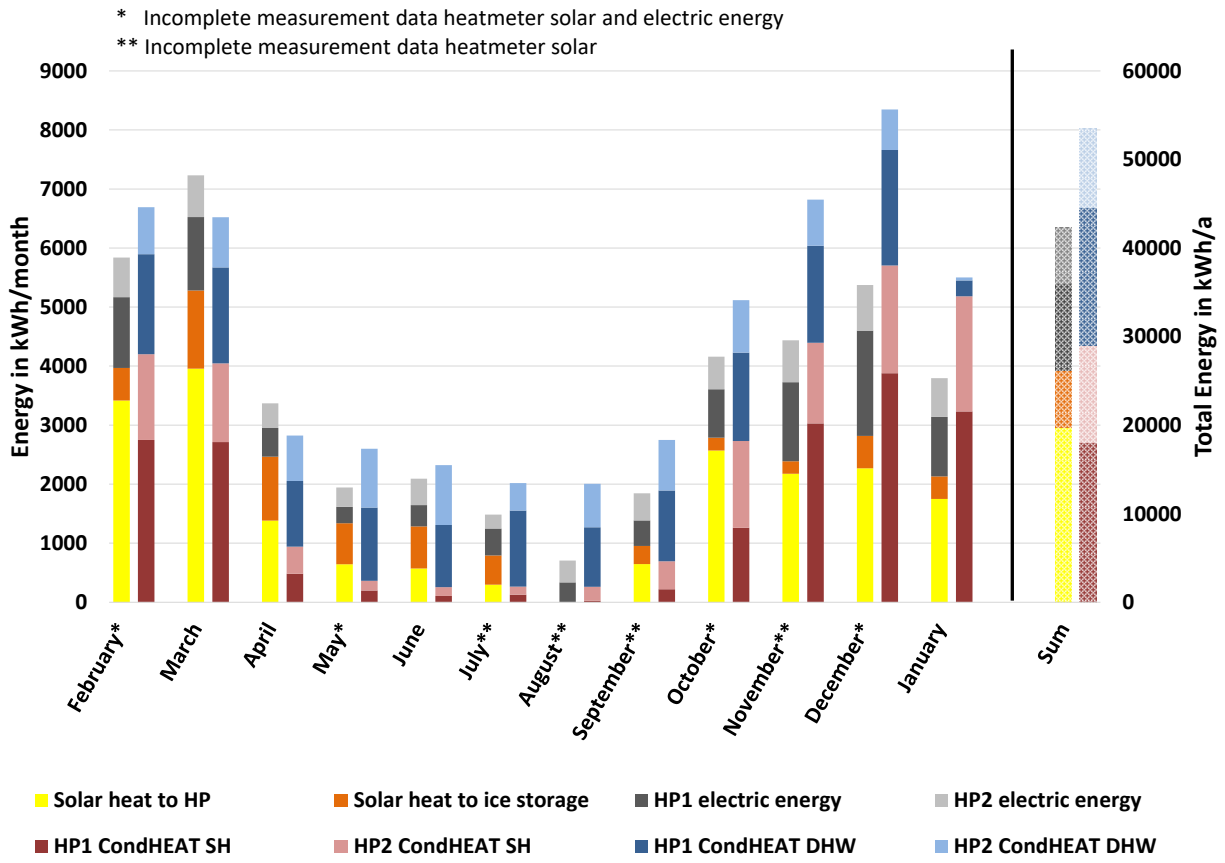

Figure 4-7: System energy balance 01.02.2016 – 31.01.2017

Looking at the measured values, it is noticeable that the major part of solar energy is fed directly to the heat pump during winter. This is the result of the current control, which always uses the solar collector as heat source for the heat pumps at a collector flow temperature above -4° C. The regeneration of the ice storage is further only allowed, if there is no heat requirement for the heat pumps. Since such a heat requirement occurs very often in winter, relatively little energy remains for the regeneration.

However, due to the division of the solar energy, it is not yet possible to evaluate whether there is too little energy left for the ice storage or not. Trough if one considers the fact that the ice storage was frozen quite fast in the winter and needed relatively long for melting again and that during this time the use of the electric heating elements was necessary, the assumption that it would be good to get more energy in the ice storage is acceptable. Ways to enable this are discussed in the doctoral thesis of Werner Lerch. (Lerch, 2017)

During the summer this is certainly no problem because there is more solar energy available and less energy needed. This shows a look at the right output bars in Figure 4-7 (less energy needed) as well as at the temperature of the ice storage, which in the summer reaches the maximum permissible temperature without problems (enough solar energy available to regenerate the ice storage immediately after using as source for the heat pumps). The right bars also show that the energy demand for the DHW heating is only slightly changing over the year. In the winter it is with 2500 kWh/month a bit higher than in the summer with about 2000 kWh/month.

The main difference between summer and winter is, of course, the SH requirement during the winter, which makes about 2/3 of the total heat requirement. Since even in the summer the SH storage was kept at a temperature level of 55-60 degrees, a small amount of heat for the SH storage was needed too in these months. During this time, of course, no heat for heating was taken out of the store, which means that the energy appearing in the energy balance corresponded to the losses to the environment. This is obviously a mistake of the controller, since this approach only resulted in unnecessary losses. Therefore, a change was requested in July 2016, so that this storage could be switched off during summer. As seen from the data from August, this change was only made for “heat pump 1”. As a result, the same heat quantity has still been used to keep the storage warm during summer, with the small difference that the energy has now been only generated by “heat pump 2”. Whether the control of the second heat pump was corrected properly in the meantime, can only be evaluated with the data of the next summer, since a heating requirement from September onwards is quite realistic.

Furthermore, it is noticeable that in January hardly any energy was provided by the heat pumps for the DHW storage. In this month, the capacity of the heat sources for the heat pump was not sufficient. For this reason, the built-in auxiliary heater was active in the DHW storage. Because of the reason that the energy produced by the auxiliary heater is not shown in Figure 4-7, the energy supply seems to be very low in January at first view. The SH storage was still heated with the heat pumps, but for some periods the auxiliary heater was activated too for this storage. In the other considered months, the storages were never heated electrically.

The difference in Figure 4-7 between the in- and output bar of the total energy per year is mainly because of not considering the gains or losses of the ice storages to the soil and because of the incomplete measurement data of the solar heat meter. For the monthly consideration, the fact that the ice storage is a long-time storage which stores energy across months, is a third reason of the deviation between the two bars. In January, for example, much more energy was extracted from the ice storage than supplied. In March, the opposite was the case while the ice storage was melted.

The annual energy supply to the SH storage, referred to the heated area of 957 m^2, gives a specific heat demand of 30.7 kWh/(m^2*a) for the year 2016 including the losses of the storage as well as of the pipes (no auxiliary heating for this storage 2016). According to the energy performance certificate, the heat demand without losses should be 9.44 kWh/(m^2*a). Even if one considers the losses of a few kilowatt hours, the actual SH demand of the building is much higher than that calculated for the energy performance certificate! This means that the entire heating system was designed under the assumption of lower demands than actually occur.

Referred to the gross area of 1477 m^2, the specific heat demand, including the losses (storage and pipes) is still at 19.9 kWh/(m_{gr}^2*a). Since these losses cannot be determined on the base of the measured data, a small advance is made on the data obtained from the simulation (Table 6-4), to classify the situation. For the case of the gross area, a specific heat demand without losses of 17.2 kWh/(m_{gr}^2*a) occur in the simulation model of the validated system. This specific heat demand is used in Table 4-1 to classify the house according to the energy performance certificate.

Since a standard climate is used for the classification in Table 4-1, no direct comparison is possible, but it can be said that the heat demand determined for the building in Weiz is relatively high for a passive house. This relatively high energy demand is a further reason why the capacity of the system is not sufficient during longer cold periods in the winter.

Table 4-1: Categories for the energy performance certificate (Greml, 2017)

specific heat demand at standard climate [kWh/(m_{gr}^2*a)]	Category	
≤ 10	A++	passive house
≤ 15	A+	lowest energy house
≤ 25	A	
≤ 50	B	low energy house
≤ 100	C	technical building regulation
≤ 150	D	old, not sanified building
≤ 200	E	
≤ 250	F	
≤ 300	G	

The energy demand for DHW heating in 2016 amount 27.4 kWh/(m^2*a) or 17.7 kWh/(m_{gr}^2*a), depending on whether the heated or the gross area is used as reference. Again, all losses of the distribution system are included, which can be considerable due to the circulation. Since the actual DHW demand is not measured, these losses cannot be quantified in detail.

In the energy performance certificate, much lower demands are expected as well. Without losses, there are only 12.78 kWh/(m^2*a) indicated.

4.3.2 Energy balance of the heat pumps

After looking at the whole system, Figure 4-9 shows the heat quantities in relation to the heat pumps. In this figure, the two heat pumps are considered together. The left bars show the energy which is delivered to the heat pumps. It is distinguished whether the solar collector or the ice storage was used as source. In addition, there is the electrical energy which was supplied to the compressors. The right bars show the energy output of the heat pumps. As in Figure 4-7, this is the amount of heat which is supplied to heat the DHW and the SH storage; however, in this figure, the distinction between the two heat pumps is dispensed with. For a better understanding, this energy flows are visualized in Figure 4-8. Since this energy flows are the same for both heat pumps, only one heat pump is shown exemplary in Figure 4-8.

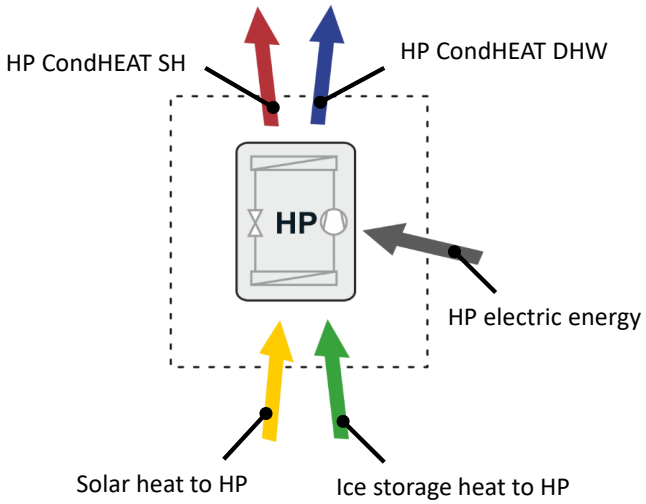

Figure 4-8: Considered energy flows in the energy balance of the heat pumps

The heat quantity of the ice storage as source cannot be measured directly because there is no heat meter installed at this location. Therefore, the detour via the source side of the heat pump had to be taken. With the sensor of the valve position of the heat source for the heat pumps, it is possible to distinguish whether the ice store or the solar collector function as primary source. With that, the amount of heat supplied to the evaporator can be calculated as the difference of the energy output at the heat sink side and the electrical energy. The error, which is caused by the failure to not take account of the losses in the heat pump, is negligibly small.

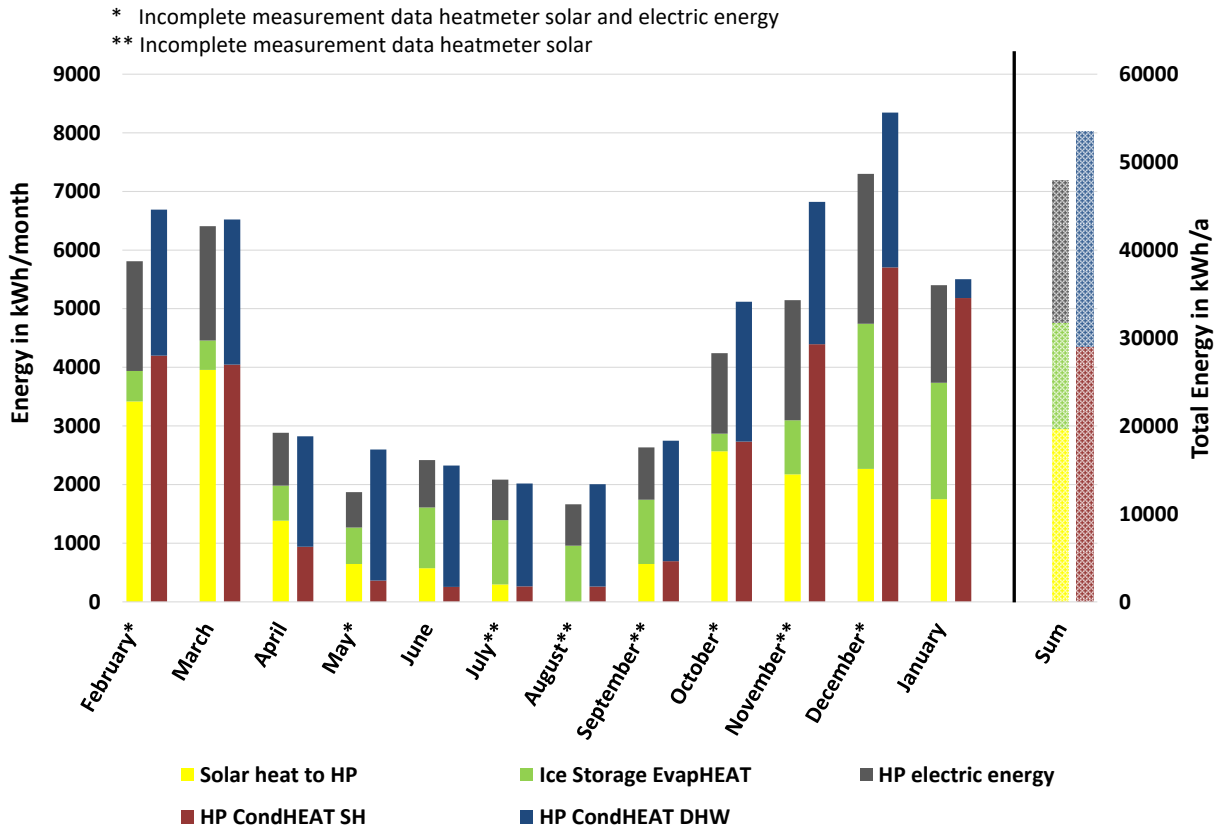

Figure 4-9: Energy balance of the heat pumps (01.02.2016 – 31.01.2017)

The other shown heat quantities are calculated the same as described in chapter *4.3.1 System energy balance*. The deviation between the input (left) and the output (right) bars in Figure 4-9 are mainly because of the incomplete measurement data of the solar heat meter ("Solar heat to HP) and the electric meters (HP electric energy).

If one looks at the heat quantity that is delivered to the heat pump, it is noticeable that only a small part of it is coming from the ice storage in February and March. This energy is less than 6 % of the whole delivered energy to the heat pumps, while the necessary electric energy is up to 20 %. The biggest part (~74 %) comes from the solar collector during this period. To determine the reason for this distribution, it is necessary to have a look at the ambient and the ice storage temperature too. These are shown in Figure 4-4. One can see that the ice storage temperature is around zero degree for the most time. In March, it even rises up to 5 °C. This means that the ice storage temperature is all the time in a temperature range that can be used for the heat pump. However, relatively high collector temperatures of up to 20 °C are also achieved. In addition, the collector temperature rarely drops below -4 °C and it recovers quickly during short running times of the ice storage as source for the heat pump, so that the system switches back to the collector mode soon. From the current point of view, there is nothing to say against the practice to use the collector as source for the heat pump as long as the necessary energy is available there. Nevertheless, other operation modes will be investigated for better results in the doctoral theses of Werner Lerch. (Lerch, 2017)

In the summer, the percentage of the ice storage as source rises rapidly. That is because the collector temperature is too high for the heat pump. The system works in the combined mode in which the ice storage is being regenerated and serves as a heat source at the same time (see chapter *3.2.5)*. A look at Figure 4-4 shows that this often happens in summer during the daytime. In October, it is again similar to the months of spring. The ice storage is hardly needed because the collector flow temperature is not too high, but there is still enough solar energy available to use it directly. In winter, the available solar energy decreases and the collector temperature drops more often below -4 °C. The ice storage contributes significantly to the energy supply during this phase so that the ice storage temperature drops down as well and it works as a latent storage soon. As far, this energy distribution has been quite in line with expectations. However, in the middle of December 2016, the already discussed fact occurred that the ice storages were completely frozen. As a result, in January the energy supply could no longer be covered by the heat pumps alone and the auxiliary heater had to be activated. The auxiliary heating was mainly activated in the DHW storage. Despite the fact that the auxiliary heater was not part of this energy balance, this can be seen from the heat quantity provided from the heat pumps for the DHW storage, which was quite low in January.

4.3.3 Energy balance of the ice storage

The energy balance of the ice storage shown in Figure 4-11 gives us further insights into the functioning of the system. The energy flow, which are considered in this energy balance, are visualized in Figure 4-10 as well. The data of the amount of heat flowing from the soil into the ice storage or from the storage to the soil were calculated by using the formula (4-1).

$$Q_{Soil} = \int_{0}^{8760} U_{Store} * A_{Store} * \left(T_{Soil,m} - T_{ice}\right) * dt \qquad (4\text{-}1)$$

A_{Store} is the area of the walls of the two stores, including the floor plate. The ceiling plate is neglected because there is no direct contact with the medium. T_{ice} is the temperature of the ice storage and $T_{Soil,m}$ is the mean soil temperature calculated from those four sensor values which measure the temperature at the storage surface. Moreover, dt is the time step and U_{Store} is the heat transmission coefficient. It has to be noted that the amount of heat from the soil is an approximate estimate and not an exact calculation.

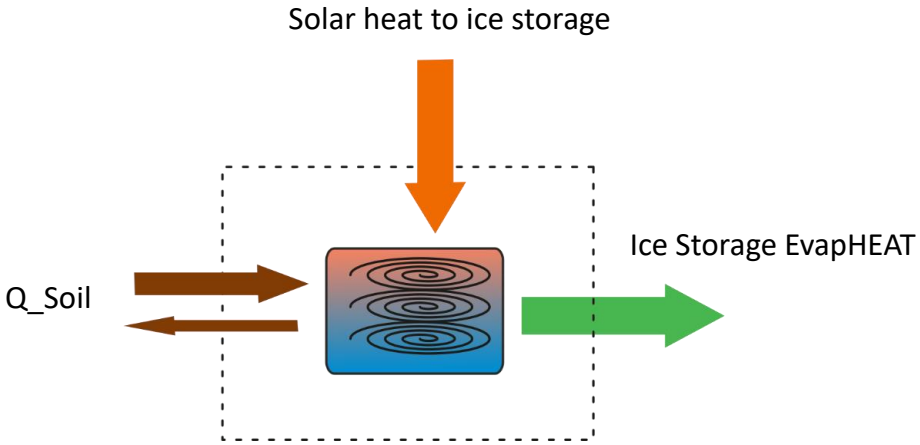

Figure 4-10: Considered energy flows in the energy balance of the ice storage

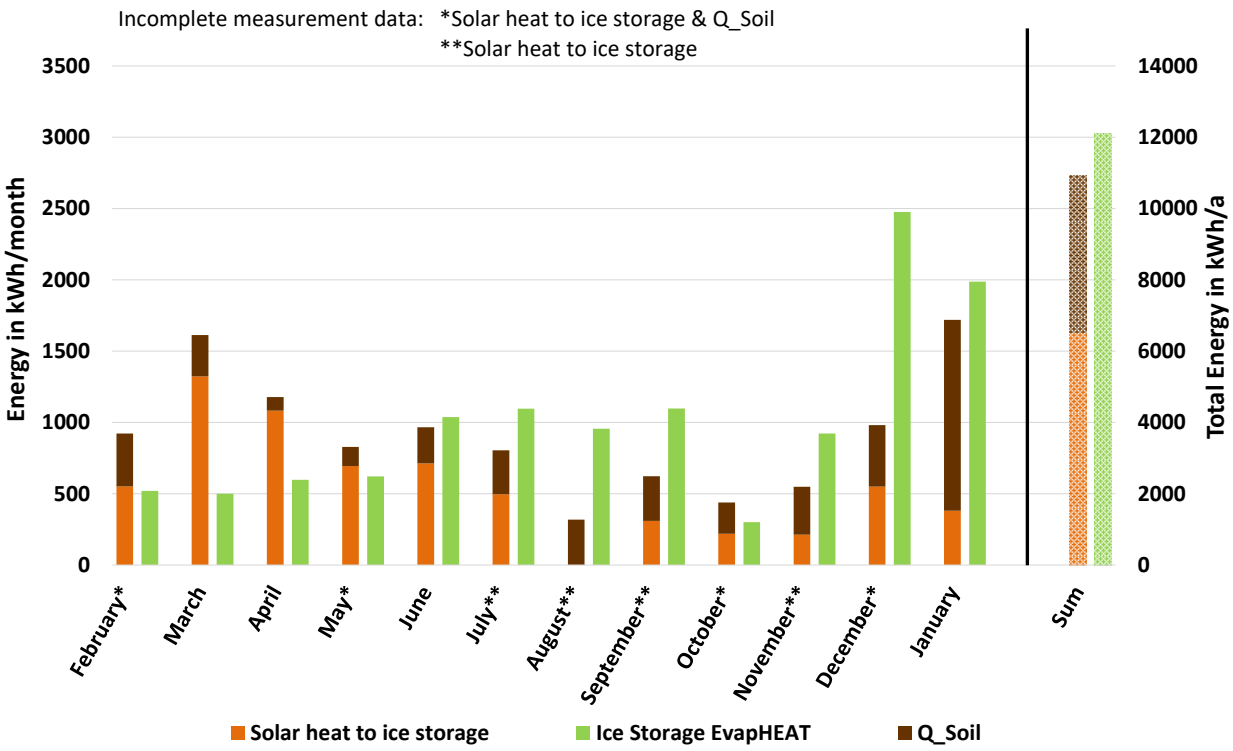

Figure 4-11: Energy balance of the ice storage

The data shows that for every month the amount of heat which flows from the soil into the ice storage is higher than the one which flows in the other direction. This is confirmed by Figure 4-4 which shows progression of the ice storage temperature in comparison with the soil temperatures. The soil temperature is only a short time in April lower than the storage temperature. This means that in the rest of the time energy is extracted from the soil. Moreover, it is shown that this heat amount is a considerable part, which confirms that the burying of the ice storage in the soil pays off.

Figure 4-11 also shows that the ice storage stores the energy over a longer period. At the end of winter or in the early spring, for example, much more energy is fed into the ice storage than it emits as source for the heat pumps. During this time, the ice melts with the now again available energy. During summer, the charge and discharge energies are approximately the same because enough energy is available at the collector to reheat the ice storage to the maximum permissible temperature in a short time again after using it as source. At the beginning of the heating season, more energy is extracted from the store. This imbalance is particularly evident in December and is the reason why the storage gets completely frozen. Due to the completely frozen storage, particularly high gains from the soil result in January, since temperature differences between ice storage and soil of up to 12 degrees occur in the meantime. However, the balance sheet should almost balance itself over the entire year. The reason why this is not the case, is mainly due to the data failures of the solar heat meter.

Whether a complete freezing of the ice storages is to be avoided or a certain share of auxiliary heating is even desirable, will be discussed in chapter 6.5.*Results for the design guideline*

4.4 Performance of the System

In order to assess the performance of a heat pump, two characteristic numbers are used. These are the coefficient of performance (COP) and the seasonal performance factor (SPF). Moreover, the share of auxiliary heating is interesting too to evaluate the heating system.

4.4.1 Coefficient of performance

The COP of electric heat pumps is the ratio of the useful heat output given at certain operating conditions in relation to the electrical power consumption. Therefore, the COP is measured at constant operating conditions in the laboratory and is indicated by the producer in the data sheet (Viessmann, 2015). In this case, it is 4.51 for the 6 kW and 4.72 for the 10 kW version, both for an operation point of B0W35. These values correspond to the current state of the art. However, since the system is not always operated in the standard state, the system cannot be adequately assessed alone on the base of the COP.

4.4.2 Seasonal performance factor

The SPF of the heat pumps (4-2) is the ratio of the annual heat produced (for SH and DHW) and the amount of the used electricity (excluding the circulation pumps). It considers all operation points and other influences of the heat pump in real operation. Therefore, it is the decisive value for assessing the actual efficiency. For the calculation, the measurement data of the year 2016 is

used. This results in a SPF of 3.32 for the 10 kW and 2.96 for the 6 kW heat pump. The efficiency of both heat pumps together results in a SPF_{HP_mean} of 3.19 (4-3).

$$SPF_{HP,i} = \frac{Q_{cond\_HP,i}}{W_{el\_HP,i}} \qquad i = 1,2 \tag{4-2}$$

$$SPF_{HP\_mean} = \frac{Q_{cond\_HP1} + Q_{cond\_HP2}}{W_{el\_HP1} + W_{el\_HP2}} \tag{4-3}$$

In addition, the values were also determined monthly. It is shown in Figure 4-12 that the monthly SPF is lower in summer than in winter. This can be explained by the fact that in summer the heat pump is only used for the DHW heating, which requires a higher temperature level than the SH. The SH is, therefore, more economical than the DHW. However, differences can also be seen in the heating season. It is shown that the SPF is highest at the beginning of the heating period and then decreases with the ambient air temperature. This is because during the winter months the heat source temperatures are lower on the average than at the beginning of the heating period and the heat pumps work more efficiently at a lower temperature difference.

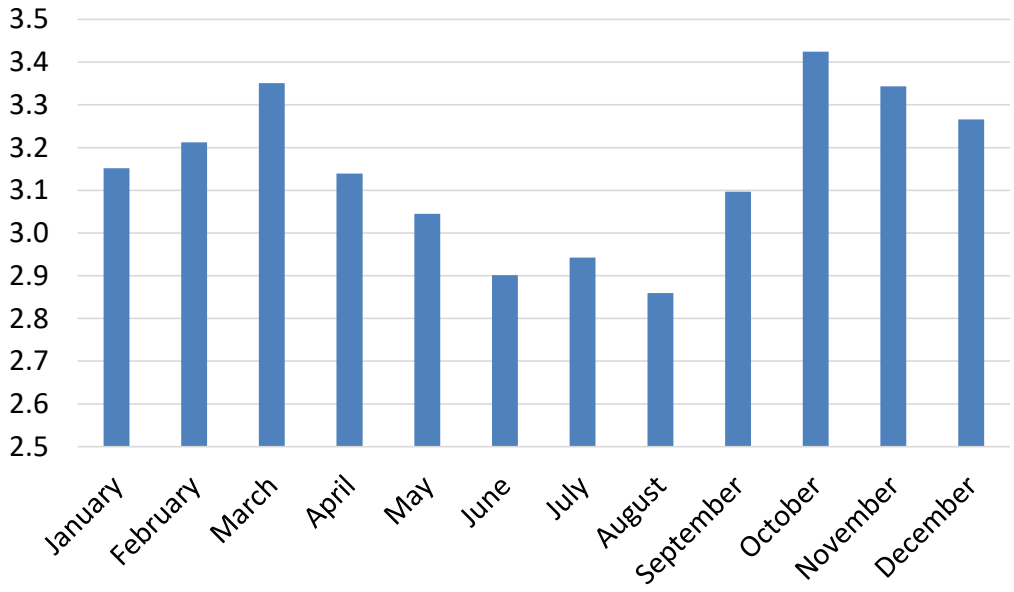

Figure 4-12: monthly distribution of the SPF_{HP_mean} (01.2016 - 12.2016)

Furthermore, it would be interesting to know the SPF of the overall system because it has an even greater significance than the consideration of the heat pumps alone. The SPF of the overall system would also be a good indicator for comparing this system to other heating systems as, for example ground-source heat pumps. Since, however, the necessary measured values are missing, this consideration must be dispensed with at this point. But in chapter *5.4.4 System Performance Factor*, it is calculated on the base of the simulation results for the validated system.

4.4.3 Share of the auxiliary heating

The share of the auxiliary heating is also an interesting value of a heating system. In the considered year 2016, the auxiliary heating was only active in January during the subcooling of the ice storage. Moreover, it was only activated in the DHW storage. With the equation (4-4), the share of the auxiliary heating results in 3.4 % what are 1982 kWh/a in total numbers.

$$EHeat = \frac{Q_{aux}}{Q_{cond\_HP1} + Q_{cond\_HP2} + Q_{aux}} \tag{4-4}$$

This share of 3.4 % is quite satisfying, if one considers the subcooling of the ice storage for a period of about two weeks. But an evaluation of the system on the basis of this share is difficult since the share of auxiliary heating can change considerably between years. Therefore, a consideration of a longer period (some years) would be necessary for a meaningful evaluation.

5 VALIDATION OF THE SIMULATION MODEL

This chapter deals with the validation of the, in large parts already existing, simulation model (Lerch, 2017) as well as with its fine-tuning. First, the solar collector, the ice storage and the ground model were validated with the measured data in order to compare the simulation model with the real system. Second these components were integrated in the overall heating system model to validate this as well. On the one hand, the validated model will be used to elaborate a design guideline for such systems, and on the other hand, it also serves as a basis for further improvements.

All simulations were carried out with the program TRNSYS (TRNSYS_17, 2011), which is briefly explained first.

5.1 The simulation program – TRNSYS 17

The simulation program TRNSYS (Transient System Simulation) was originally developed at the Solar Energy Laboratory (SEL) of the University of Wisconsin (USA). The simulation environment provides the possibility to perform transient calculations of various forms of energy systems (e.g. solar energy systems, conventional heating systems, wind energy conversion, etc.), their components (e.g., TESS (TESS, 2012), heat exchangers, solar collectors, etc.) as well as building structures in dependence of their environment (climate data). (SEL, 2012) In the following, the basic operating mode of TRNSYS is explained. (Moisi, 2014)

5.1.1 Simulation Studio and TRNSYS-types

The graphical user interface (GUI) of TRNSYS is called "Simulation Studio". It can be understood as a sort of canvas where the different mathematical models, called "types", are placed via "drag and drop". Figure 5-1 shows a screenshot of the simulation studio with an example program for TRNSYS beginners. On the right side, the variety of type libraries is shown. Connected types of a system simulation can be seen in the centre. The standard types come along with the TRNSYS program. Non-standard types for special applications or a different level of detail can either be provided by institutions or developed individually. Examples of this are the solar collector, the ice storage and the ground type. In the TRNSYS 17 version, the types are implemented in FORTRAN90, older versions work with FORTRAN77. (Moisi, 2014)

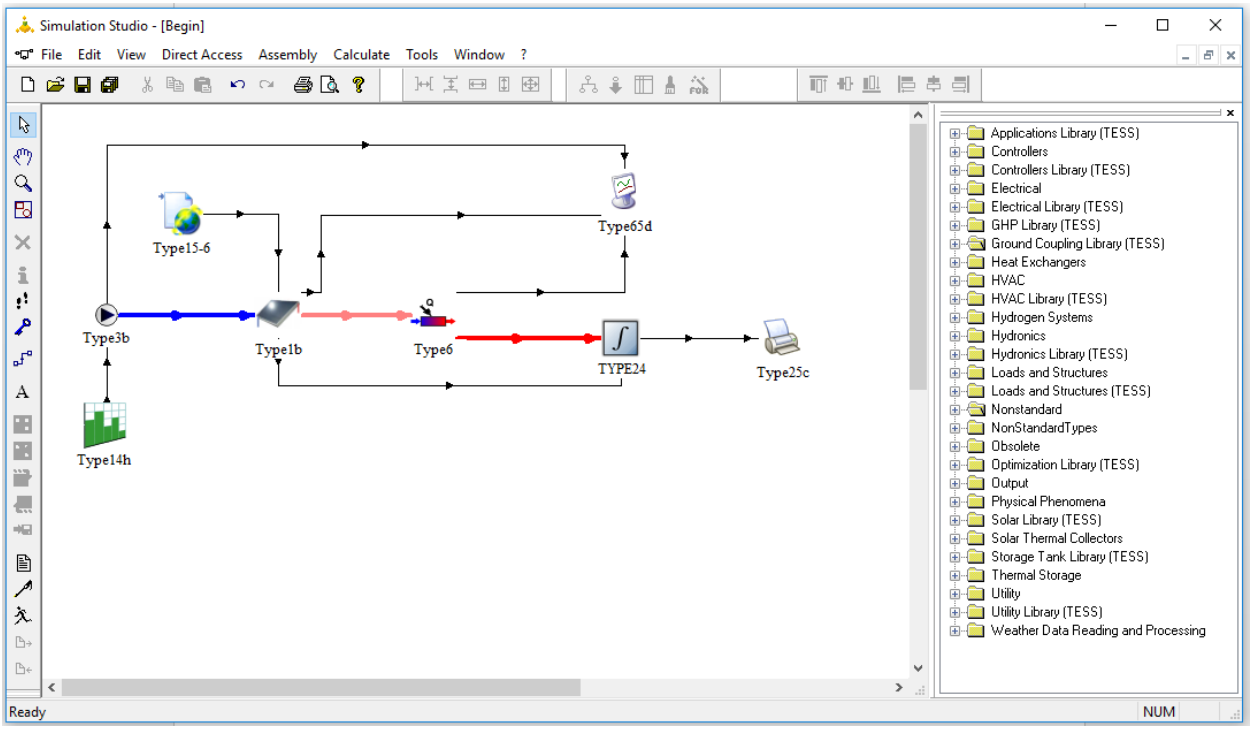

Figure 5-1: TRNSYS Simulation Studio user interface

TRNSYS uses a modular approach. These modules are called "types" and represent the physical models of the different system components. These types are interlinked with each other in order to assemble the desired system. The output of one type provides the input for another. For example, in Figure 5-1, the outlet temperature of the solar collector (type 1b) becomes the inlet temperature for the auxiliary heater (type 6). The user must ensure that the hydraulic circuit between the connected types is closed to avoid a violation of mass conservation. In general, TRNSYS does not check mass or energy balances, therefore, it has to be performed by the user. Every type has a so called "Proforma" Figure 5-2 which serves as some kind of form where necessary parameters can be entered and/or changed. The Proforma gives an insight into the required inputs and accessible outputs as well as special applications of the considered type. (Moisi, 2014)

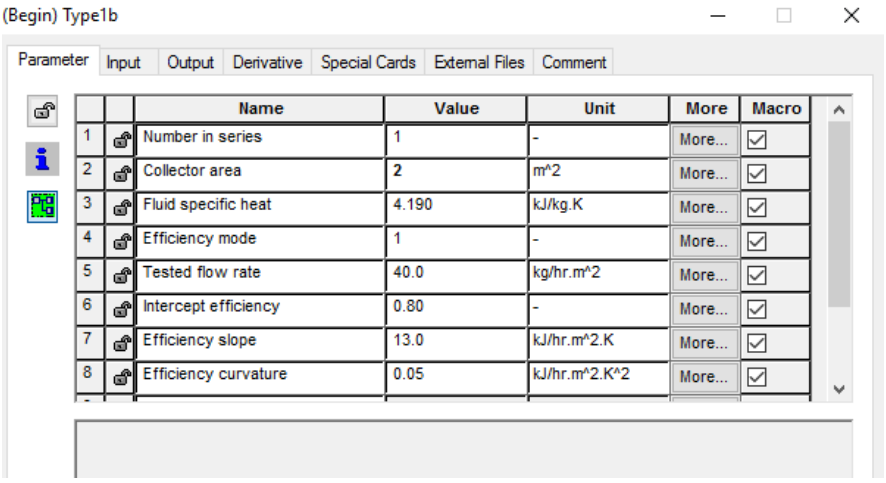

		Name	Value	Unit	More	Macro
1		Number in series	1	-	More...	☑
2		Collector area	2	m^2	More...	☑
3		Fluid specific heat	4.190	kJ/kg.K	More...	☑
4		Efficiency mode	1	-	More...	☑
5		Tested flow rate	40.0	kg/hr.m^2	More...	☑
6		Intercept efficiency	0.80	-	More...	☑
7		Efficiency slope	13.0	kJ/hr.m^2.K	More...	☑
8		Efficiency curvature	0.05	kJ/hr.m^2.K^2	More...	☑

Figure 5-2: Proforma of TRNSYS type 1b

The information of the utilized types, their connections and the simulation parameters are stored in the so called "DECK" file. This file collects all the required information which is used in the simulation and is sent to the program kernel, where the calculations are performed (Heimrath, 2004). The calculation is performed in a specific order which can be changed by the user if desired. During one time step iterations are performed until a convergence criterion is met. If this is not the case, the next iteration begins but only types which had not converged in the previous iteration are recalculated (Moser, 2012).

5.1.2 The EQUATION statement

The EQUATION statement as mentioned in the sections above were utilized to perform the exergetic and energetic evaluation of the systems and their components. Within the EQUATION statement it is possible to include user defined arithmetic equations and let them interact with TRNSYS types. These interactions can be, for example, special control strategies, elementary Boolean operations (as "greater than") statements, unit conversions or other simple calculations. The equation statement is used like a type. It can be placed in the Simulation Studio via drag and drop and linked to the considered TRNSYS types. (Moisi, 2014)

5.1.3 Loads and structures with TRNBUILD

Behind every heating system is a structure serving as boundary and dimensioning condition. The user interface TRNBUILD provides a very useful tool to define the desired building. TRNBUILD gives the possibility to define "Multizone Buildings" considering internal and electrical gains. Multizone buildings can be described as structure with several so called "Airnodes" at which the entire thermal capacity is lumped. These Airnodes can represent, for example, one single storey or several nodes can be defined within a room. (Moisi, 2014) Since the generation of the building type was not part of this work, TRNBUILD is not described in detail. Further information can found in the refereed literature.

5.1.4 Implementation of GenOPT with TRNOPT

GenOpt is an optimization program for the minimization of a cost function that is evaluated by an external simulation program. It can be used with any simulation program which reads inputs and writes outputs to text files. (Kummert, 2007)

TRNOPT is a dedicated TRNSYS interface for GenOpt. It was created by TESS (TESS, 2012) to streamline the optimisation process and it is distributed as part of the TESS libraries Version 2. With TRNOPT, the entire process of optimizing the results from a TRNSYS simulation reduces to choosing the TRNSYS input file, choosing the variables which will be varied to optimize the results, and choosing the simulation result to be optimized. In this respect TRNOPT is highly recommended to any TRNSYS user wishing to experiment with GenOpt. (Kummert, 2007)

5.2 Validation of the single components

Before it was possible to create the design guideline with the simulation model of the overall system, the single components had to be validated. This was necessary because some important parameters, such as the characteristic curve of the solar collector, have not been disclosed. In addition, the ice storage (type 843) is a rectangular storage with only one heat exchanger, while the real ice storage is cylindrical with a separate regeneration and extraction heat exchanger. To parametrize the ice storage model in such a way that it corresponds well to the real one anyway, was one of the biggest challenges in validation.

5.2.1 Procedural method

For the validation, meaningful data ranges of the different operating modes were selected from the available measured data. This data was selected as input for the respective model to be validated. As far as possible, the one minute values were taken, as a larger number of measured data has a positive effect on the validation result. The known parameters were set as constants in the respective type, while the others were varied between defined limits. These should be selected in such a way that a minimum is obtained between the simulated and the measured output data. By comparing several operating modes and data areas, it was tried to find the best configuration of the simulation model so that the behaviour was as realistic as possible.

5.2.2 The solar collector

The used collector type is an unglazed photovoltaic-thermal (PVT) collector model from “Jansen Energieplanung” called Type 203. In the PVT collector model, the incident solar radiation is partly converted into electrical energy in the PV module. This share is no longer available for thermal use. Therefore, the usable radiation for the thermal part of the PVT collector is lower by the amount of energy, which is dissipated in form of electrical energy. This energy is still reduced by the infrared balance and then absorbed by the absorber. If the surface temperature of the collector drops below the dew point temperature of the ambient air, there is an additional gain of heat from the condensation. Considering the losses, the useful energy can be determined out of this. Figure 5-3 shows this energy flows of the collector type. (ISFH, 2011)

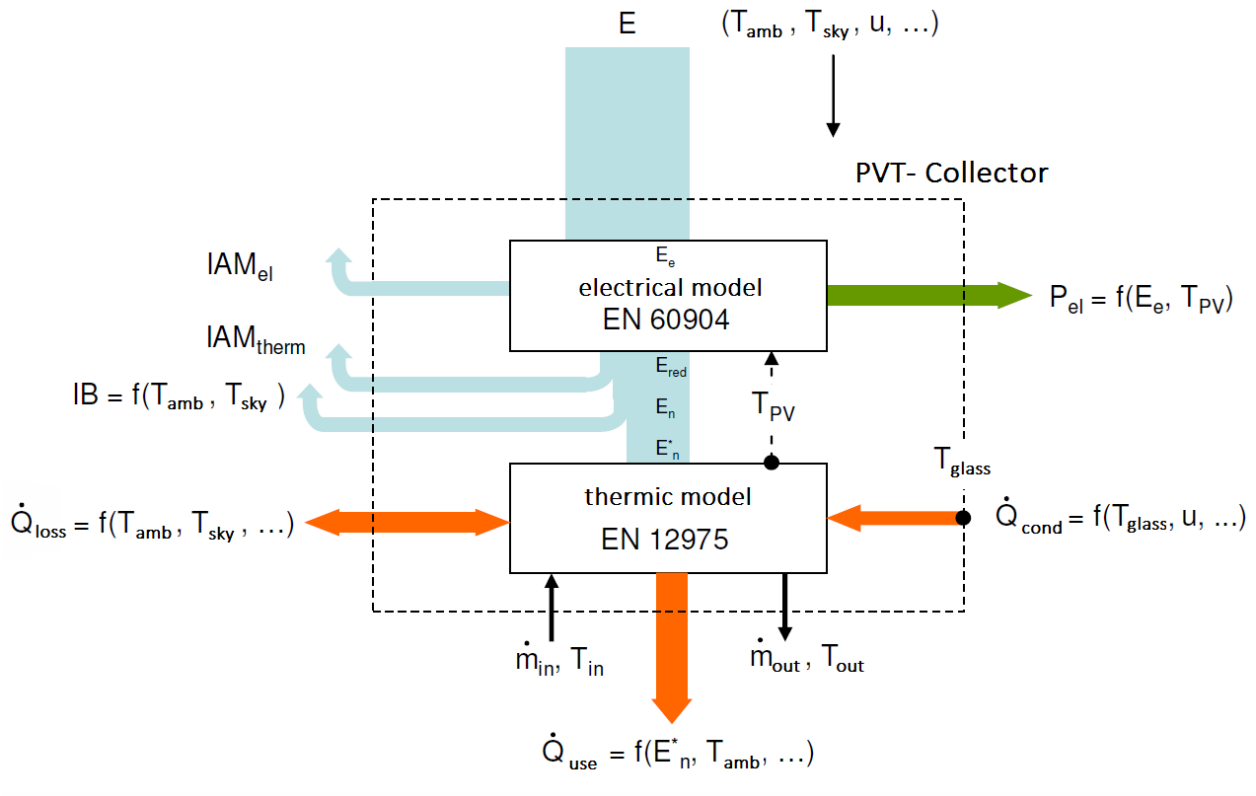

Figure 5-3: Energy flows of the collector type 203 (ISFH, 2011)

In type 203, the thermal characteristic of the PVT collector is based on the non-steady collector model described in EN 12975-2 for testing the performance of unglazed collectors. For the photovoltaic characteristic, there are two different models available: the “efficiency model” and the “effective solar cell characteristics model”. (ISFH, 2011)

Since the installed collector is a purely thermal one, the simulation type operates in an according operation mode. Concretely, this is mode 2 for the operation as a thermal collector with consideration of condensation. In Figure 5-3, only the orange part is activated. In this case, the solar radiation is, of course, not reduced by the PV module, so that the whole radiation is available for the thermal collector.

Parameter setting

As far as possible, the parameters were taken from the data sheets or from other documentations (e.g., collector angles, specific heat capacity of the fluid, etc.). However, the problem was that relatively little information was available. For this reason, some parameters were preliminary based on empirical values or assumptions.

The factors of the characteristic curve, the collector area and the heat capacity of the collectors were identified as the most important unknown parameters. For the characteristic curve, only the first two parameter, the conversion factor (a0) and the heat loss coefficient (a1), were used in the simulation model. The area of the collector was unknown because the installed collector was a two-layered one. This means that depending on the position of the sun, different levels of occlusion of the lower layer occurred. As the simulation type had only one layer, an equivalent

area had to be found. Therefore, this 4 parameters were varied in TRNOPT. A list of all parameters and their selected values can be found in the appendix (Table A- 1 - Table A- 3).

Input data

The input data is the measurement data of the selected ranges, or therefrom, calculated values. The following input data was required for the collector validation:

Table 5-1: Input data of the solar collector

	Name	Unit
1	global irradiance on collector surface	kJ/(h*m^2)
2	direct irradiance on collector surface	kJ/(h*m^2)
3	incidence angle	degrees
4	zenith angle	degrees
5	azimuth angle	degrees
6	ambient temperature	°C
7	ambient air pressure	mbar
8	ambient humidity	%
9	sky temperature	°C
10	wind velocity	m/s
11	convective heat loss coefficient	W/(m^2*K)
12	internal thermal conductance	W/(m^2*K)
13	inlet temperature	°C
14	mass flow	kg/h

The global and the direct irradiance on the collector surface as well as the three angels were calculated with the Excel tool “Solar Value Calculator” (Moser, 2017). Therefore, the global irradiance on the horizontal, the ambient temperature and the relative humidity as well as the date and the angels of the solar collector were necessary. Except of the relative humidity, all of these values were known. In order to be able to carry out the calculations yet, they were taken as 10 minutes values from the climatic data set of Graz (ZAMG, 2017). The resulting inaccuracies must be accepted since no values were available for the location in Weiz.

The air pressure was assumed to be constant at 1013 mbar because it was not measured and minor fluctuations have no big influence on the simulation behaviour of the solar collector. The convective heat loss coefficient, the thermal conductance and the necessary input file for the incidence correction factor were based on the known data for a similar collector model.

The input files are designed in such a way that a pre-simulation with constant values takes place in the first 30 minutes to allow the system to swing into.

Implementation of the validation model in TRNSYS

To validate the solar collector, the collector model is considered isolated from the other components. Nevertheless, some more types are necessary in addition to the solar collector type 203. This is shown in Figure 5-4:

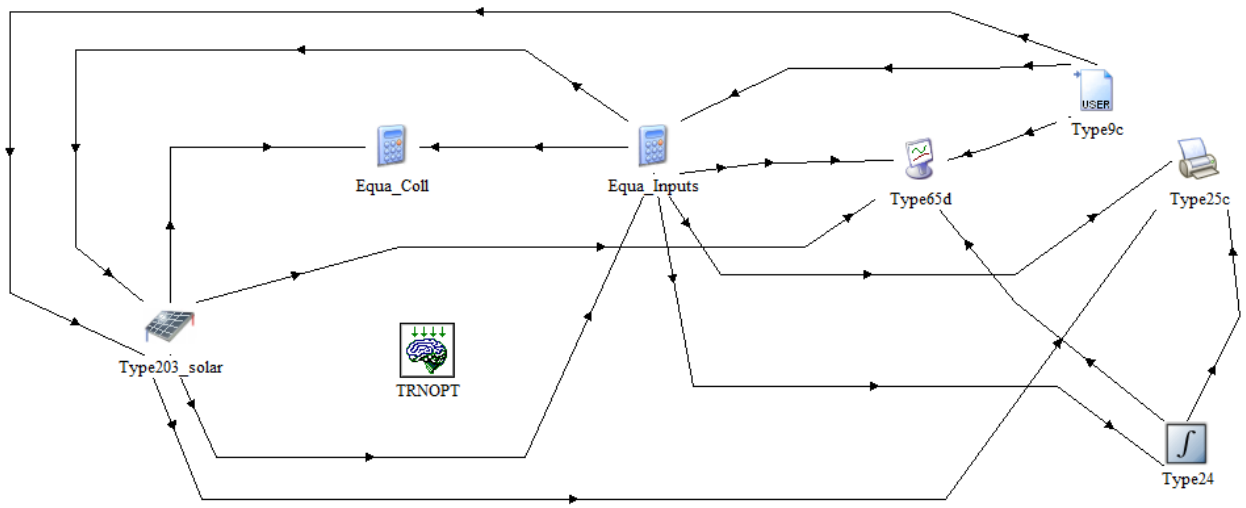

Figure 5-4: Validation model of the solar collector

To get the input data of the collector, the Type9c is needed. This is a data reader which reads, in predefined time intervals the measured data from a text file. As already mentioned, not all of the required data is directly available as measured values. Therefore, some have to be calculated in the Equation Statement first. For the sake of clarity, the calculations are divided into two Equations Statements. In addition to the inputs required, the relevant outputs are also calculated here. These are, for example, the energies from the simulation and from the measurement (could also be passed as input) as well as the equation for the minimization in TRNOPT (5-1).

$$\Delta E^2_{SimMeas} = \sum abs(E^2_{Sim} - E^2_{Meas}) \qquad (5\text{-}1)$$

Therefore, the sum of the difference between measured and simulated energy is minimized in TRNOPT, by varying the already mentioned variables. To create the sum, type 24 is required, whose output is passed to TRNOPT.

For the analysis of the results, the types 25c and 65d are used. Type 25c is called printer and produces an output file similar to the one for the input data. Type 65d is an online plotter and creates a chart with the selected data for a quick overview of the results.

In this case, the simulation runs in two stages. First, TRNOPT is started via the TRNOPT symbol to find the optimal values of the parameters. This parameter must be set in the Equation Statement. Then the actual simulation is started in TRNSYS and the result is stored in the output file as well as displayed in the online plotter.

Chosen data range and the resulting findings

As input data, characteristic ranges of the individual operating modes (*3.2.1 Heat pump with solar collector mode, 3.2.2 Heat pump with air absorber mode, 3.2.4 Ice Storage Regeneration)* were used. Since a larger number of data was advantageous, the data from the one minute measurement intervals was selected because there were much more data available for the same period. In total, five cases were examined: two cases with the solar and two with the air absorber

mode as well as one with the regeneration mode. For the *Heat pump with air absorber mode* the collector temperature is of course the lowest (once all the time below 0 °C and once under 3 °C). For the solar collector mode, it is higher up to 10 °C and for the regeneration mode, it is the highest.

In the first run the individual optimum values were searched for all cases. It turned out that it was no problem to find these values. The deviation between the simulated and the measured data was, after the settling time, in the per mill range. Figure 5-5 shows an example of the trend of the simulated and measured outlet temperature which are nearly the same.

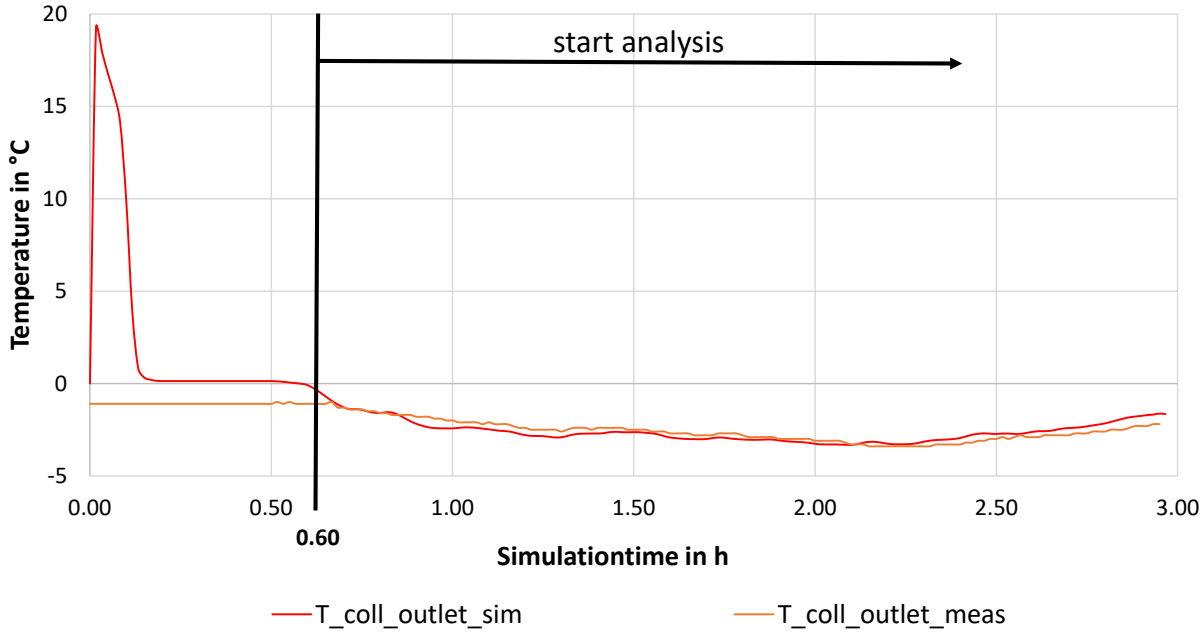

Figure 5-5: Simulation of one case with optimum values

Since the searched values are parameters and not inputs, a configuration should be found that satisfies all cases sufficiently. If this is not feasible as little as possible configurations should be made since they must be integrated via an additional collector model and a control which switches between them. The necessity of several collector models was considered because the simulation model is not a two-layered system, as it is the case with the actually installed collector. With this, the reduction of the area by the overlapping in the case of solar radiation could be considered, if necessary. Therefore, all cases were simulated again with the same configuration. It was found that the configuration of the regeneration sample fulfils the other cases well, so that no additional collector model had to be installed. Table 5-2 shows the mean temperature difference between the simulated and the measured outlet temperature in the optimum case according to TRNOPT and with the values optimal for the regeneration example. For this purpose, the absolute values of the temperature difference were considered after a settling time of 40 min. The temperature difference between the measured and the simulated temperature in case of the optimal values was, of course, lower, but it is seen that the selected values did not cause much higher differences.

In addition to the temperatures, the heat quantity of the collector is important too. Therefore, in Table 5-2, the differences of the heat quantities between simulation and measurement are shown for both cases (optimum and regeneration). The heat quantities are again considered after 40 min of settling time. The magnitude of the deviation itself depends strongly on the duration of the considered case, which means that primarily the difference between the two cases is interesting. It is seen that the highest deviation occurs at case 4. Since with case 3, which has similar boundary conditions, a much better result was obtained, this deviation was not seen as a sufficient reason for a second collector model.

Table 5-2: Temperature und heat quantity differences between simulation and measurement for different cases and different parametrisation

	Case	ΔT_{Opt} [K]	ΔT_{Reg} [K]	ΔQ_{Opt} [kWh]	ΔQ_{Reg} [kWh]
1	Solar collector mode (04.02.2016 09:57 – 12:49)	0.60	0.68	3.12	3.51
2	Solar collector mode (05.02.2016 11:56 – 12:26)	0.38	0.60	0.28	0.53
3	Air absorber mode (29.01.2016 09:02 – 10:54)	0.62	0.77	1.53	1.99
4	Air absorber mode (01.02.2016 06:10 – 08:40)	0.29	0.36	0.14	1.47
5	Regeneration mode (01.02.2016 13:20 – 15:20)	0.29	0.29	0.22	0.22

Table 5-3 shows the chosen values of the determined parameters as used in the simulation of the overall system.

Table 5-3: Determined parameters of the solar collector

Parameter	Value	Unit
Conversion factor a_0	0.75	-
Heat loss coefficient a_1	42.5	W/(m²*K)
Collector area A_{coll}	29	m²
Heat capacity collector c_{coll}	40	kJ/(m²*K)

5.2.3 The ice storage

For the simulation of the ice storage, type 843, developed at the Institute of Thermal Engineering (Institute of Thermal Engineering, 2017), was used. This model allows the simulation of a cuboid-shaped ice storage with an integrated pipe heat exchanger. It is very important to consider that during discharging an ice layer form on the outside surface of the heat exchanger pipes, when the temperature drops below the freezing point. This layer of ice acts like an insulation layer and reduces the heat transfer between the liquid water in the tank and the heat transfer fluid in the heat exchanger pipes depending on the ice layer thickness. Ice formation and growth on the tubes and the increasing thermal resistance of the ice is considered by means of a finite difference formulation of the transient Fourier equation in cylindrical coordinates. For the

modelling of the phase change from solid to liquid, the enthalpy method is used (Claußen, 1993) (Visser, 1986). As a simplification, the temperature of the liquid water in the storage is assumed to be the same in the whole tank. (Lerch et al., 2016)

As shown in Figure 5-6, the heat exchanger is assumed as a pipe, which is laid in loops inside the storage. The pipe material, the diameter, the wall thickness, the pipe spacing distance and the number of the parallel cycles can be chosen as parameters. The heat exchange between the heat carrier fluid and the inner wall of the heat exchanger pipes is calculated using an empirical model for the flow in cylindrical pipes (VDI Wärmeatlas, 1997). The heat losses/gains of the storage to/from the ambient (soil in our consideration) are calculated through a heat loss coefficient UA_{Loss} [W/K] which is provided as an input. (Lerch et al., 2016)

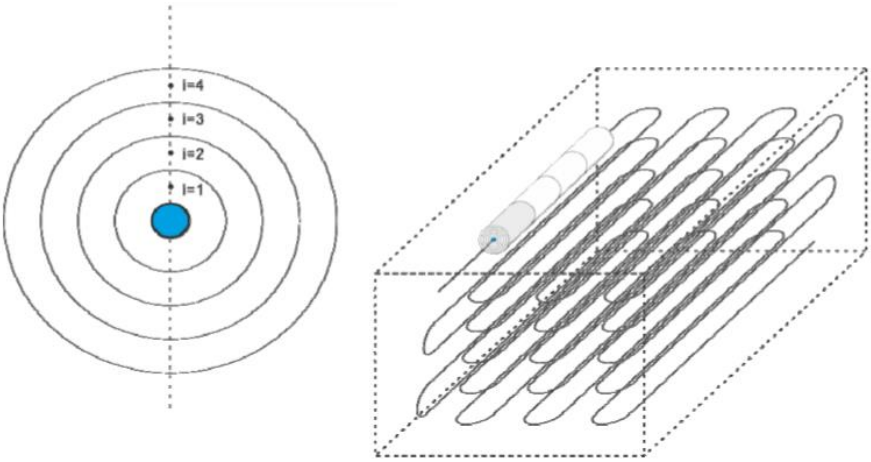

Figure 5-6: Brief schematic of ice storage model for TRNSYS Type 843 (Cao et al., 2013)

Parameter setting

As for the parameterization of the solar collector, all known parameters were taken from the data sheets. The difficulty was that the simulation model was rectangular with only one heat exchanger, while the real ice storage was a cylinder with two heat exchangers. The volume and the height of the storage model were selected the same as the real storage. The same applied to most parameters of the heat exchanger as well as to the entire substance property data. The only parameter to optimize was the maximum distance between two heat exchanger pipes, which also defines the maximum diameter of the ice cylinder.

Input data

The mass flow and the temperature of the fluid coming from the solar collector during the regeneration phase as well as the return temperature and mass flow on the side of the heat pump are required as inputs. These are the values measured by the heat quantity meter, respectively, in case of the temperature from the collector, it is the collector outlet temperature itself because the solar heat quantity meter measures the temperatures only in integers, which is not accurate enough. In addition, the ambient temperature around the ice storage (soil temperature) is required as a further input. This temperature is given by the ground sensor 1/2, which is placed on the outer storage wall (Figure 3-6).

Since the simulation model has only one heat exchanger, a solution had to be found, so that the simulation model correlated with the real storage as good as possible. The method to flow through the heat exchanger alternately turned out not to be very realistic because the ice formed was immediately defrosted at the next regeneration cycle, which is not the case in reality. Therefore, it was decided to operate only the extraction of the ice storage (heat pump source side) with the heat exchanger of the simulation model. The regeneration, instead, was operated with the double port which was also available in the simulation model. This means that the fluid flowed without a heat exchanger directly into the ice storage. Since the fluid in the solar collector was brine and the ice storage was filled with water, an external heat exchanger in front of the ice storage was required in the overall system model. (For the real system, such a solution would of course not be possible because it would no longer work when the phase transition starts. However, in the simulation model this solution achieved the best results.) For the validation, this means that the maximum distance between two heat exchanger pipes must be determined with the heat pump data. The external heat exchanger for regeneration was later validated together with the overall system.

Implementation of the validation model in TRNSYS

The model for ice storage validation, shown in Figure 5-7, is similar to that of the solar collector. The ice storage is also separated from the other components. The idea of a common validation with the soil coupling (Type 708) was discarded because this did not work with TRNOPT.

Since both ice storages are identical and are operated the same, the validation must be carried out only once.

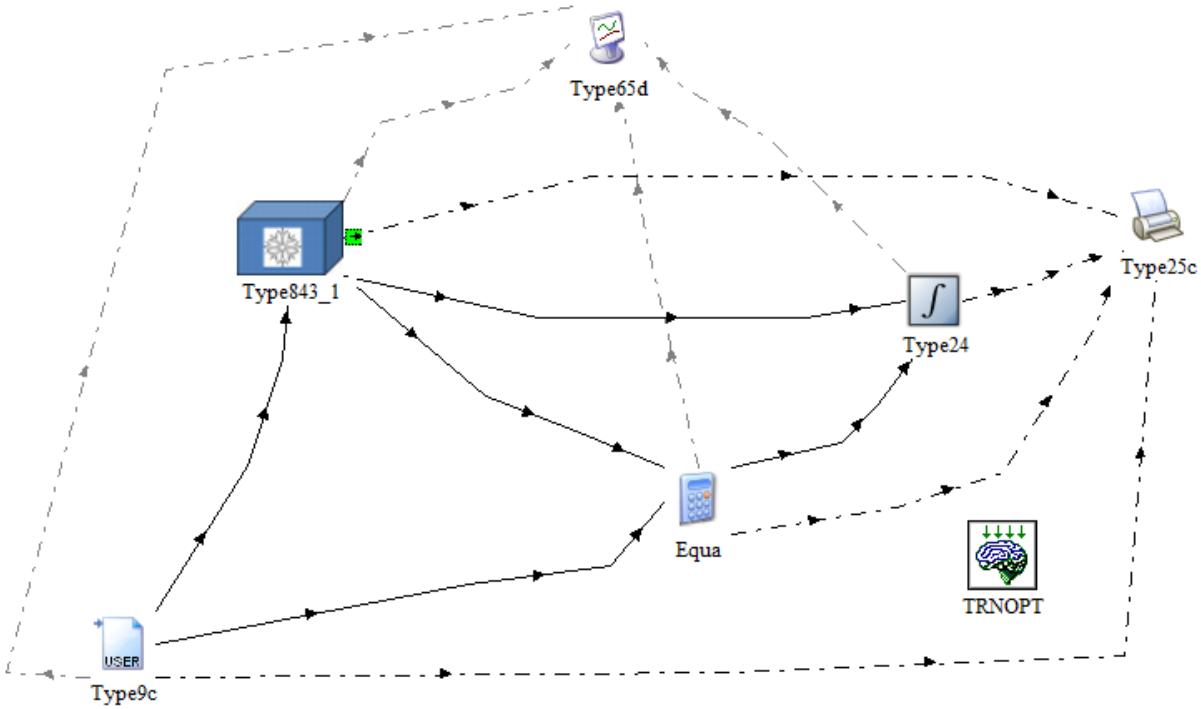

Figure 5-7: Validation model of the ice storage

Type9c provides again the required inputs. The absolute difference of the flow temperature of the ice storage unit between simulation and measurement was selected as the quantity to be minimized (5-2). This is calculated in the equation type, summed with the integrator, and then passed to TRNOPT for the optimization.

$$\Delta T_{SimMeas} = \sum abs(T_{Sim} - T_{Meas}) \tag{5-2}$$

Chosen data range and the resulting findings

Since during the monitoring of the one minute interval the ice storage was never operated as source for the heat pump for more than a few minutes, the 15 minutes data had to be used in this case. A period with a duration of approximately 16 hours could be found, so that a meaningful validation was possible. The selected case is shown in Figure 5-8. Since the ice storage was in the phase transition, the simulation model had to be brought in this condition through a presimulation.

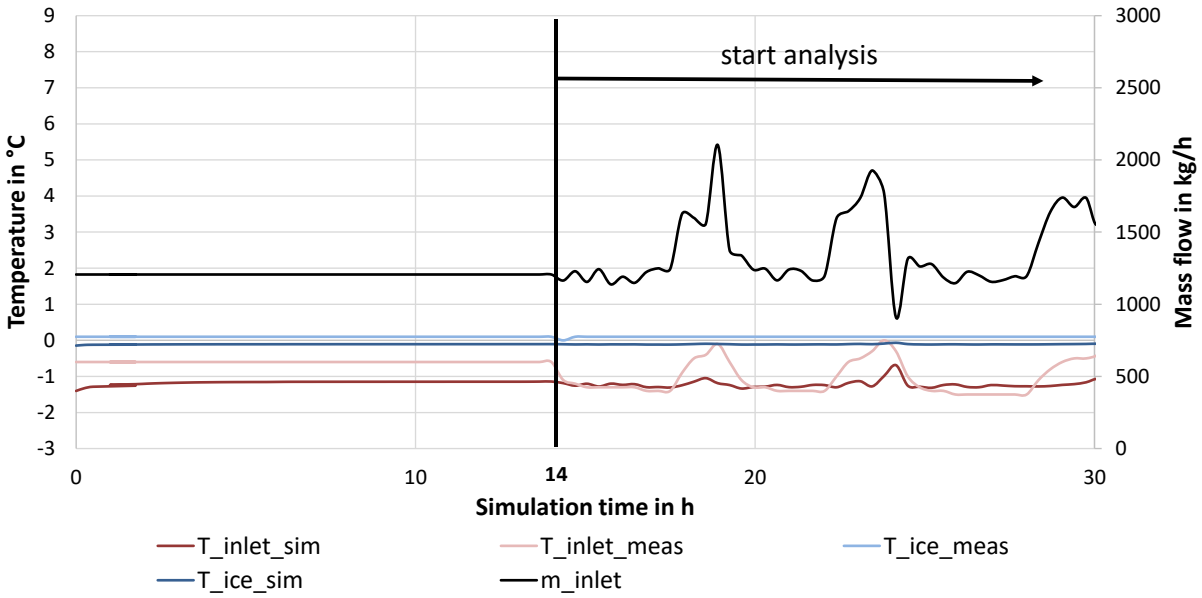

Figure 5-8: Validation model of the ice storage

In Figure 5-8, the optimum value of 14.7 cm for the distance between the heat exchanger pipes, determined by TRNOPT, has already been used. This is only valid for the extraction heat exchanger of the ice storage. The external heat exchanger for the regeneration is validated together with the soil coupling.

The peaks of the measured data are smaller in the simulation. However, the deviation in this range is only about 1 K For the heat quantities, this results in a difference of 2.8 kWh (Q_{sim} = 33.4 kWh, Q_{meas} = 36.2 kWh). Since the validation of the ground type together with the ice storage type confirms the permissibility of this configuration too, the distance of 14.7 cm is also used for the simulation of the overall system.

5.2.4 Soil coupling

The used ground model (Type 708) maps the unsteady temperature field within a ground segment with an enclosed cistern. This type allows the coupling with external hot water storages as well as with ice storages. For this purpose, the storage fluid temperature is transferred to the Type 708 as input variable. The temperature calculated in Type 708 on the inner cistern wall surface and the cistern cavity are transferred again as input variables to the external storage model. There they form the boundary condition for the calculation of the thermal storage losses to the environment. The heat loss coefficient of the storage, which is decisive for this, is also used in Type 708 for the calculation of the temperatures. (Janßen Energieplanung, 2010)

The temperature field is assumed to be rotationally symmetric, therefore, the two-dimensional non-stationary temperature field is mapped in the radial and vertical directions. The model allows a differentiation of the thermal soil properties in both directions. On the surface of the ground, Type 708 considers the absorption of solar radiation and the heat transport to the environment by convection and heat radiation. The lateral boundary of the mapped soil segment is assumed to be adiabatic. For the lower limit, undisturbed soil is assumed. This temperature is to be specified as a parameter. (Janßen Energieplanung, 2010)

Parameter setting

To reproduce the soil with Type 708 correctly, a series of parameters is necessary: the parameters of the external storage model with its geometric dimensions, heat loss coefficients, etc. as well as the parameters of the soil itself. Figure 5-9 shows the geometric parameters which must be specified.

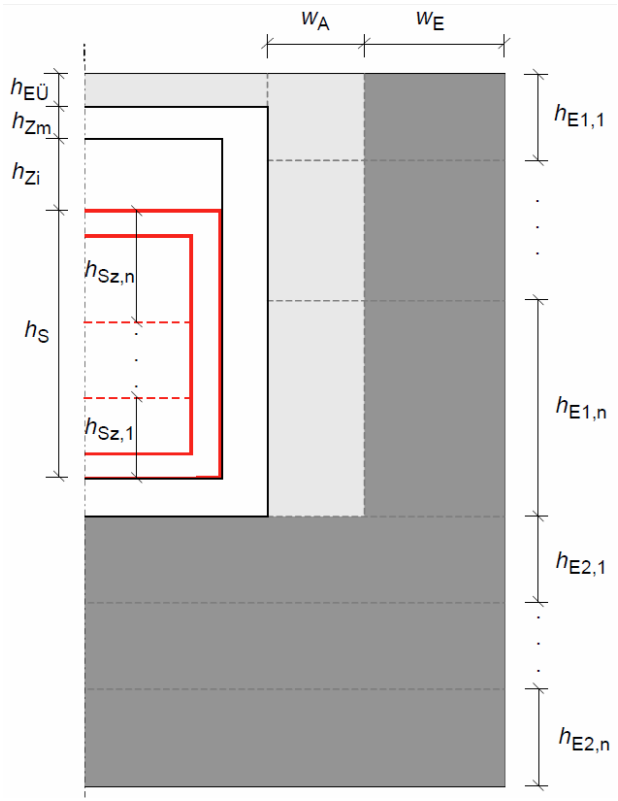

Figure 5-9: Geometric parameter of type 708 (Janßen Energieplanung, 2010)

The storage height h_s, the cistern height h_{zi}, the cistern wall thickness h_{zm} and the overlap $h_{EÜ}$ must be specified in the vertical direction. While the storage height and the overlap were taken directly from the data sheets, the other two parameters were determined during the validation since the simulation model deviates slightly from the real model. The storage is modelled as a mixed system with only one zone. The soil itself is divided into two zones in vertical direction, h_{E1} for the area next to the ice storage and h_{E2} for the area below. The second zone indicates the lower limit of the soil to be modelled and is selected in that way that the assumption "undisturbed soil" is fulfilled. In the horizontal direction, no differences in the soil in the proximity of the storage are assumed. Therefore, the soil is only calculated with one horizontal zone w_E.

Apart from the geometrical parameters, the heat loss coefficients play an elementary role. A distinction is made between the heat losses at the side walls, at the top and at the bottom of the storage. In addition, the heat transfer coefficient between the cistern surface and the storage top in the cistern cavity is to be specified. These are together with the efficiency of the external heat exchanger for the regeneration of the ice storage the essential parameters to be determined during validation.

Furthermore, some climatic data, as the yearly average of ambient temperature, the amplitude of monthly averages of ambient temperature, the day number of the simulation start, etc. are needed. These data were determined by using the standard climate and adjusted accordingly to the simulation data.

Moreover, it should be noted that the Type 708 has two operating modes. Mode 0 is a pre-simulation in which the already properly parameterized ground type operates in a separate TRNSYS project over a long period of time with repeated climate data. This creates a starting temperature field file, which shortens the settling time in the further simulation. In this case, ten years were simulated with the standard climatic data for one year. This operation was iteratively performed to determine both the correct parameters and the correct start temperature field file.

Input data

First, the required variables to define the boundary condition at the ground surface were to be specified as input variables. These were the global radiation, the reflectance, the sky temperature, the ambient temperature and the wind speed. These inputs were generated by the weather data reader (Type 15-2) with the climatic data of Graz for the year 2016 (ZAMG, 2017). The data from Graz was chosen because this is the closest measuring station to Weiz.

Furthermore, the material data of the soil as well as the temperature of the ice storage had to be specified. The material data of the soil was chosen constantly for the entire simulation period for dry clay soil and the temperature of the ice storage was given from the ice storage type.

Implementation of the validation model in TRNSYS

First, it was thought to validate the soil type together with the ice storage in a separate TRNSYS file, as the other components before. However, since an optimization with TRNOPT was not possible due to the programming of the type and moreover an isolated consideration did not

yield the best results, the soil was validated directly in the overall system. For this purpose, the overall system was set up in advance in such a way that the characteristic figures and the energy balances of the single components matched the measurement data as exactly as possible. More about this is described in chapter *5.3 The simulation model of the overall system.*

In addition, the discussed parameters of the soil type were varied in such a way that the ice storage temperature of the simulation matched with the measured as good as possible. The focus was primarily placed on the ice storage and not on the soil temperature, as this is ultimately the decisive factor for the simulation model to represent the real system well. After a few iterations, it was, thereby, possible to find a configuration which represented the system satisfactorily.

Resulting findings

As seen in Figure 5-10, the ice storage temperature in the simulation model matches very well with the measured one. The subcooling in January 2016 takes place exactly at the same time and to the same temperature level. The cooling down in the autumn and the phase transition are also matched very well. Only the thawing after the phase transition is a bit faster in the simulation. Due to the fact that the other temperature sensors installed in the ice storage also differ from each other in this area, this slight deviation should not be serious.

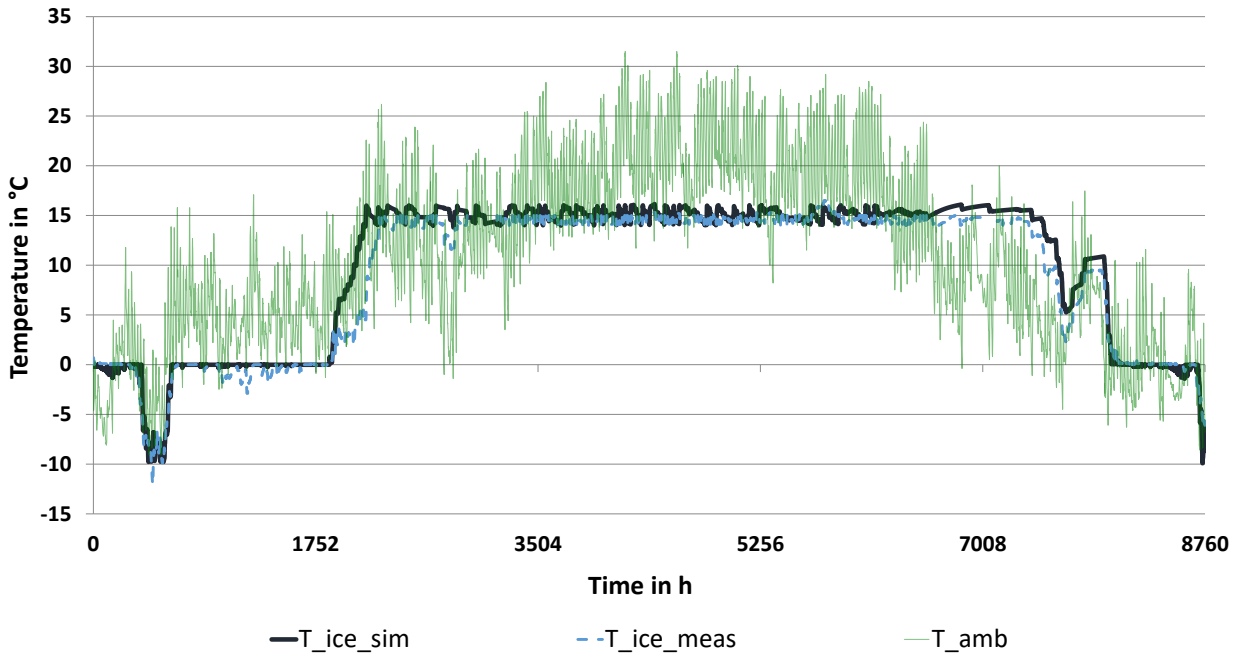

Figure 5-10: Trend of ice storage temperatures for the year 2016 (01.01 – 31.12)

A detailed listing of all selected, or during validation process determined, parameters can be found in the appendix (Table A- 2).

5.3 The simulation model of the overall system

After the validation of the individual components, except of the soil model (Type 708) which was validated together with the overall system, their determined parameters were taken over in the overall system. This system model was already setup by Lerch Werner. A detailed description of it can be found in Lerch (2017), which is why here follows only a brief discussion of the most important details.

The overall system was divided in three layers. The first layer, as shown in Figure 5-11, included the building (Type 56) and some necessary information like the ventilation, the internal loads as well as the weather data. The building was setup with TRNBUILD and designed in such a way that it correlated to the real building. Each apartment as well as basement and ground floor were designed as a separate zone. With the weather data reader, the according weather could be imported from a ".tm2 file". For the validation, this was the weather data from Graz for the year 2016 (ZAMG, 2017) since this was the closest measuring point.

In addition, the printer which stores all important values for the evaluation in a one hour interval in a text file is placed here.

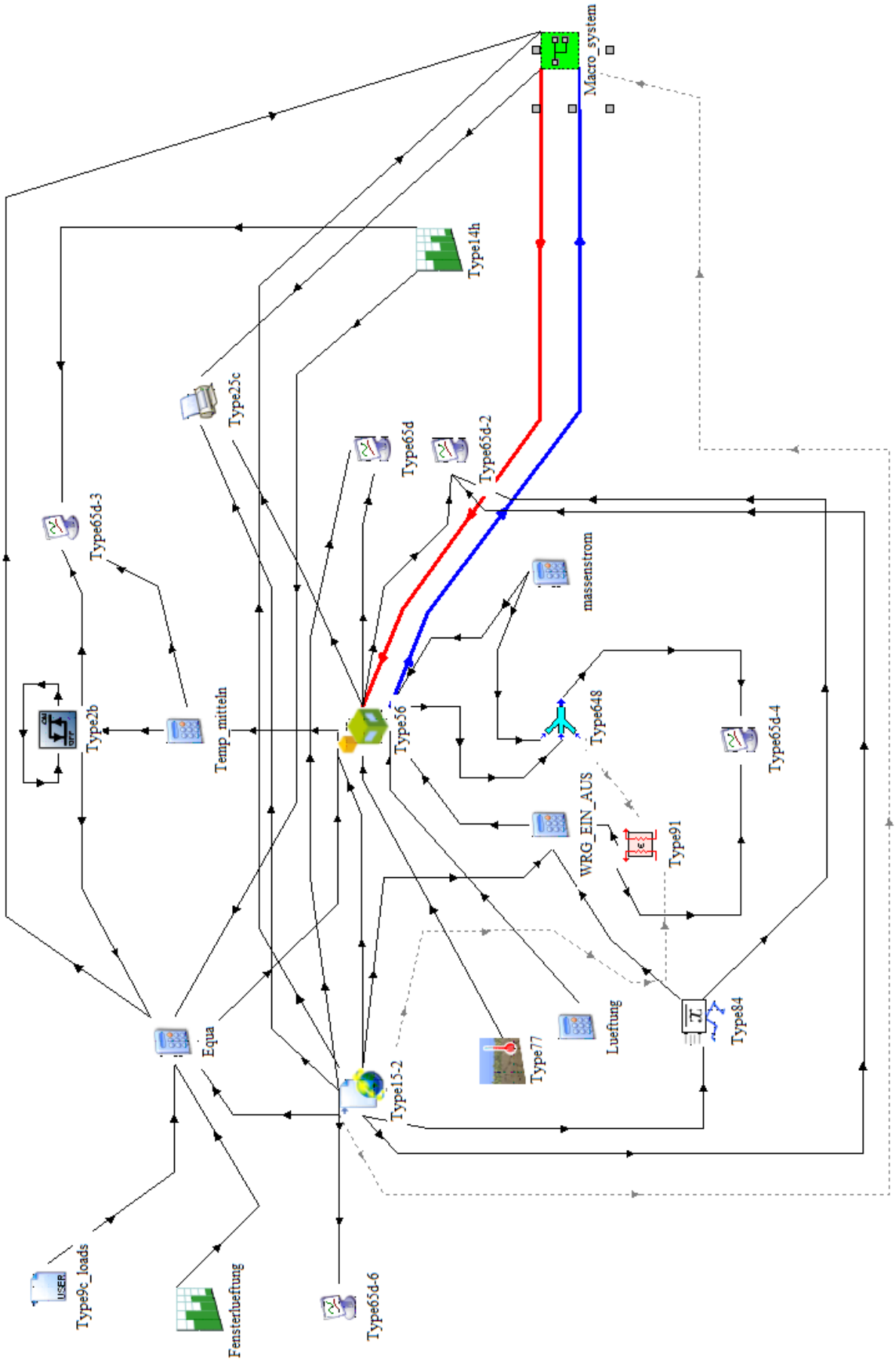

Figure 5-11: Overall system layer 1 – climate/building

The second layer is shown in Figure 5-12. This layer comprises the actual heating system and is the place where the components validated are installed. The connections which are marked with colours are the connections representing the real connections where actually the fluid flows. Red colour represents the inlet and blue the return pipes. The grey ones are for information transport, for example, for the controlling, the visualization, or the input. The green ones are for the output data of the “Printegrator” (Type 46a).

As determined in the validation, one solar collector model is sufficient to cover all operating conditions. As a result of the validation, the external heat exchanger was installed for the regeneration of the ice storages because of using the double port. The ground type is now connected with the ice storage and calculates the ambient temperature (soil temperature). The built-in heat pump models are pure characteristic curve models which have been parameterized using the data sheets.

On the consumption side, the apartments were grouped into three zones to reduce the complexity. Therefore, the identical apartments were combined in each case. The apartments 1, 4, 5, and 8 were the outlying apartments on the ground floor and on the first floor. The apartments 2, 3, 6 and 7 were the ones on the inside with an additional room for children and the apartments 9 and 10 were the bigger ones on the second floor. A building plan can be found in the appendix (Figure A- 16).

It should be noted that the pipe losses were only considered in one heating circuit (apartment 9, 10) but for the entire pipe length. The domestic hot water requirement is depicted by a tap system, which receives a tap profile from an input file. This profile is based on the measured DHW demand for the validation. Here too, the pipe losses were considered. For the DHW and the SH storage, the same model (Type 340) only with different parameters was used. Both were non-stratified storages, which means that they had no stratified charging pipe but the naturally occurring stratification was calculated. They also considered the losses to the environment. In addition, in both an electric heating element was included which was activated when the ice storage temperature dropped below -10 °C.

The control of the simulation system is designed in such a way that it corresponds to the real system. This is explained in chapter *3.2 Operating modes.* The only exception of this is the operation of the heat pumps. While in the real system sometimes only one of the two heat pumps is in operation, they operate always in parallel in the simulation model, which means that one heat pump never works alone. This simplification had to be made because the real control algorithm was unknown.

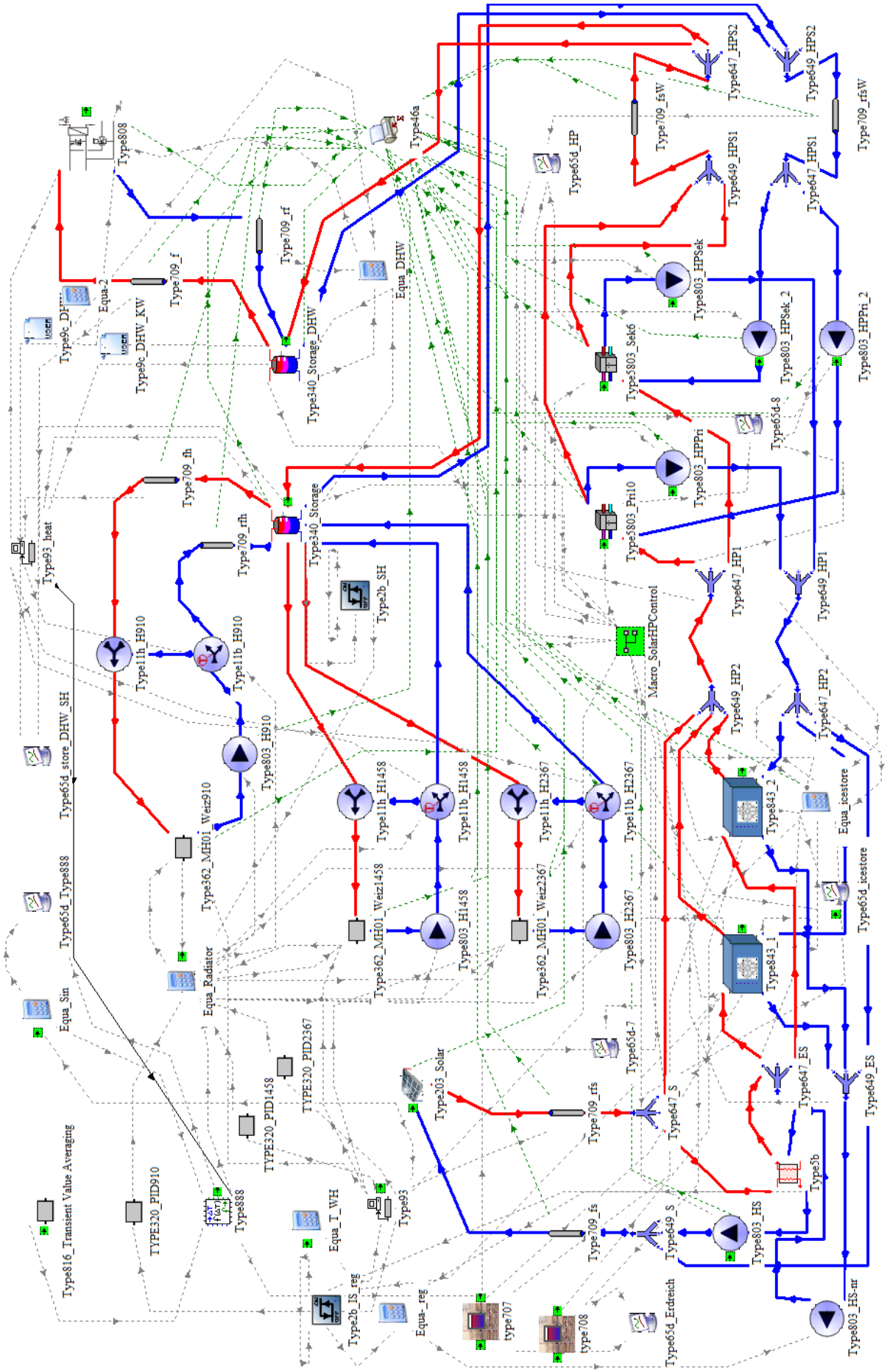

Figure 5-12: Overall system layer 2 – heating system

The already mentioned Printegrator is a combination of an integrator and a printer and is used for the output of all energies. These energies will be issued on a monthly base to compare them with the monthly balance sheets in chapter *4.3 Energy* during the validation process.

The third layer contains some further types for the control of the system. These are mainly hysteresis controllers, which regulate the storage temperatures or the activation of the auxiliary heater.

5.4 Validation of the overall system

In order to ensure that the simulation model provides the same results as the real system, a validation of the overall system was necessary in addition to the validation of the single components. For this purpose, the system was adjusted in such a way that the specific SH demand and the specific DHW demand matched with the measured data. Moreover, the measured and simulated ice storage temperature should also match as good as possible. Finally, the energy balances of the individual components, such as the solar collector, the ice storages, and the heat pumps, were compared with each other too.

The parameters still to be determined were the room temperature, the window ventilation and the shading as well as the already described validation of the ground type (see chapter *5.2.4 Soil coupling*), which was also carried out within the overall system.

In the simulation model for all apartments and rooms the same set temperature was used. This temperature was estimated from the measured data (T_{room_i}) by the equation (5-3).

$$T_{mean\_room} = \frac{T_{room\_1} * A_{room\_1} + T_{room\_2} * A_{room\_2} + \cdots + T_{room\_n} * A_{room\_n}}{A_{ges}} \qquad (5\text{-}3)$$

Thus, a room size weighted average temperature value of all heated rooms was calculated. With the measured data for the year 2016 (only heating period), this resulted in a temperature of 22.7 °C. Due to the inaccuracy of the measurement and the fact that this was a simplification, it was decided that a variation of ±1 K was allowed. This means that this temperature was used as starting point and was varied between 21.7 and 23.7 during the validation.

To determine the infiltration, equation (5-4) was used. The variable v_{inf} stands for the infiltration and the factor *i* is a ramp function which is 0 between 22 and 5 o'clock and 1 all the other time. With this equation, the infiltration behaviour is to be simulated as realistically as possible. The ventilation through open windows v_{vent_window} was varied within reasonable limits during the validation.

$$v_{ges} = v_{inf} + i * v_{vent\_window} \qquad (5\text{-}4)$$

The shading was modelled in such a way that it was activated when the set room temperature was exceeded. Then the radiation was reduced to 15 % of the without shading occurring

radiation. In addition, a certain percentage of standard shading was supposed by balconies or by manual activation of the shading system. This percentage (*shd_{offset}*, equation (5-5)) was also to be determined by the validation.

$$shd = shd_{offset} + i_{on/off} * (0.85 - shd_{offset}) \quad (5\text{-}5)$$

These three parameters (T_{mean_room}, v_{vent_window}, shd_{offset}) gradually varied in several simulations to find the best configuration. The result is shown in Table 5-4.

Table 5-4: Validation result

T_{room_set} [°C]	v_{vent_window} [h^{-1}]	shd_{offset} [%]
23.7	0.155	32

Due to the relatively high energy consumption, these values are also quite high, but this was necessary to achieve a good match between the simulation model and the real system. This consistency respectively the deviations occurring are analysed in more detail in the following sub-chapters.

It should be noted that the validation discussed so far relates only to the SH. The profile for the DHW requirement has already been adapted to the measurement data, so no further validation is necessary.

5.4.1 SH and DHW demand

As shown in Table 5-5, a good match between the measured and the simulated values could be found in the validation. Since the measured values also contain the storage and pipe losses, these had to be added to the simulated values to ensure comparability. The considered pipe losses are the losses between the storages and the apartments as well as the losses between the heat pumps and the storages. Comparing the simulation values including the losses with those of the measurement, it is shown that the deviation is below 0.1 %. This is a great result for the validation concerning the specific demands.

Table 5-5: specific demands (based on heated area)

	simulation	sim incl losses	measured
specific SH demand [kWh/(m^2a)]	26.64	30.74	30.71
specific DHW demand [kWh/(m^2a)]	20.09	27.37	27.36

The specific demands are referred in this case to the heated area of 957 m^2. The meaning of the magnitude of these values is discussed in chapter *4.3.1 System energy balance*. A comparison of the simulation to the measurement in absolute numbers for the year 2016 is shown in Figure 5-13. The left bars show the distribution where the energy is provided, and the right ones for what it is used.

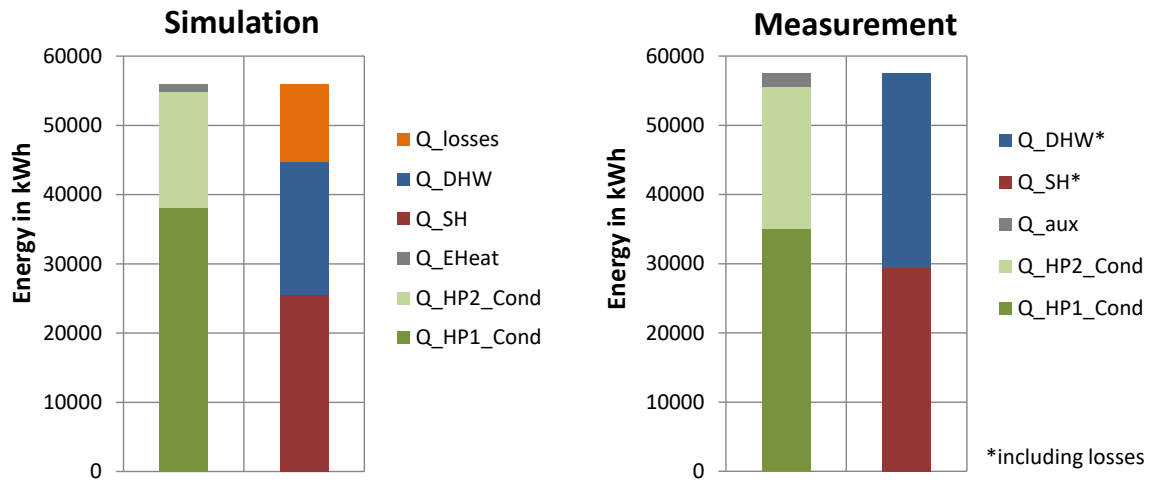

Figure 5-13: Total energy requirement (01.01.2016 – 31.12.2016)

5.4.2 Ice storage temperature profile

The second indicator for the correct validation of the system was the ice storage temperature profile. In addition to the parameters discussed above, especially the ground model (type 708), which was also validated in the course of the validation of the overall system, was crucial for this. The result is shown in Figure 5-10 and has been already discussed in chapter 5.2.4 Soil coupling. As shown there, a satisfactory result could also be achieved in this aspect.

It is also important to ensure that a pre-simulation is carried out, so that the ice storage temperature at the start of the actual simulation is consistent with the real data. Since during the phase transition it is neither known in the simulation nor in the real system how many percent of the storage are frozen, the duration of the pre-simulation was determined in such a way that the first sub-cooling occurred in both systems at the same time.

5.4.3 Balance sheets of the individual components

Despite the good conformity regarding the specific demands and the ice storage temperature profile, the simulation model differs slightly from the real system in some points. This is shown on the basis of the energy balances of the individual components. Each of them compare the measured values with the simulated ones for the year 2016.

Figure 5-14 and Figure 5-15 show the energy balances of the heat pumps. It can be seen that heat pump 1 provides more energy in the simulation than in the real system and that it is the other way around for heat pump 2. Due the fact that the used control algorithm is unknown, which is why the simplification had been made that both heat pumps always operate simultaneously in the simulation model, deviations were expected at this point. In addition, the control of the real system has been modified during of the considered year, which makes an exact comparison even more difficult. Since then, as can be seen in Figure 5-13, the overall energy of the two heat pumps together has matched very well and the solution has been classified as satisfactory.

Since the heat quantity of the ice storage as source for the heat pump was not measured and the solar heat quantity meter made many problems, the heat quantity on the evaporator side was calculated as the difference of the heat quantity on the condenser side and the electric energy. Consequently, the losses occurring at the heat pump cannot be considered.

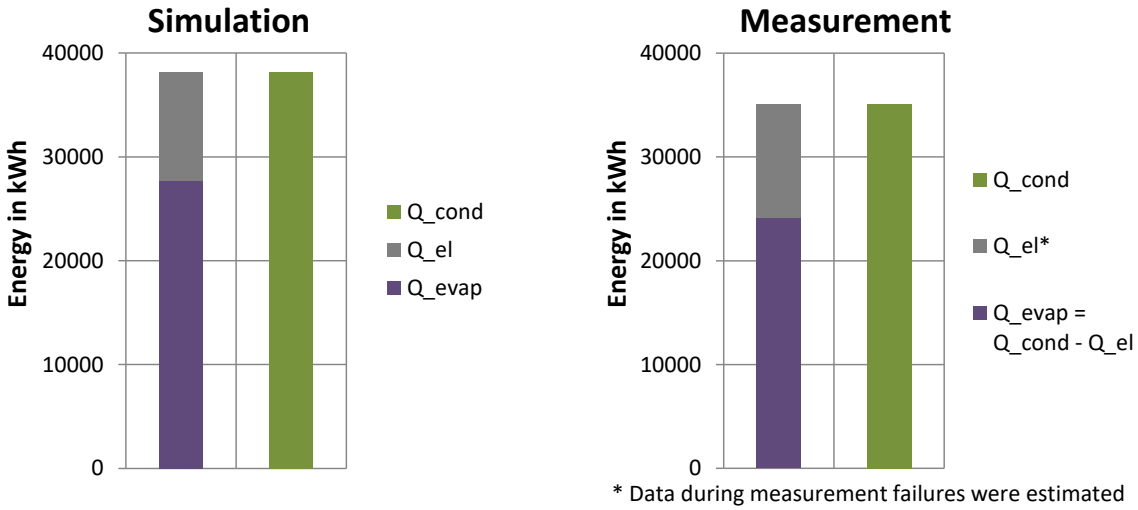

Figure 5-14: Heat pump 1 (2016)

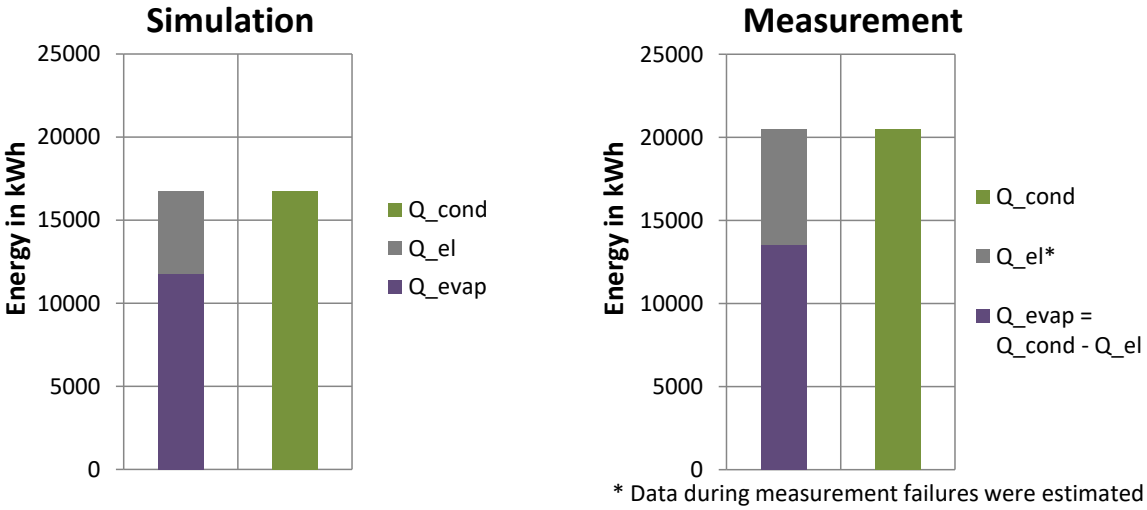

Figure 5-15: Heat pump 2 (2016)

The most significant difference between the simulation and the measured data appears for the ice storage. Figure 5-16 shows that the ice storage is much less used in the simulation model than in the real system. Since the ice storage temperature profile matches very well, the assumption is made, that the difference occurs during the summer months, when enough energy is available to reheat the ice storage immediately after use. One reason for this was a control error, which is why the SH storage temperature was maintained at 60 degrees throughout the whole summer. This energy is mainly supplied by the ice storage, since during the summer the collector temperature is often too high to be used as source for the heat pumps.

Figure 5-17 shows that in the DHW storage approximately 3000 kWh of losses occur over the year. Considering further losses in the pipelines between heat pump and the storage as well as the fact that the SH storage is smaller than the DHW storage and it was heated up to the temperature of the DHW storage for about six months, an additional use of at least 1000 kWh for the ice storage as source for the heat pumps can be assumed. With this explanation, the gap cannot be closed completely but the difference is in a range that can be tolerated now.

The energy content of the ice storage (Q_store) between 01.01.2016 and 01.01.2017 was not measured but can be understood as the difference of the input and output side of the balance sheet.

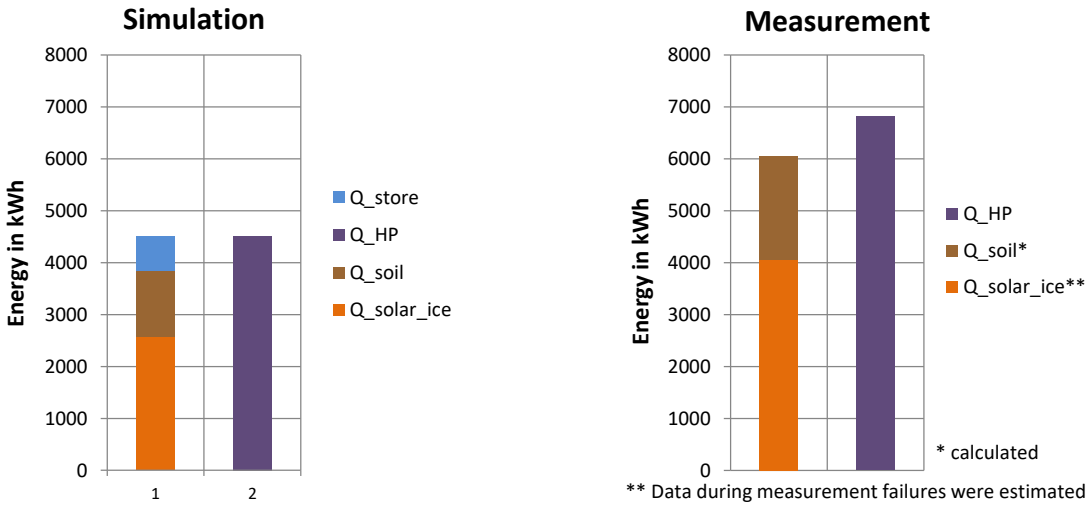

Figure 5-16: Ice storage (2016)

Figure 5-17 and Figure 5-18 show the energy balances of the DHW and the SH storage. Because of the reason that the system was validated concerning the specific SH and DHW demands, the balances had to match. As already mentioned, the losses in the measured data cannot be determined, which is why they are included in Q_DHW and Q_SH in the measured energy balance (system boundary condenser side of the heat pumps). Due to the size and the higher temperature level, the losses in the DHW storage are larger. Furthermore, it is shown that the energy demand of the auxiliary heating in the simulation model is slightly lower. The different distribution to the storages occurred because the auxiliary heating was activated in the real system only for the DHW storage.

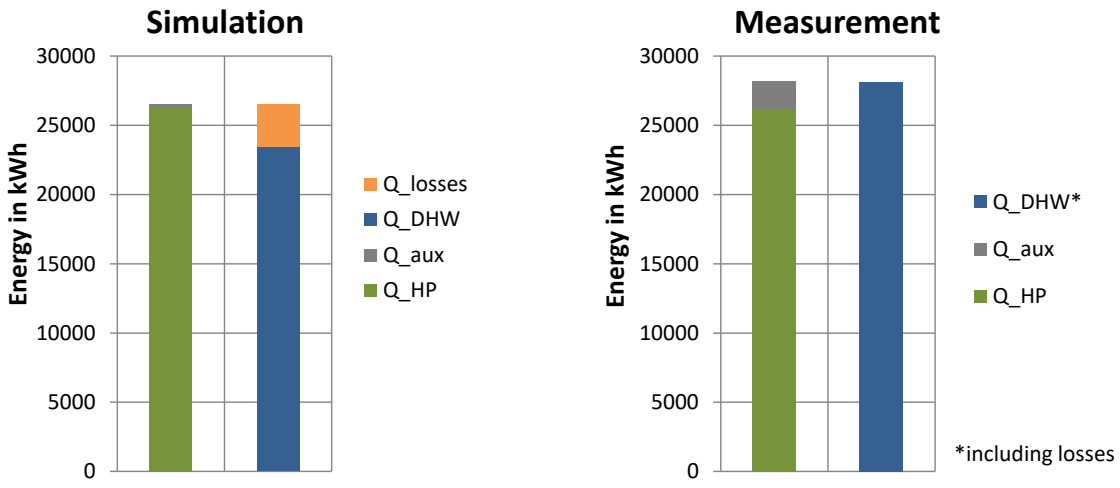

Figure 5-17: Domestic hot water storage (2016)

Figure 5-18 also shows the distribution of the heating energy to the single apartments in the simulation model. It can be seen that the two apartments 9 and 10 in the second floor require more energy than the others. This is due to the fact that they are larger and located on the last floor, which means that in addition to most of the wall also the ceiling of these apartments is in contact with the environment.

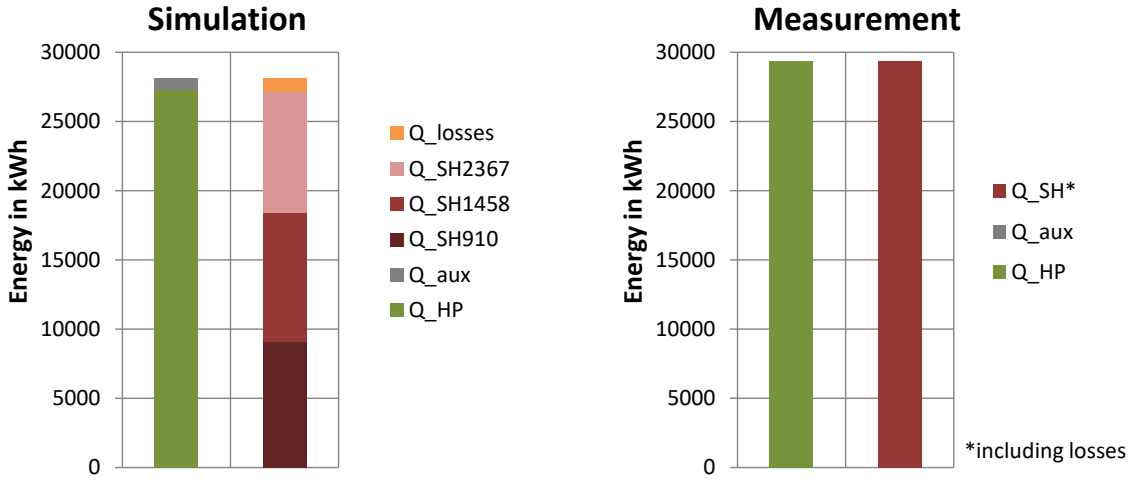

Figure 5-18: Space heating storage (2016)

Moreover, the balance of the solar collector shows that the solar collector is more often used directly as source for the heat pump in the simulation, than in the real system. Because of numerous failures in the measurement of the solar data, as well as the fact that no data was available in January, the measurement data is here rather to be understood as a rough estimation. That is why an analysis of the difference between measurement and simulation is dispensed with.

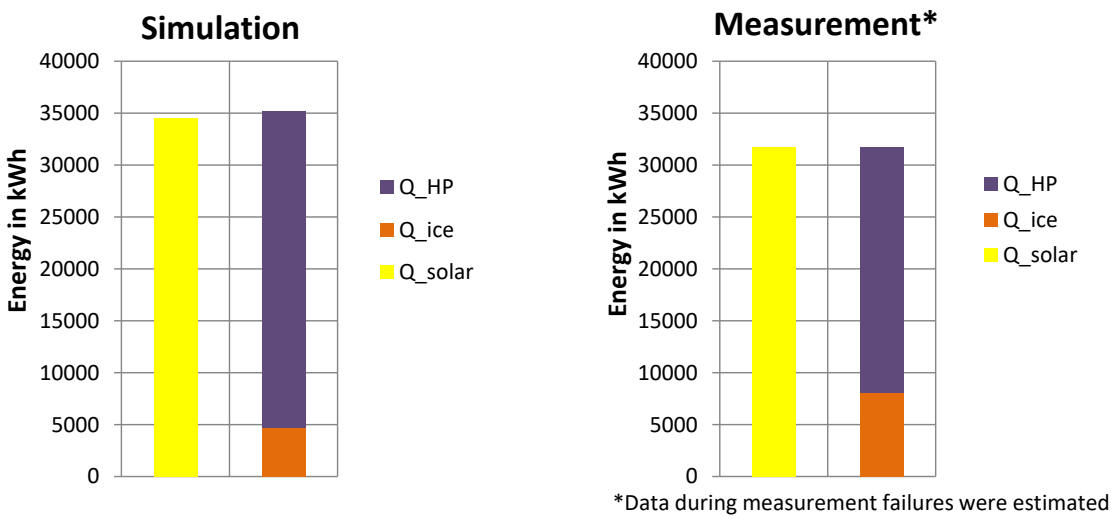

Figure 5-19: Solar collector (2016)

5.4.4 System Performance Factor

It is interesting to compare the SPFs between measurement and simulation. Table 5-6 shows that significantly higher SPFs of the heat pumps are achieved in the simulation model. This is possible due to the characteristic model of the heat pumps used. However, it is also a strong indicator that in the optimization of the system a collective mode of operation of the heat pumps, as used in the simulation model, should be examined more closely. Especially in view of the regeneration time (more time for the regeneration available because of shorter working times of the heat pumps) that could have a positive influence.

Table 5-6: System Performance Factor

	Simulation	Measurement
SPF HP1	3.65	3.32
SPF HP2	3.39	2.96
SPF mean	3.57	3.19
SPF System	2.67	-

Furthermore, it is shown that the SPF of the overall system (5-6) is much lower than the SPF of the heat pumps. This SPF considers the electrical consumption of the heat pumps, the auxiliary heaters as well as all other in the system needed pumps shown in Figure 5-20. Since the share of the auxiliary heating (4-4) is with 1.9 % not too big and the other pumps also need not much electric energy (287.5 kWh/a), this is mainly because of the high heat losses in the pipes as well as in the SH und DHW storage, which are also considered because of referencing the SPF_{System} to the effective energy.

$$SPF_{System} = \frac{Q_{eff\_SH} + Q_{eff\_DHW}}{Q_{el\_HPs} + Q_{el\_pumps} + Q_{aux}} \quad (5\text{-}6)$$

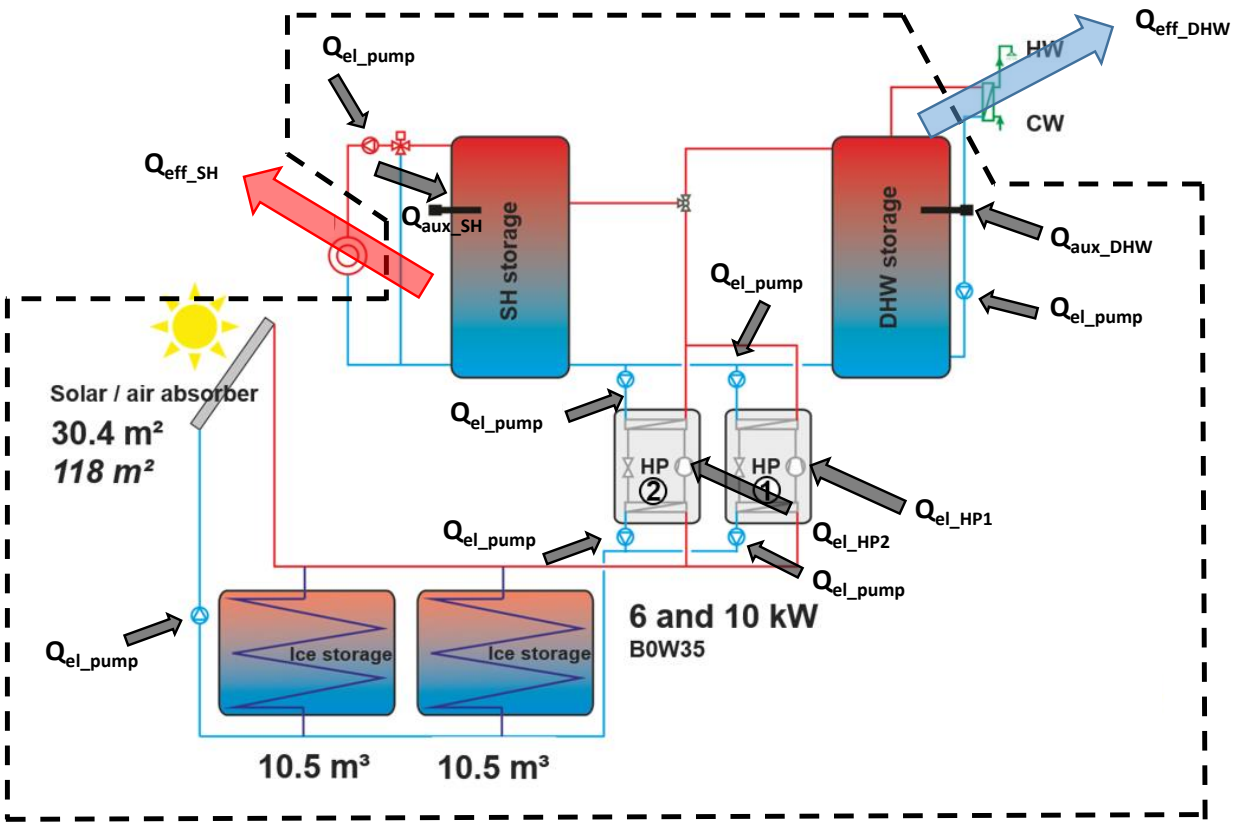

Figure 5-20: Energy flows for calculating the SPF_{System}

6 DESIGN GUIDELINE

Based on the validated simulation model, a design guideline for such systems has been created. Thus, the required size of the ice storage volume and the solar collector area can be selected for multi-family buildings with different heat demands. For this purpose, a sensitivity analysis with the validated system was carried out first, to estimate how a change in the ice storage volume or the collector area affects the system. Afterwards, different multi-family buildings with a heat demand between 8 and 64 kWh/(m^2a) for a heated area of 957 m^2 were simulated by adapting the set room temperature, the window ventilation, the shading and the insulation of the walls. These buildings were used to determine the optimal parameters considering different climate data. For this purpose, a sensitivity analysis of the collector area and the ice storage volume was carried out for these buildings too. With gained knowledge, it could be determined how the system should be designed for a desired system performance or a certain percentage of auxiliary heating.

6.1 Climate data

Before explaining the sensitivity analysis and the generation of the design guideline, the underlying climate data should be discussed in this chapter. These are generated with the program METEONORM (Meteotest, 2009) for the location in Weiz and are divided into a standard climate, a worst (cold climate data) and a best (warm climate data) case.

6.1.1 Standard climate data

For generating the standard climate, the climate data from the years 2000 to 2009 were used for the temperature model and the data from 1991 to 2010 for the radiation model. This results in the average values shown in Table 6-1.

Table 6-1: Yearly average values for the standard climate data (Meteotest, 2009)

	yearly average value	unit
Global radiation	1186	kWh/(m^2*a)
Direct radiation	131	W/m^2
Diffuse radiation	68	W/m^2
Global brightness	14816	Lux
Scattered brightness	8466	Lux
Rate of overclouding	5	Octas
Air temperature	9.8	°C
Dew-point temperature	5.0	°C
Relative humidity	72	%
Air pressure	960	hPa
Wind velocity	0.5	m/s

In addition, the monthly average values of the radiation are shown in Figure 6-1 as well as the monthly values of the ambient air temperature in Figure 6-2.

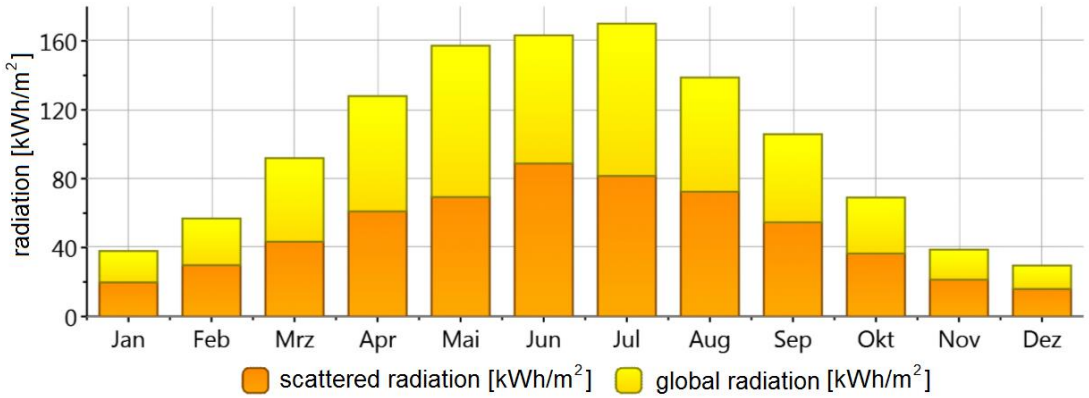

Figure 6-1: Monthly average value of radiation for standard climate data (Meteotest, 2009)

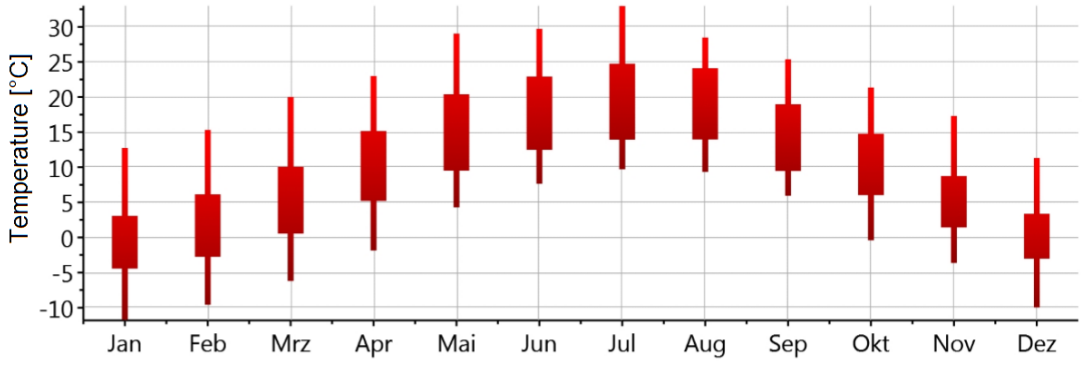

Figure 6-2: Monthly ambient air temperature for standard climate data (Meteotest, 2009)

6.1.2 Cold climate data

The same years as for the standard climate applied as reference but this time a worst-case scenario was generated out of them. Comparing both cases with each other shows that, for example, the mean direct radiation is more than 30 % lower in this scenario. Moreover, the yearly average value of air temperature is, as shown in Table 6-2, also clearly lower with only 7.7 °C (- 2.1 K). This results in significantly higher demands on the heating system during simulations with this climate.

Table 6-2: Yearly average values for the cold climate data (Meteotest, 2009)

	yearly average value	unit
Global radiation	988	kWh/(m²*a)
Direct radiation	89	W/m²
Scattered radiation	66	W/m²
Global brightness	12450	Lux
Scattered brightness	7992	Lux
Rate of overclouding	6	Octas
Air temperature	7.7	°C
Dew-point temperature	3.0	°C
Relative humidity	72	%
Air pressure	960	hPa
Wind velocity	0.5	m/s

Figure 6-3 and Figure 6-4 show again the monthly average values of the radiation and the values of the ambient air temperature. Here it can be seen too that this year is much colder. While in the standard climate data only one clearly negative monthly average temperature value occurs in January, it is shown that in this case three months are in the negative range.

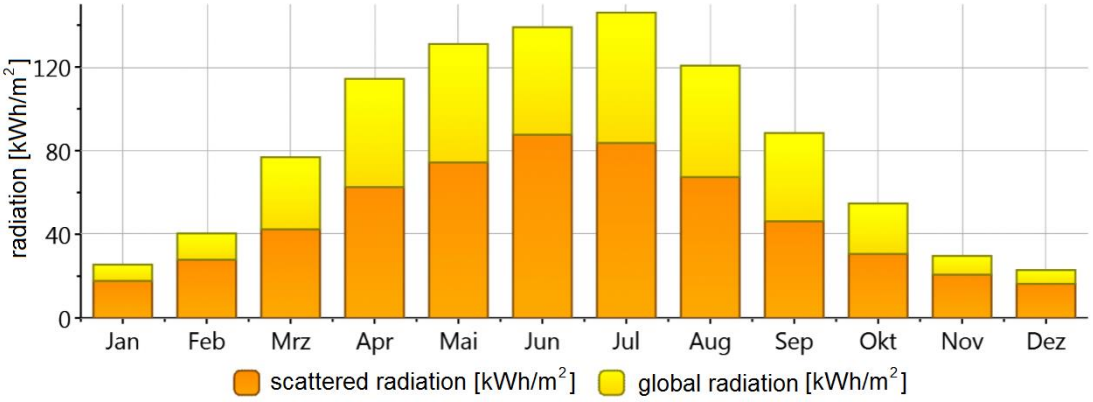

Figure 6-3: Monthly average value of radiation for cold climate data (Meteotest, 2009)

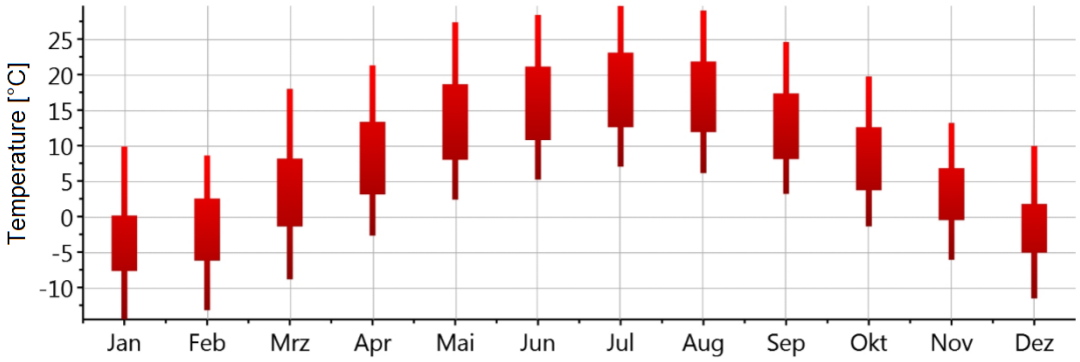

Figure 6-4: Monthly ambient air temperature for cold climate data (Meteotest, 2009)

6.1.3 Warm climate data

In contrast to the worst-case scenario, a best-case scenario was generated from the climate data. Here, both radiation and ambient air temperature are higher than before. As in the other two cases, the yearly average values are shown in Table 6-3 as well as the monthly average values for radiation and the ambient air temperature which are shown in Figure 6-5 and Figure 6-6.

Table 6-3: Yearly average values for the warm climate data (Meteotest, 2009)

	yearly average value	unit
Global radiation	1352	kWh/(m²*a)
Direct radiation	175	W/m²
Scattered radiation	65	W/m²
Global brightness	16830	Lux
Scattered brightness	8266	Lux
Rate of overclouding	5	Octas
Air temperature	11.9	°C
Dew-point temperature	7.0	°C
Relative humidity	73	%
Air pressure	960	hPa
Wind velocity	0.5	m/s

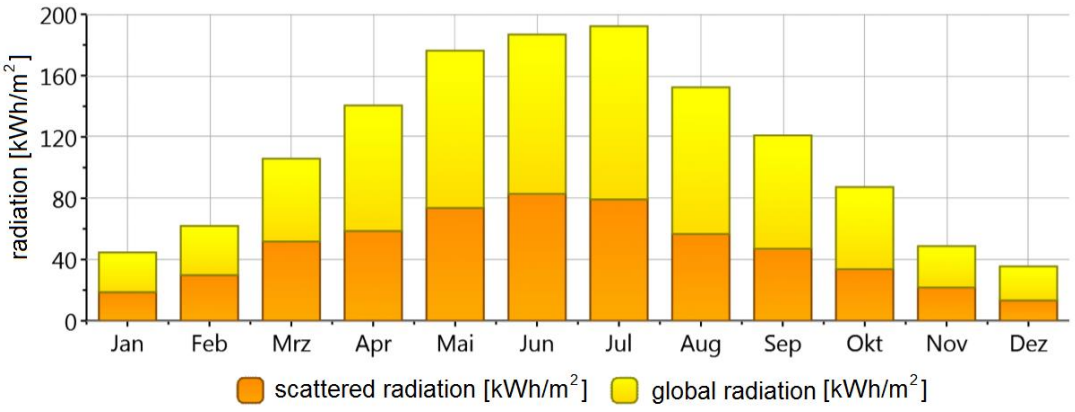

Figure 6-5: Monthly average value of radiation for warm climate data (Meteotest, 2009)

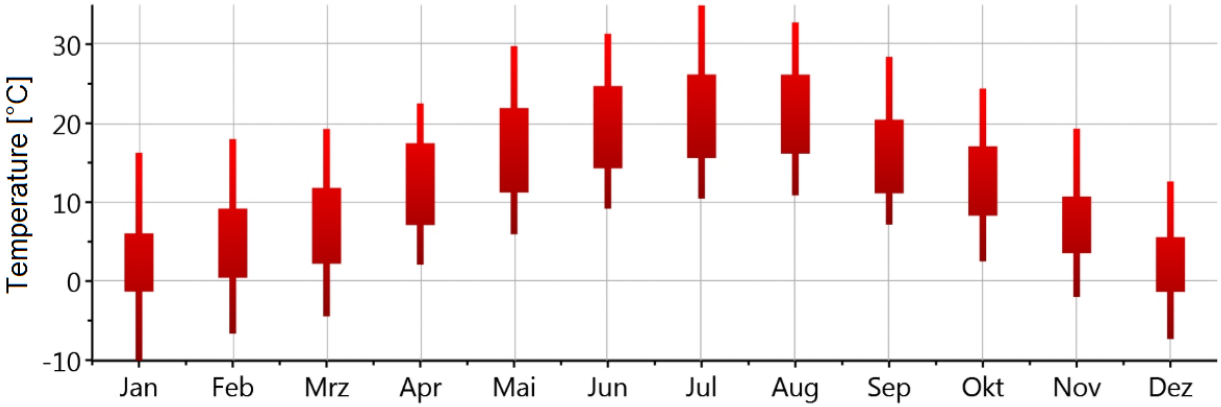

Figure 6-6: Monthly ambient air temperature for warm climate data (Meteotest, 2009)

6.2 Sensitivity analysis of the validated system

With the validated system and the generated weather data a sensitivity analysis was carried out as a first step. For this purpose, the solar collector area and/or the ice storage volume was gradually increased from the base of the validated data. For each step the SPF of the system (5-6) and the share of the auxiliary heating (4-4) was calculated. This was done for all three climate data scenarios. On the one hand, it shows how the system currently in operation works with the different climate data, which is particularly interesting for the cold climate because 2016 was a comparatively warm year, and on the other hand, it gives an insight how the system changes if the solar collector area or the ice storage volume are varied.

The result for the cold climate data is shown in Figure 6-7. At “variation of the component dimensions = 0 %”, the validated configuration is plotted from which the components are enlarged individually or together in 5 % increments up to 50 %. With the validated system, the auxiliary heating is almost 18 % and the SPF of the system is below 2. As expected, the values are significantly worse with the cold climate data than with the climate of the year 2016, where a SPF of 2.67 and share of auxiliary heating from 1.9 % are reached. Since significantly higher SPFs are desirable, a variation in the negative direction, i.e., a reduction of the size of the components, has been dispensed with.

It is shown that the change of the collector area has a similar effect as the change of the ice storage volume. If both are increased at the same time, an even better result can be achieved. The values “SPF both var.” and “EHeat both var.” are to be understood in such a way that the collector area and the ice storage volume are both increased 5 % at the 5 % mark on the x-axis. In addition, it is seen that in this worst-case scenario, even when the two components are enlarged by 50 %, the share of the auxiliary heating is still relatively high (ca. 10 %). This is to be compared with the two other climate data sets before making further analysis.

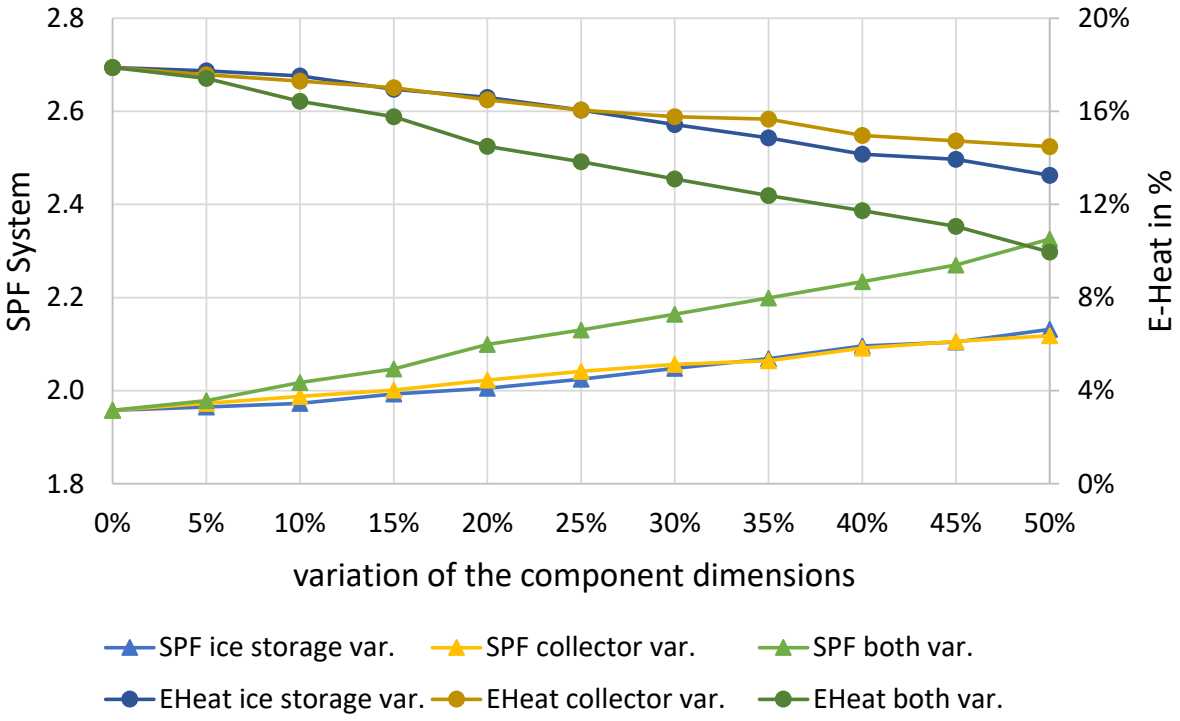

Figure 6-7: Sensitivity analysis with cold climate data

Figure 6-8 shows the diagram for the same configuration but with the standard climate data. The initial situation with the validated system is already much better. Now only an auxiliary heating of about 6 % is necessary, while with the cold climate, despite 50 % increase of both components, the 10 % mark could not be underrun. In this way, the great influence of climate on the system performance can be observed. Apart from this, the effects of an enlargement of the two components are similar to those already described for the cold climate.

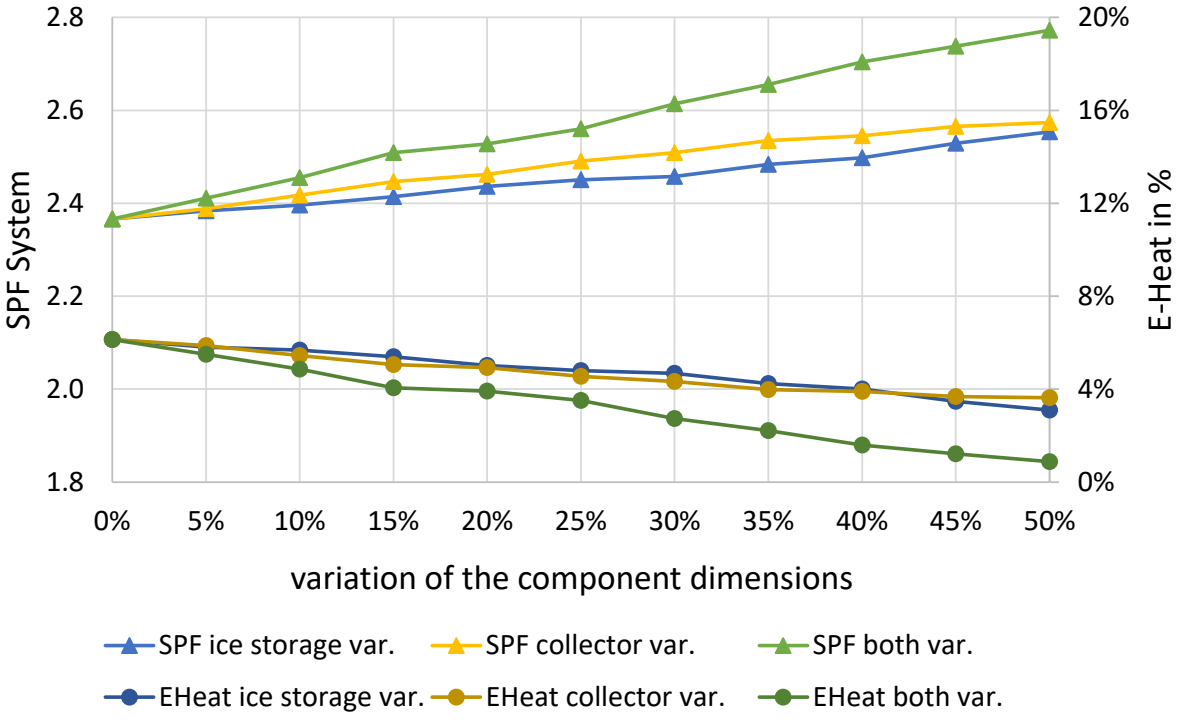

Figure 6-8: Sensitivity analysis with standard climate data

Moreover, the sensitivity analysis was carried out with the warm climate too. This is shown in Figure 6-9. With the validated system, the auxiliary heating is with only 0.5 % hardly necessary and with a further increase of 5 % of one of the two components it finally becomes zero. Furthermore, from this point on, an increase of the ice storage volume is no longer useful. An enlargement of the collector still has a positive effect on the SPF_{System}, however, this is also significantly lower from this point onwards. This is because a larger collector area results in a higher flow temperature on the evaporator side of the heat pumps, which is why they can operate more efficiently. It also shows that the SPF_{System} in this configuration is limited at approximately 2.8. For a further improvement of the SPF_{System}, the occurring heat losses must be reduced.

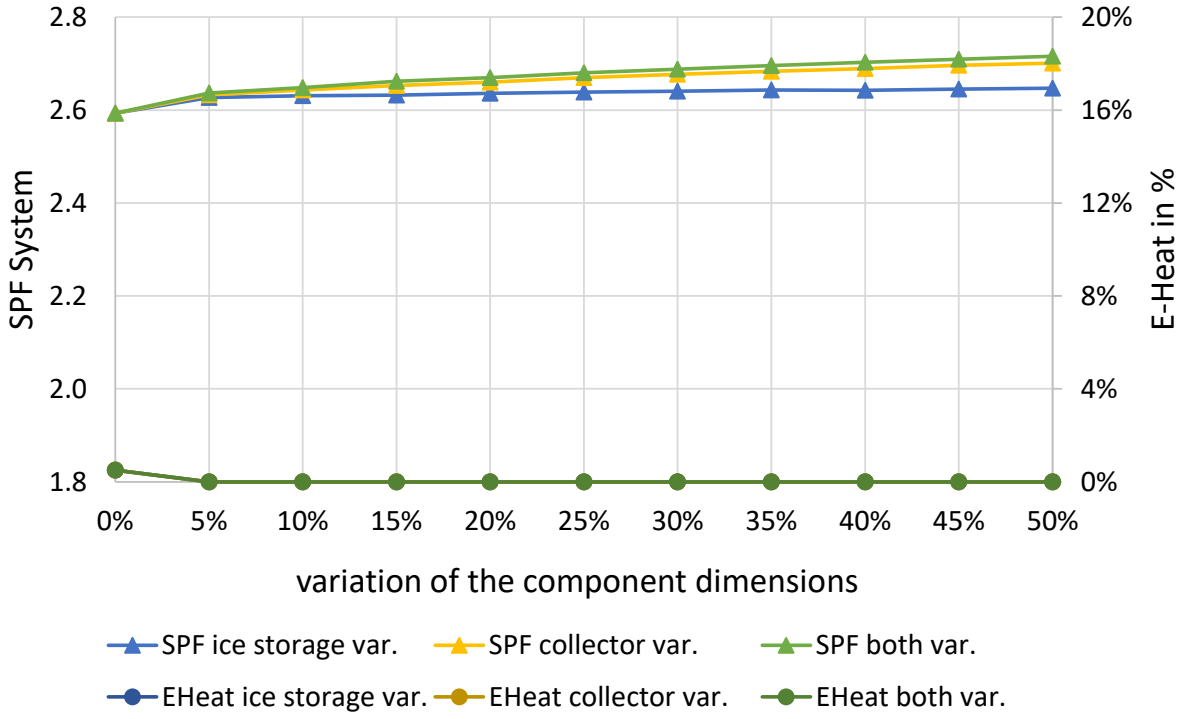

Figure 6-9: Sensitivity analysis with warm climate data

The discussed situation of the system in Weiz simulated with the different climate data is summarized in Table 6-4. The data of the year 2016 best match with the warm climate, if comparing the share of auxiliary heating. Therefore, it is not excluded that years with a significantly higher share of auxiliary heating, respectively a lower SPF_{System} may occur. Nevertheless, it is seen that the specific SH demand according to the simulation of 2016 is much closer to the standard climate than to the warm one. This confirms that the amount of the SH demand alone does not directly fit to the share of the auxiliary heating.

Table 6-4: Effect of different climate data on the validated system

climate	SPF_{System} [-]	EHeat [%]	spec. SH demand [kWh/(m²*a)]	spec. DHW demand [kWh/(m²*a)]
Weiz 2016 sim.	2.67	1.92	26.6	20.1
standard	2.36	6.31	27.8	20.1
cold	1.95	17.96	38.8	20.1
warm	2.59	0.56	18.4	20.1

Based on this sensitivity analysis, it can be said that for a better efficiency of the system in Weiz the component to be enlarged can be chosen freely within certain limits. An enlargement of the solar collector would, therefore, make sense in order to increase the efficiency of the system. Since one cubic meter of the ice storage costs much more than a square meter of the solar collector at the moment, an expansion of the ice storage is not as recommendable. Apart from this, the enlargement of the ice storage volume would be far more complex. However, this and further improvements are discussed in more detail in Lerch (2017).

6.3 Method for generating the design guideline

As already mentioned, the design guideline has been generated for multi-family buildings with a heat demand between 8 and 64 kWh/(m²*a). Therefore, it was decided to simulate five buildings with a heat demand of 8, 22, 36, 50 and 64 kWh/(m²*a). A similar procedure as for the validation of the overall system was used. By variant calculations the room temperature, the window ventilation, the shading and the insulation of the walls were varied until the desired heat demand was reached. This was done under the assumption of "ideal heating". That means that the actual heating system (Layer 2 and 3) in the TRNSYS model was deactivated and the heating was carried out in the building type itself. The building type was thereby heated in such a way that the adjusted set point room temperature was always maintained. The necessary energy was the heat demand for which the buildings were designed. This procedure was necessary, since different heat pumps were also required for the different buildings but their parameterization was, with the chosen method, only possible with the buildings.

For the window ventilation and the shading, the same applies as described in *5.4 Validation of the overall system.* Using the standard climate, this results in the configurations shown in Table 6-5. The heat demand $Q_{\_heat\_ideal}$ is, therefore, valid with ideal heating and with the standard climate data.

Table 6-5: Used buildings with a heated area of 957 m²

$Q_{\_heat\_ideal}$ [kWh/(m²a)]	T_{room_set} [°C]	v_{vent_window} [h⁻¹]	shd_{offset} [%]	u_{wall} [W/m²K]
8	18.80	0.000	0.00	0.086
22	21.00	0.145	0.30	0.098
36	23.20	0.213	0.45	0.098
50	22.47	0.155	0.32	0.462
64	23.75	0.220	0.45	0.462

It should be noted that the main point in the parameter selection was the correct heat demand. Even if it was tried not to choose completely unrealistic values, it was unimportant how the correct heat demand was achieved. For this reason, values such as a room temperature of 18.8 °C were tolerated because a further modification of the building would have been too time consuming.

With these parameters, the five buildings were simulated again but now with the cold climate to determine the required heat pump capacity. The cold climate was selected to ensure the operability of the system even in the worst-case scenario. From the hourly recorded heat demand of the buildings, the maximum value was selected, which corresponded, transformed to kilowatt, to the required heat pump capacity. Since two heat pumps were used in the simulation model, which always operated in parallel, the determined power was distributed equally to both heat pumps. These results rounded up to the next integer in the configuration, which is shown in Table 6-6. The used procedure is a simplification, which is why a slightly over dimensioning of the heat pumps is expected.

Table 6-6: Required condenser capacity of one heat pump at B0W35

Q_{heat_ideal} [kWh/(m²*a)]	$\dot{Q}_{\_cond}$ [kW]
8	11
22	14
36	16
50	18
64	20

For these heat pumps, the characteristic curves were generated with the program EES. The data of the installed 10 kW heat pump (see in Table 3-2) were used and the capacity was scaled upwards according the needed one. That means that the efficiency of all heat pumps in Table 6-6 is the same.

The selected method of capacity determination results in a significantly higher heat pump capacity than it is installed in Weiz (Q_{heat_Weiz} ≈ 26.5 kWh/(m²*a); $\dot{Q}_{\_cond}$ = 16 kW). However, the system in Weiz was designed, according to the energy performance certificate, for a building with a specific SH demand of 9.44 kWh/(m²*a) and a specific DHW demand of 12.78 kWh/(m²*a). The building considered here with a specific SH demand of 8 kWh/(m²*a) has already a specific DHW demand of 20.1 kWh/(m²*a). In total, this building already has a higher energy demand, than the system in Weiz, which is why a higher heat pump performance appears to be useful.

This parameterization was adopted in the original TRNSYS project (real heating system), with which a further sensitivity analysis was carried out for each building. The specific heat demand was determined with the standard climate under the condition of ideal heating. In Table 6-7, it is shown what this means for the buildings with the other climate data and without ideal heating.

Table 6-7: Actual specific heat demand of the different buildings

building (Q_{heat_ideal})	specific SH demand [kWh/(m²*a)]			spec. DHW demand [kWh/(m²*a)]
	standard	cold	warm	
8	7.3	14.1	2.7	20.1
22	19.5	29.3	12.0	20.1
36	32.5	43.4	22.7	20.1
50	44.9	59.0	32.2	20.1
64	56.7	71.6	43.5	20.1

It is seen that both the switch away from ideal heating and the different climate have a great influence on the actual heat demand. Hence, the building which has a heating demand of 22 kWh/(m²*a) with ideal heating and standard climate data has only a heat demand of 19.5 kWh/(m²*a) with the real heating system and standard climate data . With the real system and the cold climate the heating demand of this building increases to 29.3 kWh/(m²*a), while it drops down with the warm climate data to only 12 kWh/(m²*a).

Furthermore, it should be noted that the size of the building is unvaried. All specific values are, therefore, referred to the same heated area of 957 m². For this reason, the specific values are well comparable and the additional specification of the absolute values is omitted.

6.4 Sensitivity analysis for the elaboration of the design guideline

As with the validated system in chapter *6.2 Sensitivity analysis of the validated system*, a sensitivity analysis was carried out with the simulated buildings as well. This was done for every building and every climate. As starting point the current configuration (V_{ice} = 21 m³; A_{coll} = 30.4 m²) was scaled on the basis of the heat pump capacity. With a current heat pump capacity of 16 kW, this results in a specific ice storage volume of 1.3125 m³/kW and a specific collector area of 1.9 m²/kW. The outcome from the specific values multiplied with the heat pump capacity from Table 6-6 is the chosen starting point for each building. From this starting point, the analysis was carried out in 25 % steps up- and downwards to identify the trend of the system behaviour. Based on this, relevant points for the design guideline were resolved more closely. Figure 6-10 to Figure 6-12 show the results for the 36 kWh/(m²*a) building (with ideal heating) for the different climate data with a more detailed resolution.

For the standard climate data, shown in Figure 6-10, the chosen starting point (0 %) would be a relatively good one. With this design, the share of the auxiliary heating is nearly zero. From the point on where no auxiliary heating is necessary anymore, the further enlargement of the components has hardly any positive influence. However, with an increasing share of auxiliary heating, the SPF drops down relatively quickly. The reduction of the ice storage has quite a stronger influence on this. This is more apparent in the share of the auxiliary heating. Considering the SPF, the influence is smaller because with a larger collector area higher flow temperatures can be achieved, which also has a positive influence on the system. If both are reduced simultaneously, this has the most significant influence. The joint increase is to be understood in such a way that the collector area and the ice storage volume are both increased (e.g., by 5 % at

the 5 % mark on the x-axis). It is shown that the decrease of the auxiliary heating down until about 1 % is relatively uniform, but that the last percent is comparatively difficult to reduce. Moreover, from the starting point on, the enlargement of the collector area has nearly any influence on the share of the auxiliary heating. To avoid auxiliary heating, a certain ice storage volume is necessary, if the collector area is not to be enlarged extremely.

The description of Figure 6-10 as "*Sensitivity analysis of the $Q_{\_heat\_ideal}$ = 36 kWh/(m^2*a) building at standard climate data*" must be understood in the sense that the building, which has a specific heat demand with ideal heating and standard climate of 36 kWh/(m^2*a), is simulated with the real heating system and standard climate. In the simulation with the real heating system and with different climate data, different actual SH demands occur for the building with $Q_{\_heat\_ideal}$ = 36 kWh/(m^2*a). Therefore, in Figure 6-10 until Figure 6-14 the actually occurring SH und DHW demand for each case is specified too. With equation (5-6) the overall electric energy consumption (heat pumps, circulation pumps, auxiliary heating) can be calculated, by knowing the SPF_{System}, the SH demand and the DHW demand. In Figure 6 10 with a SPF_{System} of 3.0 (10 % increase of both components), this would result for example in an overall electric energy consumption of 16780 kWh/a.

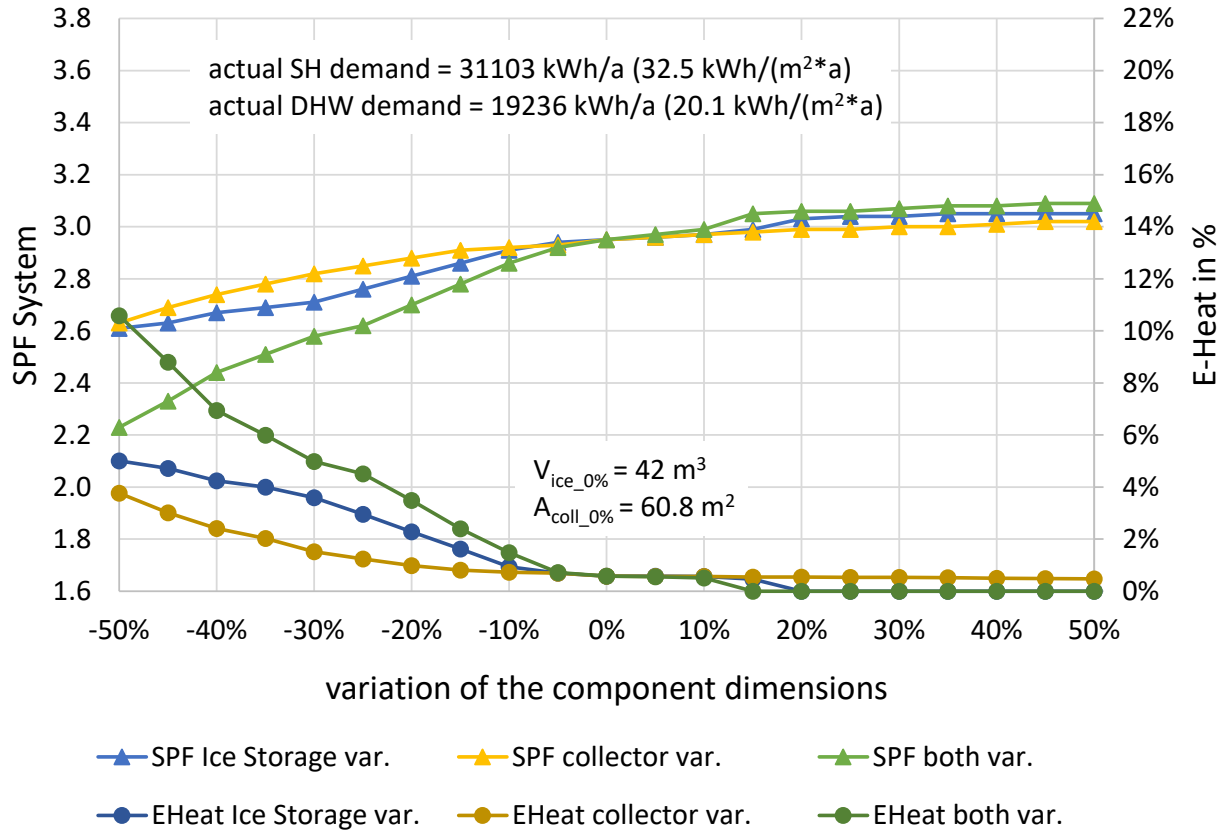

Figure 6-10: Sensitivity analysis of the $Q_{\_heat\_ideal}$ = 36 kWh/(m^2*a) building at standard climate

As expected, a much higher share of auxiliary heating is necessary for the cold climate with the same design, which also affects the SPF_{System}. To avoid the need of auxiliary heating, the components must be enlarged much more as for the standard climate data. It is also shown that with the enlargement of the collector alone, it is hardly possible to reach a lower share of auxiliary heating than 6 %.

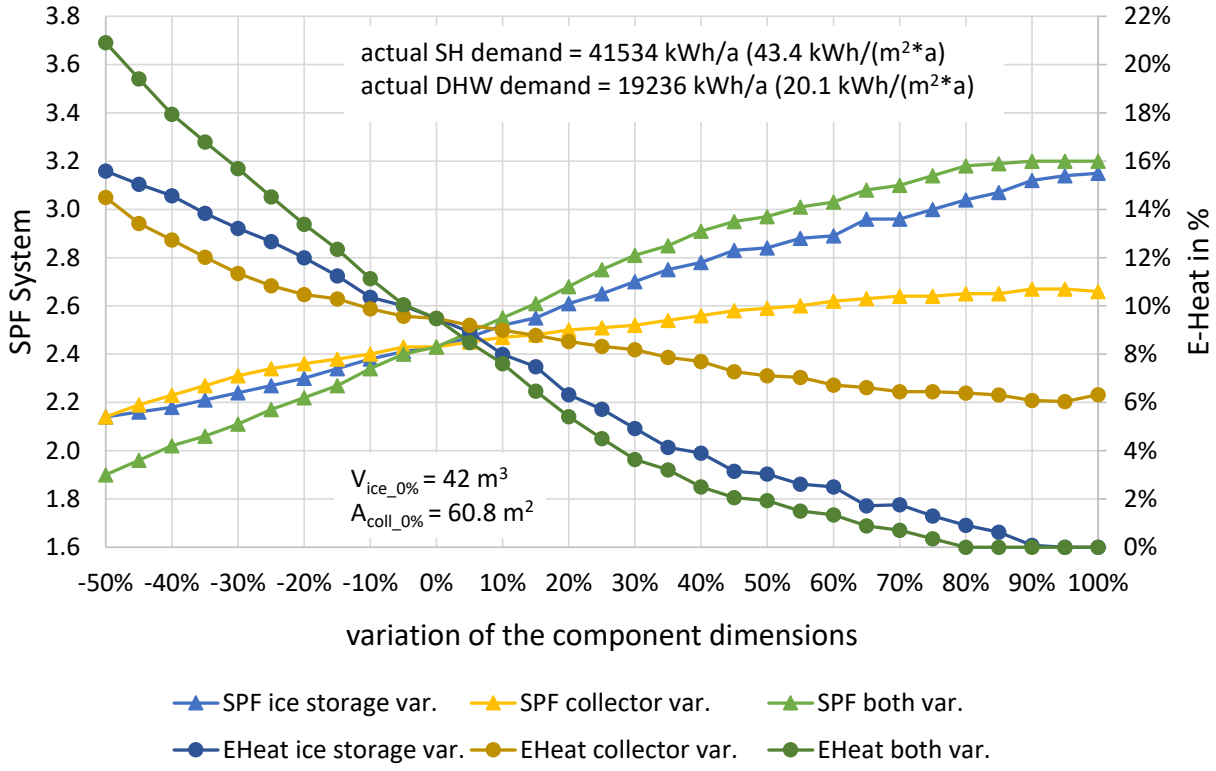

Figure 6-11: Sensitivity analysis of the $Q_{\_heat\_ideal}$ = 36 kWh/(m²*a) building at cold climate

If the system would be designed for the warm climate, in this case a reduction of the components would make sense.

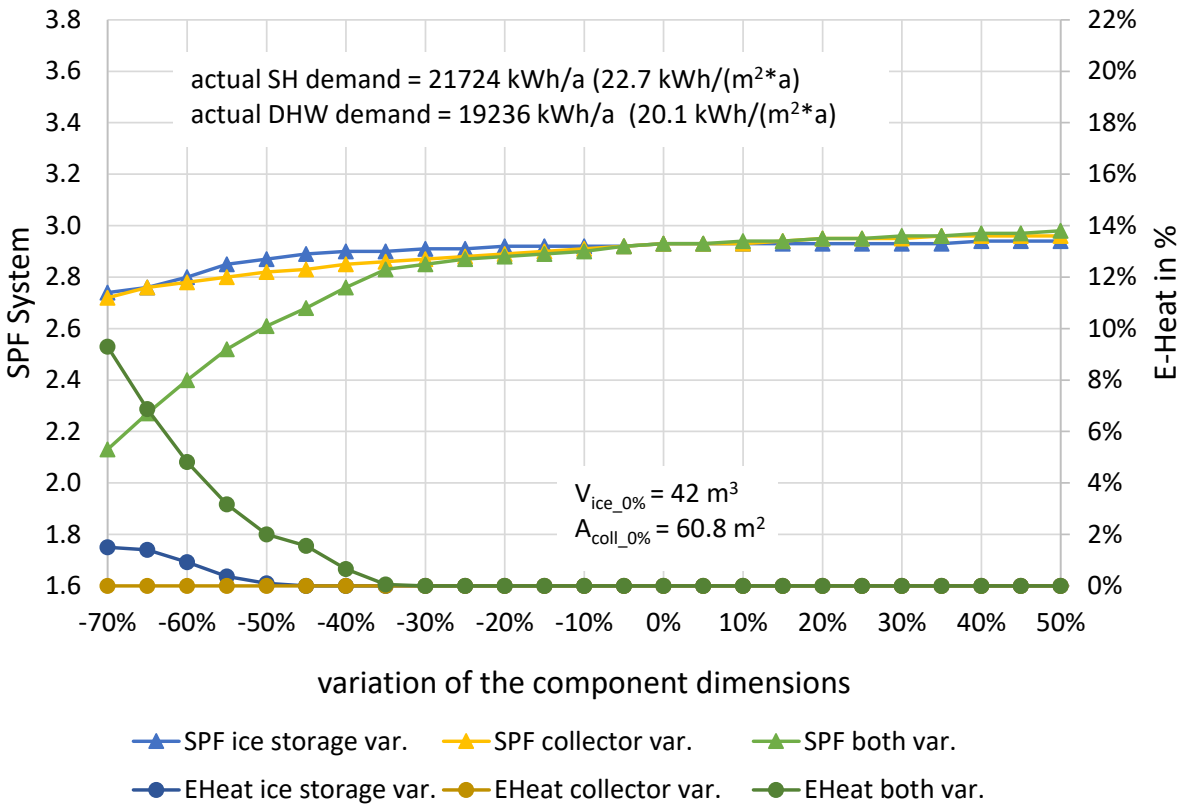

Figure 6-12: Sensitivity analysis of the $Q_{\_heat\_ideal}$ = 36 kWh/(m²*a) building at warm climate

It is shown that, for example, the design for 0 % auxiliary heating differs a lot for the different climate data. This is logical, since, as shown in Table 6-7, quite different SH demands occur. Therefore, a separate design guideline is created for each climate. It would certainly make no sense to design a building for the best possible case (warm climate) but the design guideline for the warm climate gives an insight how the system for such a building must be designed when it is built at a different place with a warmer climate.

The sensitivity analysis of the other buildings is relatively similar, which is why not all of them are discussed in detail. The other ones which are not shown here can be found in the appendix. However, one significant difference occurs between the individual buildings, namely that the maximum achievable SPF_{System} increases with the (specific) SH demand. To illustrate this, in Figure 6-13 and Figure 6-14 the building with the lowest and the biggest heat demand is illustrated at standard climate. It is shown that for the 8 kWh/(m²*a) building the SPF_{System} is limited at about 2.4 while for the 64 kWh/(m²*a) building a SPF_{System} up to 3.5 can be achieved. The 36 kWh/(m²*a) building is with about 3.1 in between.

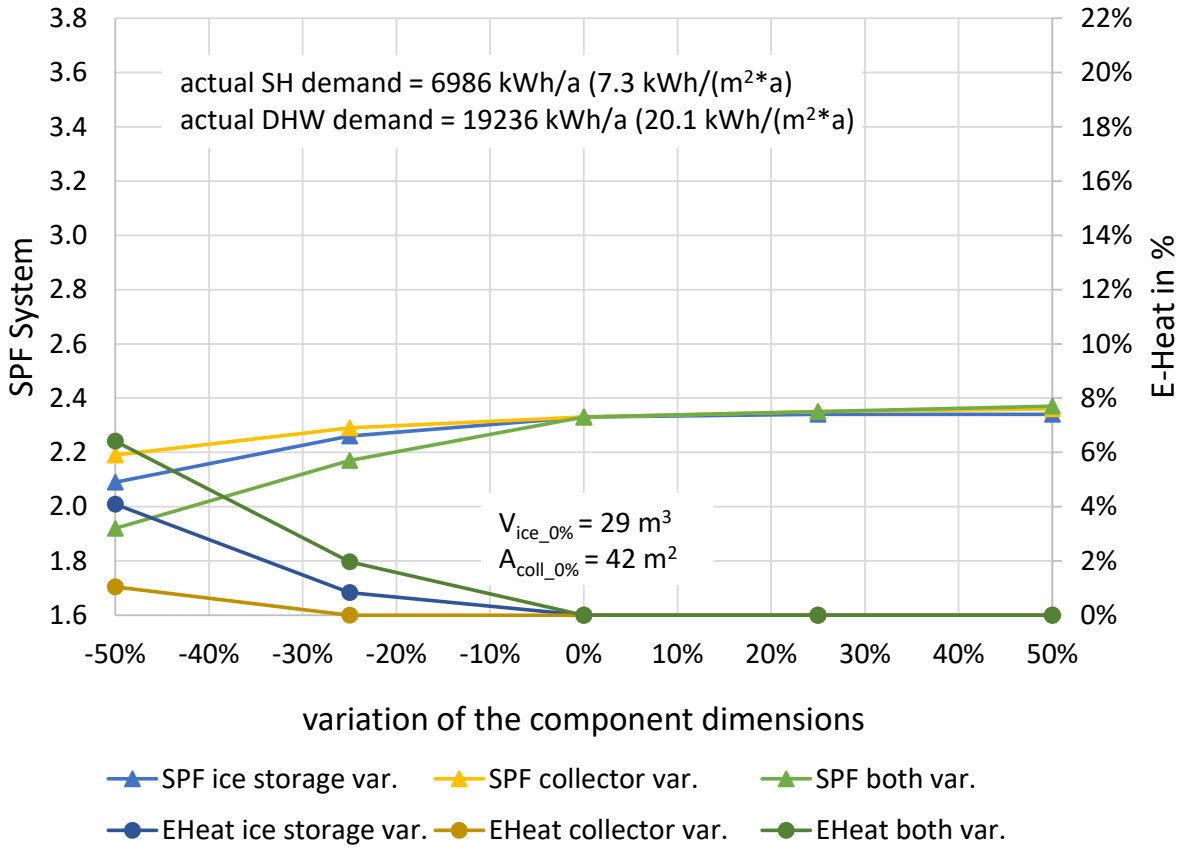

Figure 6-13: Sensitivity analysis of the $Q_{\_heat\_ideal}$ = 8 kWh/(m²*a) building at standard climate

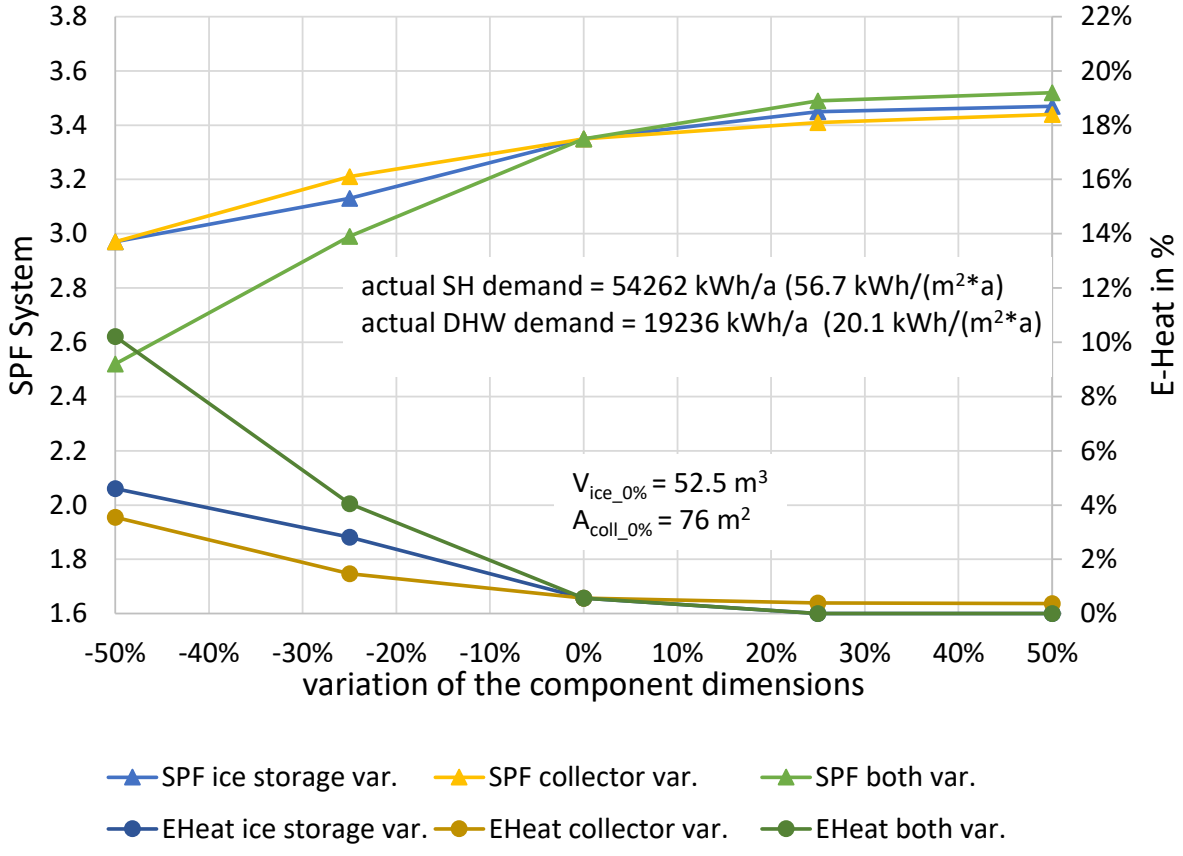

Figure 6-14: Sensitivity analysis of the $Q_{\_heat\_ideal}$ = 64 kWh/(m²*a) building at standard climate

This is because it is more efficient for the heat pump to provide heat for the SH than for the DHW storage (also shown in Figure 4-12) because for the SH storage a lower temperature level is needed. Since the DHW demand is constant for all buildings and only the SH demand is varied, the share between them also differs for the different buildings. For the standard climate, this is illustrated in Figure 6-15. As shown, the share between the buildings varies significantly. As a result, the same SPF_{System} cannot be achieved for all buildings.

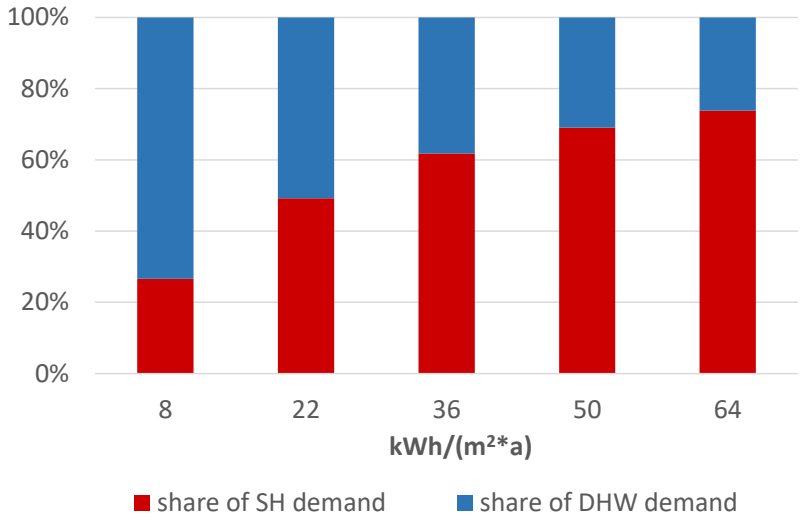

Figure 6-15: Share between SH & DHW demand (standard climate)

This effect also occurs between the different climate data which is why the in each case maximum achievable SPF of the system is for the cold climate higher than for the warm one.

Based on this, it can be said, that an installation of a solar-ice storage-heat pump system is more advisable when the share of the SH demand is comparatively large compared to the DHW demand.

Since the 8 kWh/(m^2*a) building is an extreme case, with a maximum SPF_{System} under 2.4 (SH 27 %, DHW 73 %), this building was excluded from the design guideline.

6.5 Results for the design guideline

Since the maximum achievable SPF_{System} is varied according to the building, the share of the auxiliary heating was taken as a benchmark for creating a first design guideline. As soon as no auxiliary heating was needed, the SPF_{System} could hardly be increased. Therefore the configuration in which no auxiliary heating was necessary any more was selected as one option in the design guideline. With this design, the maximum SPF could be achieved for every building. In addition, a guideline was created that allows 1 % (±0.1 %) auxiliary heating, since the reduction of this last percent required a little more effort (especially at standard climate data). With this design, some percentage of ice storage volume and collector area could be saved but small reductions in the SPF_{System} had to be accepted. The dimensions for 3 % (±0.1 %) auxiliary heating are also shown in the diagram, since in some cases it can be advisable to allow a higher percentage of auxiliary heating.

The results are shown in Figure 6-16 until Figure 6-18 for the different climate data. The additional demand of collector area and ice storage volume for the different buildings increases approximately linearly with the increasing heating demand. In Figure 6-16, a reading example for these diagrams is illustrated. For example, for a building with a specific heat demand of 40 kWh/(m²*a), a heat pump capacity of 0.035 kW/m² (heated area), an ice storage volume of 0.056 m³/m² and a solar collector area of 0,079 m^2_{coll}/m^2 are needed for the design with 0 % auxiliary heating. This design also includes a specific DHW demand of 20.1 kWh/(m²*a) and is valid for the standard climate data.

With an auxiliary heating share of 1 %, up to 20 % of collector area and ice storage volume can be saved (e.g. for a 40 kWh/(m²*a) building 0.056 m³/m² for 0% & 0.045 m³/m² for 1 % auxiliary heating is needed). With this design an around 0.2 lower SPF is to be expected. I.e., relatively much component size can be saved with relatively low efficiency declines. If the system is designed for 3 % auxiliary heating, additional collector area and ice storage volumes can be saved. However, with the standard climate data, the difference is no longer as big as between 0 % and 1 %. Which design gets selected can be decided individually depending on the respective application and the associated costs.

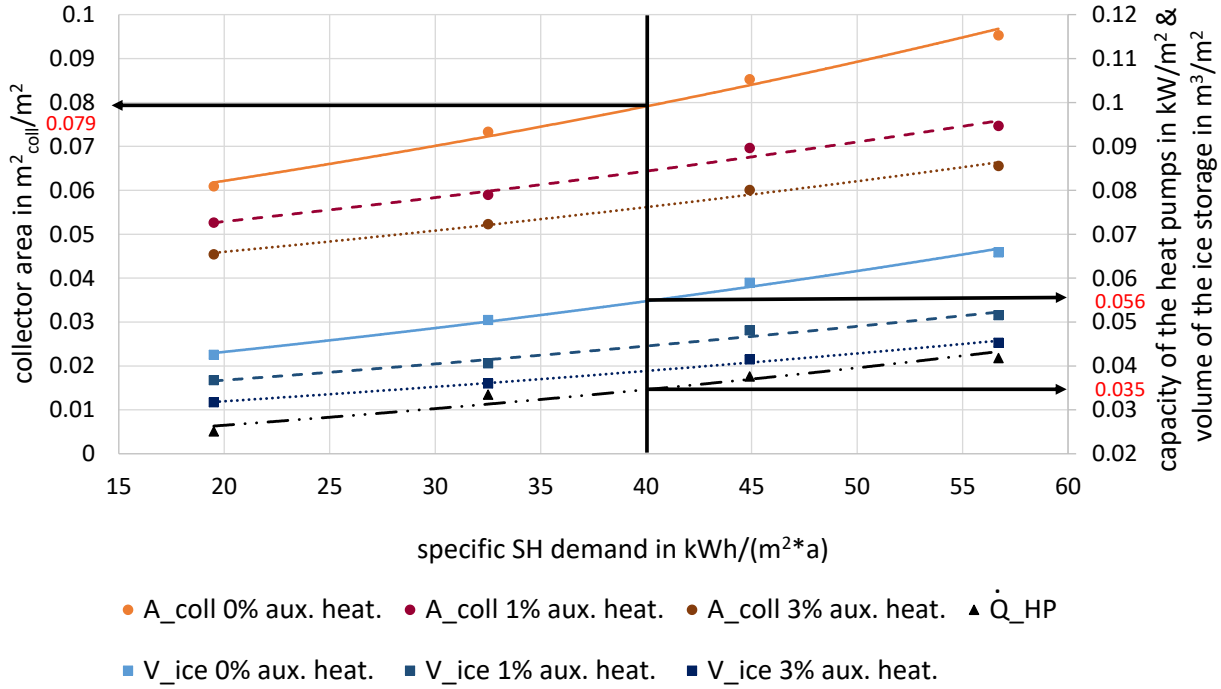

Figure 6-16: Design guideline for the standard climate data including 20.1 kWh/(m²*a) specific DHW demand

For the cold climate (Figure 6-17) and for the warm climate (Figure 6-18) the trend is similar, with the difference that for the cold climate more collector area and more ice storage volume is necessary, while it is the opposite for the warm climate data. So, if one compares a building which has a specific heat demand of 30 kWh/(m²*a) at the warm climate data with one, which has the same demand at the cold climate, it is seen that for the cold climate approximately twice as much ice storage volume and collector area is needed. This confirms, that the amount of the SH

demand alone does not directly suggest the share of the auxiliary heating. Moreover, it is shown in Figure 6-11, that with the cold climate the reduction of the auxiliary heating is almost linear. This is also shown in Figure 6-17 at the difference between 1 % and 3 % auxiliary heating, where the gradation is much more uniform.

With the warm climate, in contrast to the standard climate, the reduction of the collector area and the ice storage volume is very low at a share of 1 % of auxiliary heating. In this case, a substantial reduction of the components is only possible with the design for a share of 3 % of auxiliary heating.

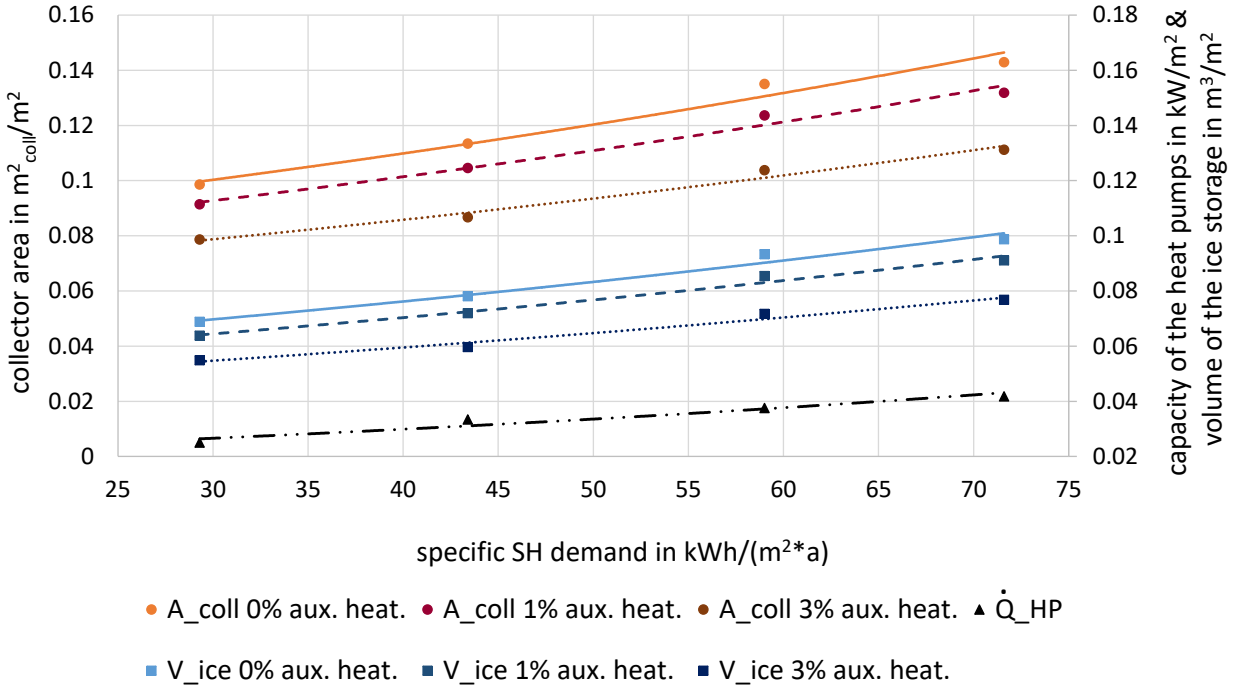

Figure 6-17: Design guideline for the cold climate data including 20.1 kWh/(m²*a) specific DHW demand

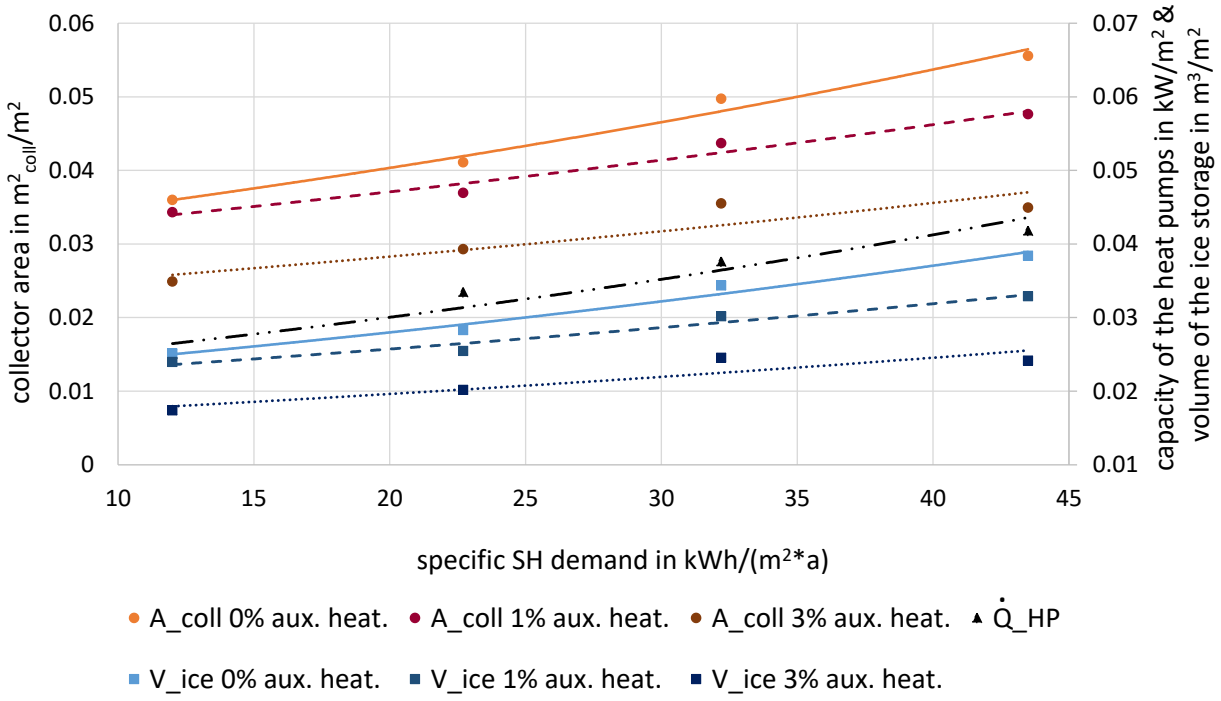

Figure 6-18: Design guideline for the warm climate data including 20.1 kWh/(m²*a) specific DHW demand

To illustrate the spread between the different climate data, they are plotted together in Figure 6-19 for the 1 % auxiliary heating case. In this figure, the buildings are referenced to the specific SH demand at ideal heating and with standard climate data to make them comparable. That means, for example, that the building, which has a specific SH demand of 36 kWh/(m²*a) with ideal heating and at standard climate data is simulated with the real heating system and different climate data. This building is marked for all climate data as 36 kWh/(m²*a) building, although it has another SH demand at the different climate data (shown in Table 6-4).

It is shown in Figure 6-19 that for the different climate data a completely different design is necessary. For example, for a building with a specific heat demand of 40 kWh/(m²*a) (ideal heating) with the cold climate, a collector area of 0.108 m^2_{coll}/m^2 with the standard climate, an area of 0.06 m^2_{coll}/m^2, and with the warm climate only an area of 0.038 m^2_{coll}/m^2 is needed. Therefore, it is important to consider carefully for which climate a building should be designed. The diagrams for the 0 % and the 3 % auxiliary heating case can be found in the appendix in Figure A- 12 and Figure A- 13.

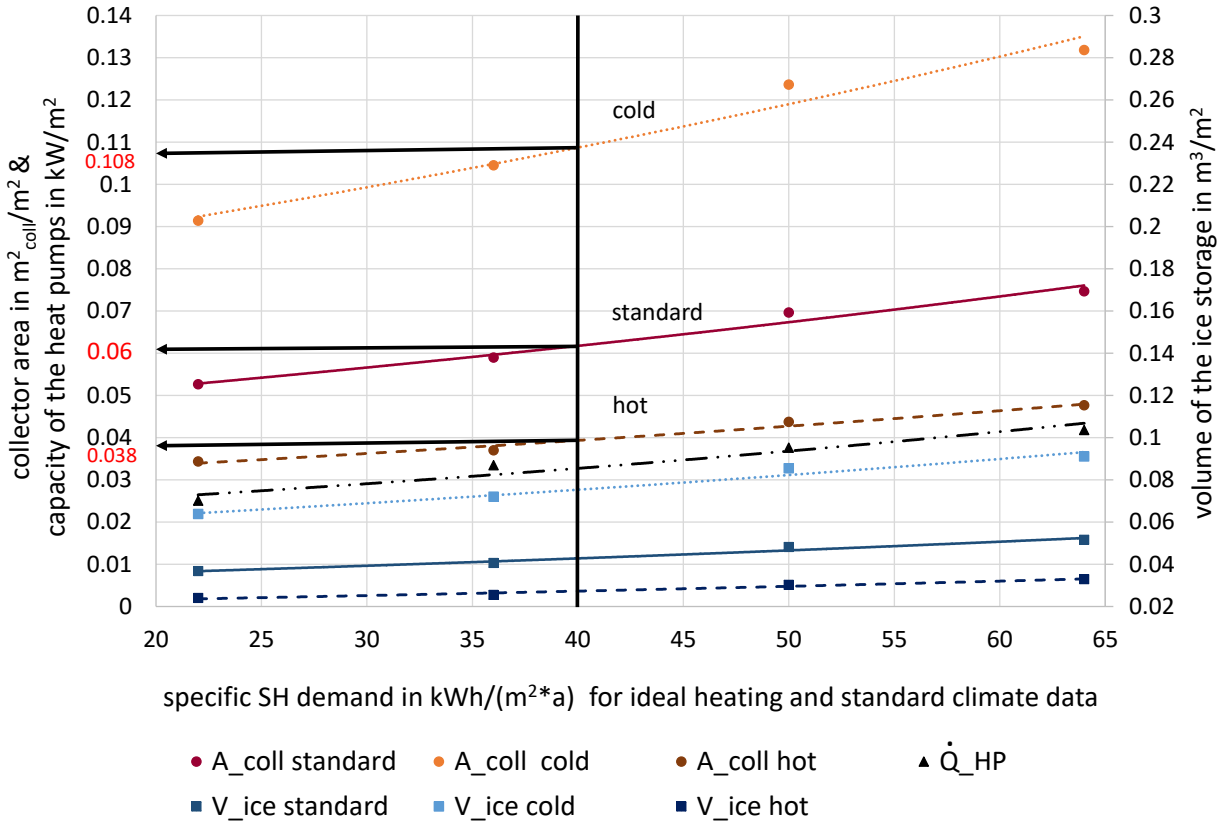

Figure 6-19: Comparison of the designs for 1 % auxiliary heating and for different climate data including 20.1 kWh/(m²*a) specific DHW demand

These results are to be understood as one possibility to design such a system. As a next step, it would also be interesting to include the costs involved as additional parameter. These further possibilities of creating a design guideline were not discussed in this master thesis as they would have gone beyond the scope of this study.

7 CONCLUSION

Summing up, it can be said that the system in Weiz partly needs some small corrections but as a whole it operates largely stable. However, a significantly higher space heating and domestic hot water requirement is needed in the building than it is stated in the energy performance certificate. What means, that the overall system was designed under the assumption of too low demands. This is why, the ice storage cooled down relatively fast during longer cold periods, what results in the fact that the entire ice storage was subcooled and could not be used as source for the heat pump any more. During these times, the building had to be heated with the auxiliary heaters, until the ice storage was regenerated again. As shown in the simulation results with a higher share of auxiliary heating, the efficiency of the system decreased relatively fast. For the considered year 2016 this share of 3.4 % was not too high but this year has been a comparatively warm one. Therefore, it is possible that years with a significantly higher share of auxiliary heating, respectively a lower SPF_{System} may occur. A simulation for estimating the trend of the next years shows that a share of more than 6 % is to be expected with the generated standard climate data for the location in Weiz. This leads to a SPF of the overall system of 2.4. The measurement data from the beginning of the year 2017 support this trend. Furthermore, this under-dimensioning makes it difficult to make a meaningful comparison by means of the system in Weiz to similar heating systems, such as geothermal ones. Moreover, it is shown that the burying of the ice store, which is also a way of using the heat of the soil, has a positive influence. In this way, a considerable share of energy could additionally be gained every month.

In addition, an already existing TRNSYS simulation model could be adjusted by validation in that way that it correlated with the real situation in Weiz. For the solar collector, it was possible to parameterize the TRNSYS type in such a way that one collector model was sufficient, even though the simulation model was not a two-layered system, as it was the case with the installed collector. The validation of the ice storage in combination with the ground type was slightly more complex, since the existing TRNSYS model differed in some respects from the actual installed one. Especially the fact that the ice storage model had only one heat exchanger, made the matter difficult. In addition, due to the programming, the used type for the soil coupling did not allow a validation with the optimization tool TRNOPT, therefore, the optimal parameterization had to be found manually. However, in the end a parameterization could be found, so that the ice storage temperature in the simulation matched with the measured data. The phase transition, the subcooling as well as the subsequent regeneration could be reproduced very well. With a final validation of the overall system, the space heating as well as the domestic hot water demand of the real system could be reproduced exactly. For this purpose, the validated single components were integrated into the overall system and the control was adjusted in the same way as in Weiz. Only the two heat pumps were always operated in parallel in the simulation model because the actual control algorithm was unknown. The unknown parameters, such as the window ventilation, were varied until the results matched with the measurement data. In this way, in addition to the heat demands, the other key figures as well as the energy flows could be represented very well.

With this validated system, a fist design guideline for such solar-ice storage-heat pump systems could be created. The design guideline was based on the system heat demand of the buildings. Since the heat demand is known from the energy performance certificate in the construction of a building, a simple dimensioning of such systems is thereby possible. However, as the situation in Weiz shows, the information of the energy performance certificate should not be trusted blindly. For elaboration the guideline, multi-family buildings with different heat demand were created and for each system the required area of the solar collector as well as the required size of the ice storage volume were determined. Since the domestic hot water requirement was not varied, the different buildings achieved different maximum SPF_{System}, depending on the share between space heating and domestic hot water requirement. Therefore, the design guideline was related to the amount of auxiliary heating to achieve the best efficiency for each building. This was created for 0 %, 1 % and 3 % auxiliary heating, since with a slightly higher percentage of auxiliary heating a significant reduction of collector area and ice storage volume could be achieved. A decision which design gets selected can thereby made individually for each case.

The elaborated design guideline is one possibility to design such a system. As a next step, it would be interesting to include the costs involved as an additional parameter.

8 REFERENCES

ABB i-bus®. 2017. KNX EM/S 3.16.1 Datenblatt. [Online] 2017. [Zitat vom: 06. 04 2017.] http://www.knx-gebaeudesysteme.de/sto_g/English/TECHNICAL_DATA/SINGLE/EMS_3161_TD_DE_V1-0_2CDC512069D0101.PDF.

Benkert, St. und Heidt, F. D. 2000. Abschlussbericht zum Projekt: Validierung des Programms "Graphische Auslegung von ErdwärmeAustauschern GAEA mit Hilfe von Messdaten im Rahmen des Verbundprojekts "Luft-/Erdwärmetauscher" der AG Solar NRW. [Online] Universität-Gesamthochschule Siegen, 02 2000. [Zitat vom: 20. 03 2017.] http://nesa1.uni-siegen.de/softlab/download/abschlussbericht.PDF.

Cao, S.; Siren, K.; Heinz, A; Bonk, S. 2013. Models of Sub-Components and Validation for the IEA SHC Task 44 / HPP Annex 38 . http://iea-shc.org/data/sites/1/publications/T44A38_Rep_C2_E_Storage_Final_Draft.pdf. 2013.

Claußen, T. 1993. Entwicklung und experimentelle Verifizierung eines dynamischen Latentwärmespeichermodells. Universität Oldenburg : Diplomarbeit am Studiengang Diplom-Physik, 1993.

Consolar. 2017. Homepage [Online] 2017. [Zitat vom: 03. 04 2017.] http://www.consolar.de.

Diehl Metering. 2017. Sharky 775 Kompaktenergiezähler. [Online] 2017. [Zitat vom: 06. 04 2017.] http://www.diehl.com/fileadmin/diehl-metering/pdb/AT_AT_Web/familie1141551633/SHARKY_775.pdf.

Elsner Electronic. 2017a. KNX PY Pyranometer Datenblatt. [Online] 2017. [Zitat vom: 06. 04 2017.] https://store.casaio.de/media/pdf/38/79/46/KNX_PY_Datenblatt_14Jul14.pdf.

Elsner Elektronik 2017b. KNX TH-UP Thermo-Hygrometer Datenblatt. [Online] 2017. [Zitat vom: 06. 04 2017.] http://www.elsner-elektronik.de/shop/de/fileuploader/download/download/?d=1&file=custom%2Fupload%2F70366-70368_KNX-TH-UP_Datenblatt_D_23Feb17.pdf.

Elsner Elektronik. 2017c. KNX AQS/TH Innenraumsensor Datenblatt. [Online] 2017. [Zitat vom: 06. 04 2017.] http://www.elsner-elektronik.de/shop/de/fileuploader/download/download/?d=1&file=custom%2Fupload%2F70161_KNX_AQSTH_Datenblatt_18Apr16.pdf.

Elsner Elektronik 2017d. Wetterstation P03/3-RS485-GPS Datenblatt. [Online] 2017. [Zitat vom: 06. 04 2017.] https://www.voltus.de/out/pictures/media/P033-RS485-GPS_Datenblatt_01.pdf.

Energie Solaire. 2017. Homepage [Online] 2017. [Zitat vom: 23. 03 2017.] http://www.energie-solaire.com/wq_pages/de/site/page-221.php.

Greml, A. 2017. ENERGIEAUSWEIS-TIROL. [Online] 2017. [Zitat vom: 15. 02 2017.] http://www.energieausweis-tirol.at/10.html.

Gutensohn, R. 2012. Viessmann Eisspeichersystem - Ein neues Versorgungskonzept. [Online] 2017 [Zitat vom: 06. 04 2017.] http://www.fws.ch/tl_files/download_d/Downloads/Gutensohn-FWS%20%2011_2012%20Eisspeicher.pdf.

Hackl, R. 2016. Analyse einer realen Eisspeicher - Wärmepumpenanlage mit Solar - Luftkollektoren. Graz : Technische Universität Graz - Institut für Wärmetechnik: Bachelorarbeit, 2016.

Halozan, H und Holzapfel, K. 1987. Heizen mit Wärmepumpen; TÜV Rheinland; Köln,1987.

Heimrath, R. 2004. Simulation, Optimierung und Vergleich solar thermischer Anlagen zur Raumwärmenutzung für Mehrfamilienhäuser. Graz : PhD thesis, Institute of Thermal Engineering, TU Graz, 2004.

Heinz, A. 2015. Wärmespeicher Päsentation zur Vorlesung Sonnenenergienutzung. Graz : TU Graz, 2015.

HMI-Master GmbH. 2017. Homepage [Online] 2017. [Zitat vom: 06. 04 2017.] http://www.hmi-master.at/.

Hutter, G. 2016. Foto Gebäude Weiz; per E-Mail zur Verfügung gestellt. Weiz : SG ELIN Weiz, 2016.

IAE SHC. 2017. SHC Task 44 - Solar and Heat Pump Systems. [Online] 2017. [Zitat vom: 03. 04 2017.] http://task44.iea-shc.org.

ISFH. 2011. Modell eines unverglasten photovoltaisch-thermischen Sonnenkollektors für TRNSYS 16. Emmerthal, 2011.

Institute of Thermal Engineering. 2017. https://www.tugraz.at/en/institutes/iwt/home/. Graz : TU Graz, 2017.

Janßen Energieplanung. 2010. Type 708 für TRNSYS 16. Hannover, 2010.

Kummert, M. 2007. Using GENOPT with TRNSYS 16 and type 56. Glasgow : ESRU – University of Strathclyde, 2007.

Landis+Gyr. 2017. T550 Ultraheat. [Online] 2017. [Zitat vom: 06. 04 2017.] http://www.landisgyr.com/webfoo/wp-content/uploads/2013/06/Landis+Gyr-T550-UC50_Projektierungsanleitung.pdf.

Lerch, W. 2017. Doktorarbeit in Bearbeitung (Entwurf). Institute of Thermal Engineering, TU Graz, 2017.

Lerch, W.; Heimrath, R. und Heinz, A. 2016. Direct use of solar energy as heat source for a heat pump in comparison to a conventional parallel solar air heat pump system. Graz : University of Technology Graz, Institute of Thermal Engineering, 2016. http://www.sciencedirect.com/science/article/pii/S037877881500198X

Leven, B.; Neubarth, J. und Weber, C. 2001. Ökonomische und ökologische Bewertung der elektrischen Wärmepumpe im Vergleich zu anderen Heizungssystemen. Stuttgart: Institut für Energiewirtschaft und Rationelle Energieanwendung, 2001. http://elib.uni-stuttgart.de/bitstream/11682/1619/1/IER_FB80_Waermepumpe.pdf

Meteotest. 2009. Meteonorm 6.1.0.9. Global Meteorological Database for Engineers, Planner and Educations, Software and Data on CD-Rom. Bern, Switzerland, 2009.

Minder, S.; Wagner, R.; Mühlebach, M.; Weisskopf, T. 2014. Eisspeicher-Wärmepumpen-Anlagen mit Sonnenkollektoren. Bern : EnergieSchweiz, 2014.

Moisi, H. 2014. Simulation based analysis of a seasonal thermal storage system using PCM. Graz : Diplomarbeit, TU Graz - Institut für Wärmetechnik, 2014.

Moser, C. 2012. Optimierte Einbindung von Energiespeichern in industrielle Prozesse. Graz: Diplomarbeit, TU Graz - Institute für Wärmetechnik, 2012.

Moser, C. 2017. Excel Tool: „Solar Value Calculator“. Graz: TU Graz – IWT, 2017

Müllers, S. 2008. Grundschule Homburg-Bruchhof Eisspeicher–Systemlösung mit hoher Effizienz. [Online] 2008. [Zitat vom: 20. 03 2017.] http://empower-deutschland.de/dokumente/thema_energie/6_Eisspeicher.pdf.

Planungsbüro Wolfgang Enthaler GmbH. 2012. Einreichplan Wohnanlage SG ELIN. Mühlgasse 12 0860 Weiz, 2012.

Projekt HOT ICE. 2017. Fotos entstanden im Zuge des Projekts HOT ICE. http://www.innovationszentrum-weiz.at/veranstaltungen-aktuelles/detail/projekt-hot-ice. Weiz, 2017.

Schlader, W. 2013. Elektrische Wärmepumpen - Einflüsse auf die Effizienz, Ökobilanz, erreichbare Jahresarbeitszahlen. Dornbirn : Energieinstitut Vorarlberg, 2013.

SEL. 2012. TRNSYS 17 User Manual. Madison Wisconsin, USA : Solar Energy Laboratory, University of Wisconsin, 2012.

Siemens AG. 2017. Ultraschall-Wärme- und Kältezähler Datenblatt. [Online] 2017. [Zitat vom: 06. 04 2017.] https://www.downloads.siemens.com/download-center/Download.aspx?pos=download&fct=getasset&id1=A6V10388513.

Streicher, W, Heimrath, R und Heinz, A. 2015. Sonnenenergienutzung, Skriptum zur Vorlesung. Graz : Institut für Wärmetechnik, TU Graz , 2015.

TB Bierbauer GmbH. 2015. Schautafel HotIce Weiz. 2015. Kontakt: http://www.bierbauer-tb.at/index.php/kontakt.

TESS (2012). TESSLibs 17: Component Libraries for the TRNSYS Simulation Environment. Thermal Energy Systems Specialists (TESS), Madison Wisconsin, USA.

TRNSYS_17. 2011. A Transient System Simulation Program: V17.02.004. Solar Energy Lab. USA : University of Wisconsin - Madison, 2011.

VDI Wärmeatlas. 1997. Wärmeübergang und Strömung in Verfahrenstechnik und Chemie, 8. Auflage. Springer Verlag, 1997.

Viessmann. 2017. Homepage [Online] 2017. [Zitat vom: 03. 04 2017.] www.viessmann.at.

Viessmann. 2015. Montage- und Serviceanleitung VITOCAL 300-G. [Online] 2015 [Zitat vom: 04. 04 2017. http://www.viessmann.com/vires/product_documents/5724818VSA00003_1.PDF. Allendorf : GmbH, Viessmann Deutschland, 2015.

Viessman. 2014. Planungsanleitung Eisspeicher. [Online] 2014. [Zitat vom: 03. 04 2017.] https://www.alternative-haustechnik.de/media/pdf/48/eb/7b/pa-vie-z013756.pdf. Allendorf : GmbH, Viessmann Deutschland, 2014.

Viessmann. 2011. Planungshandbuch Wärmepumpen. [Online] 2011. [Zitat vom: 20. 03 2017.] http://www.viessmann.at/de/bereiche/heizsysteme/service-plus.html

Visser, H. 1986. Energy Storage in Phase Change Materials, Development of a component model compatible with the TRNSYS transient simulation program. Delft University of Technology : Department Applied Physics, 1986.

Wenzel, W.; Zivkovic, M.; Huber, H.; Köfinger, C.; Rieberer, R.; Em, G.; Studer, H.; Haage, U.; Wieshammer, G. 2006. Endbericht: Wärmepumpen, Erdkollektoren, Garten- und Wohnqualität. [Online] 2017. [Zitat vom: 09. 04 2017.] https://www.konsument.at

ZAMG. 2017. Erfassung der Klimadaten am Standort Inffeldgasse, Graz, im Zuge des Projekts: MPC-Box - Model Predictive Control of thermal activated Building Components and Measurements in Test-Boxes. https://online.tugraz.at/tug_online/fdb_detail.ansicht?cvfanr=F33110&sprache=2. Österreich, 2017.

APPENDIX

A.1 Sensitivity analysis

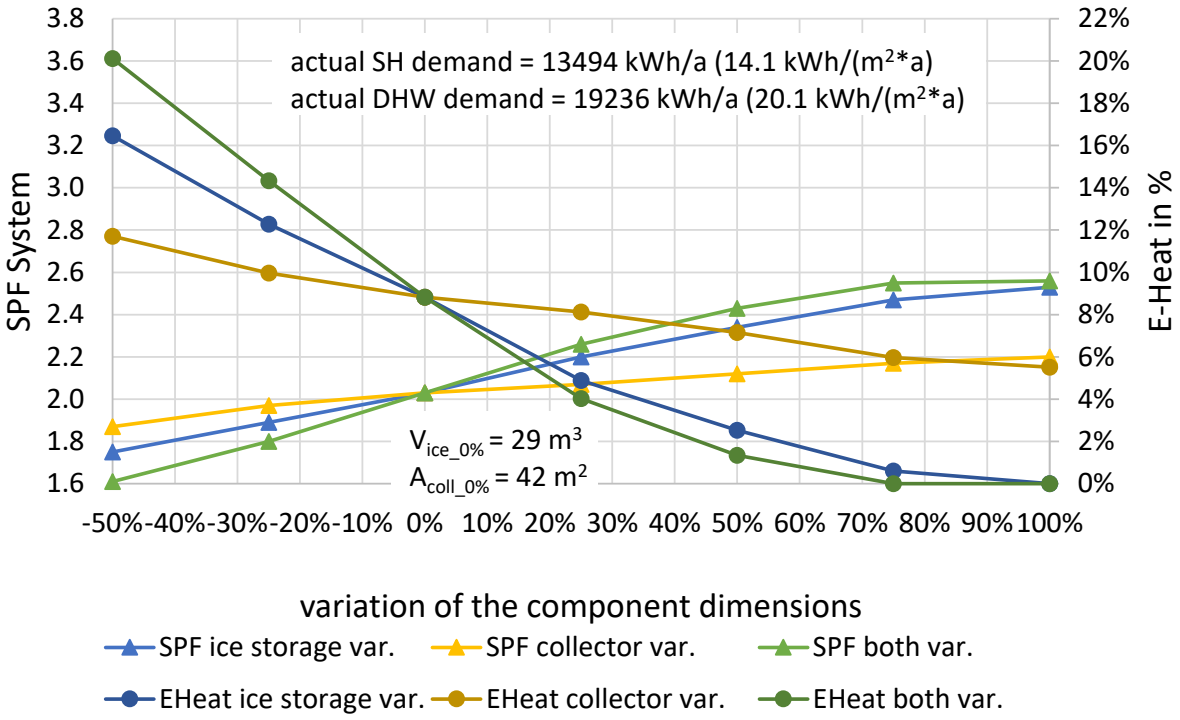

Figure A- 1: Sensitivity analysis of the $Q_{\_heat\_ideal}$ = 8 kWh/(m²*a) building at cold climate

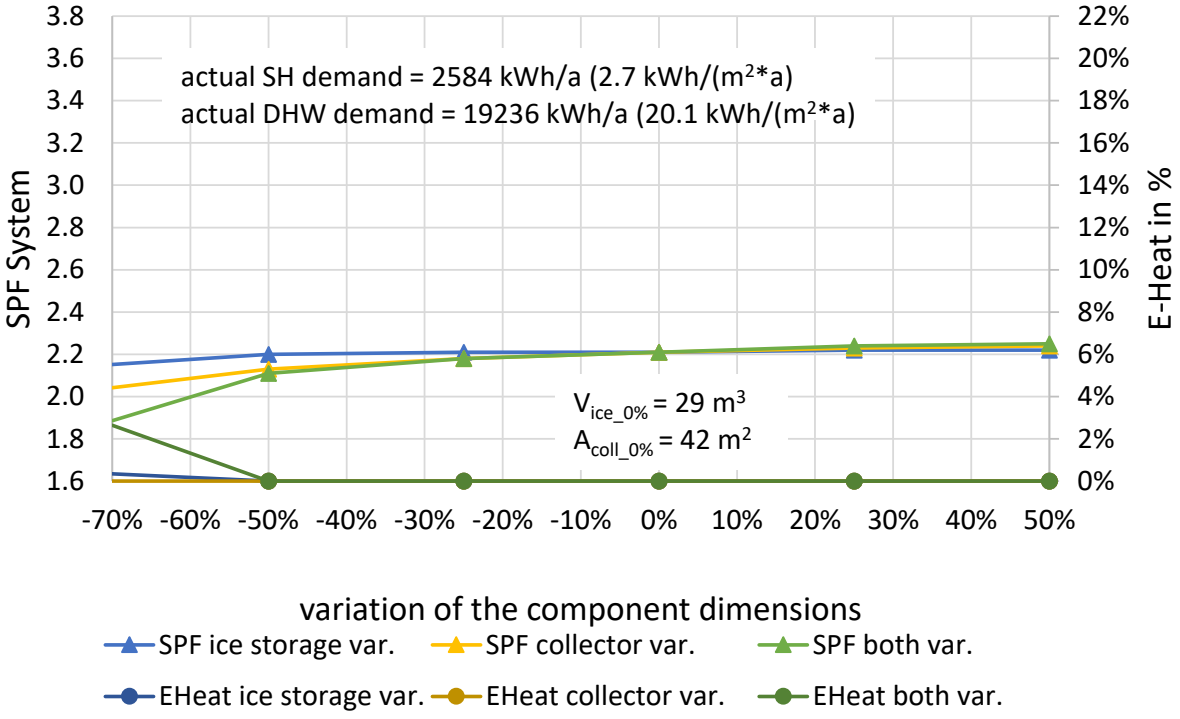

Figure A- 2: Sensitivity analysis of the $Q_{\_heat\_ideal}$ = 8 kWh/(m²*a) building at warm climate

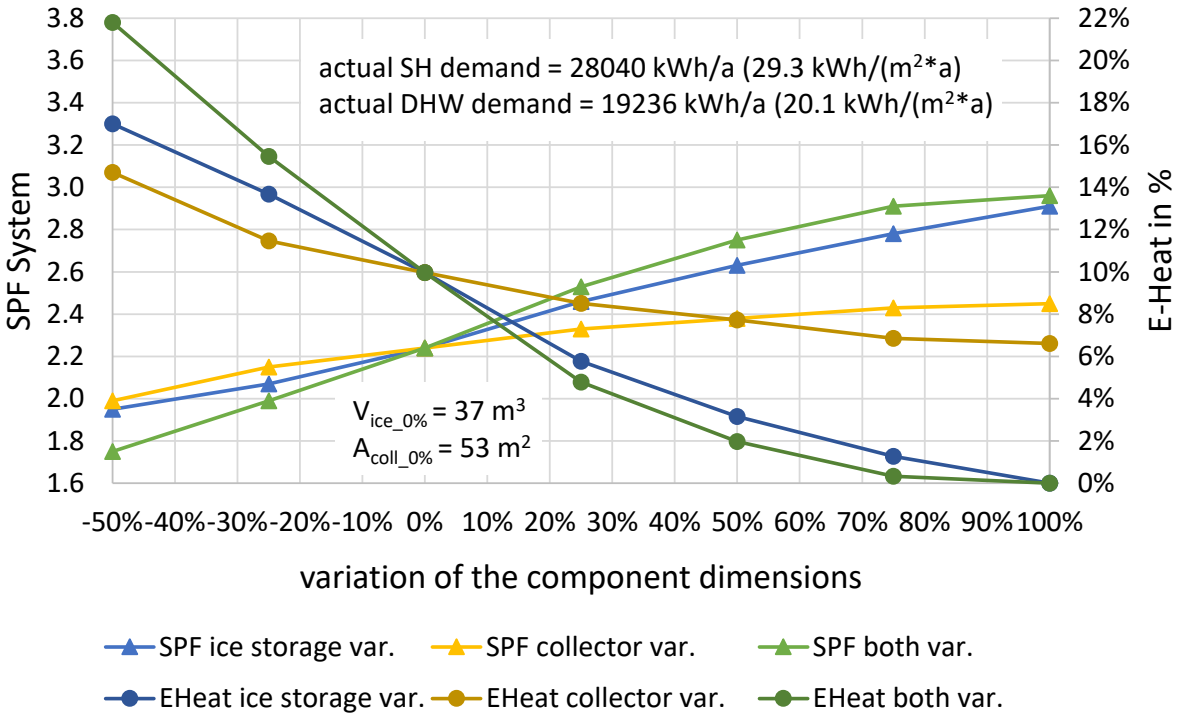

Figure A- 3: Sensitivity analysis of the $Q_{\_heat\_ideal}$ = 22 kWh/(m²*a) building at cold climate

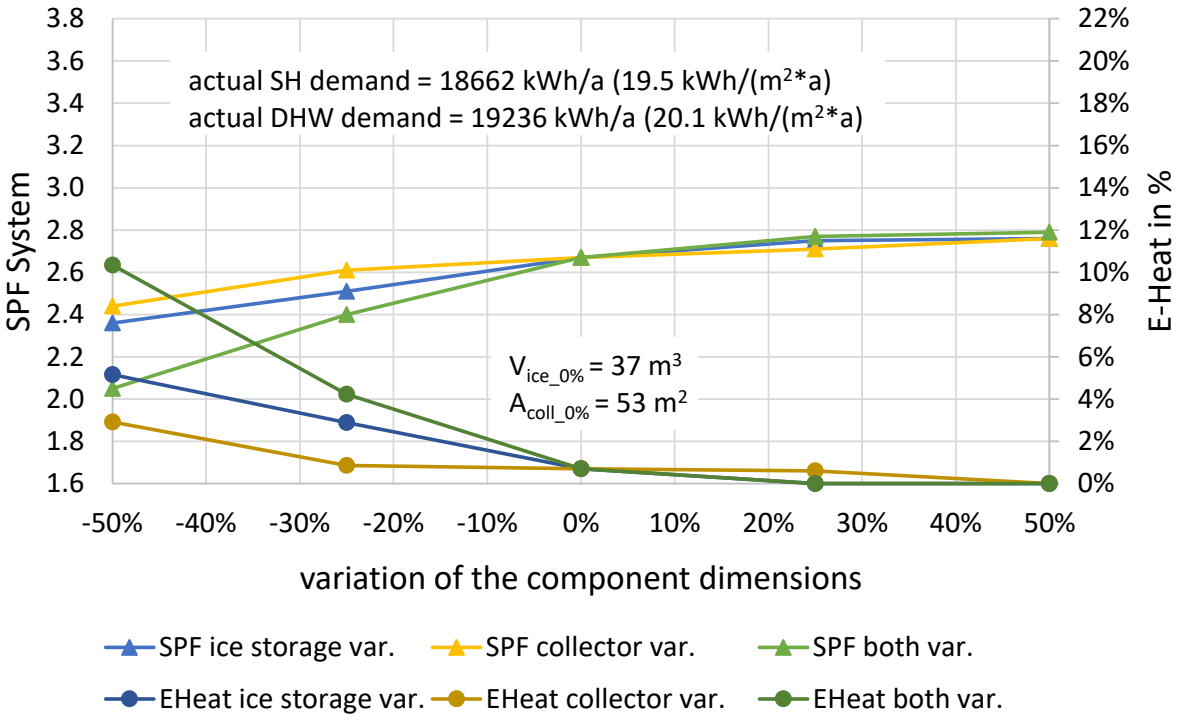

Figure A- 4: Sensitivity analysis of the $Q_{\_heat\_ideal}$ = 22 kWh/(m²*a) building at standard climate

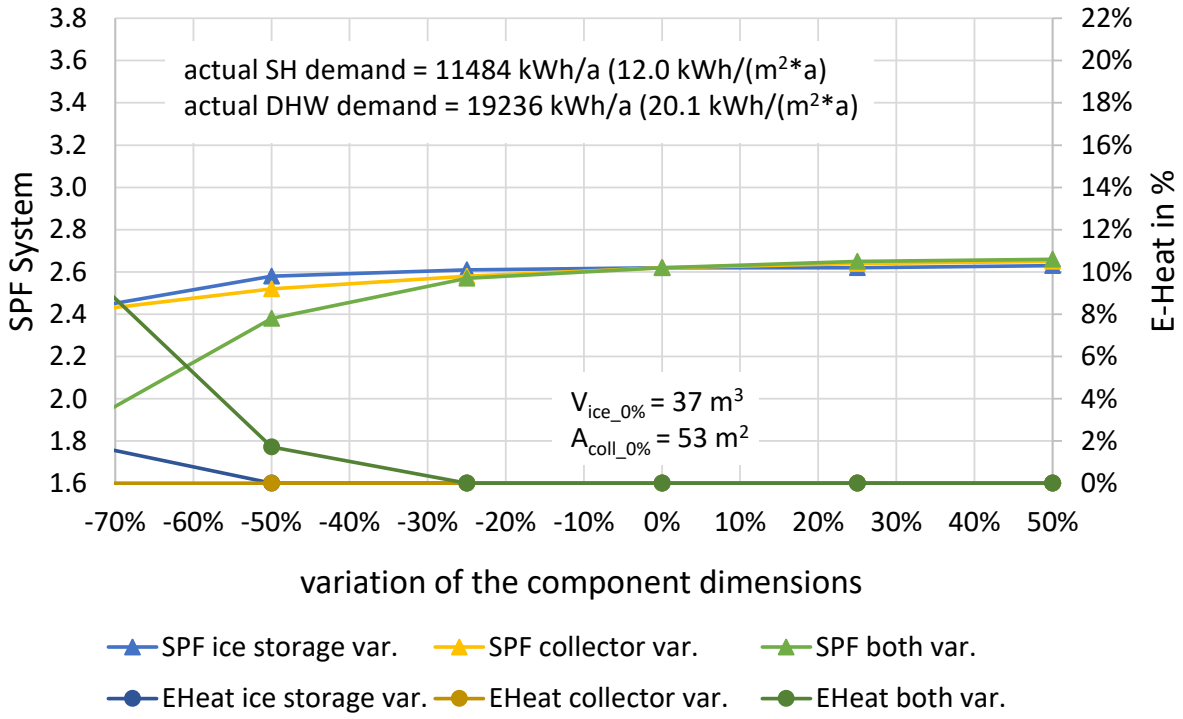

Figure A- 5: Sensitivity analysis of the $Q_{\_heat\_ideal}$ = 22 kWh/(m²*a) building at warm climate

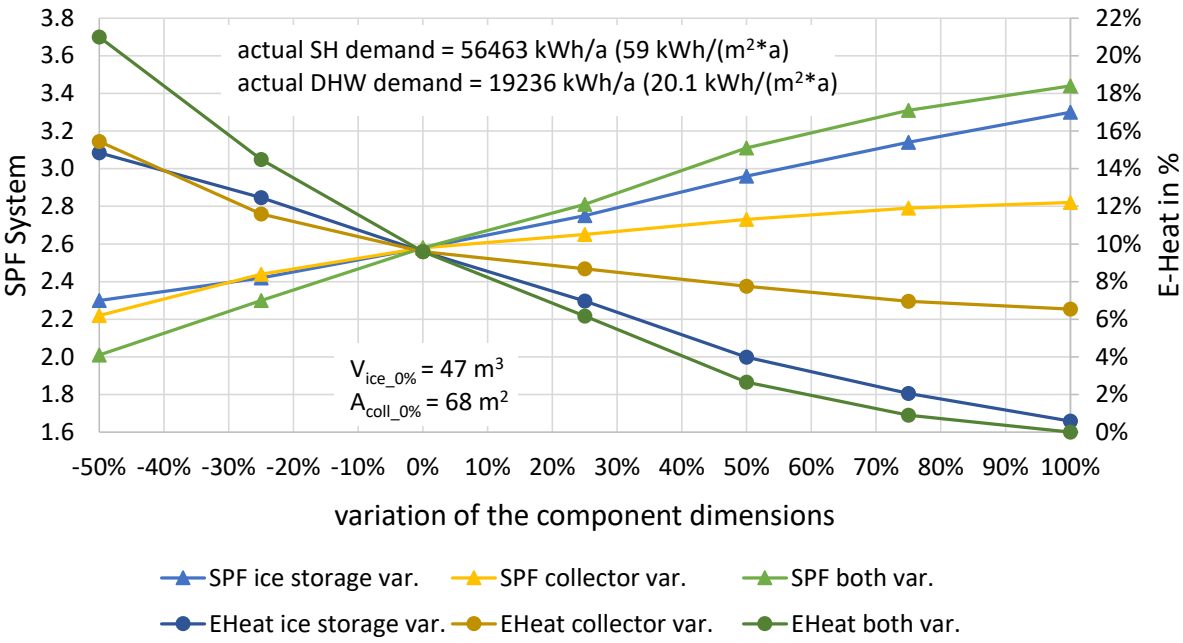

Figure A- 6: Sensitivity analysis of the $Q_{\_heat\_ideal}$ = 50 kWh/(m²*a) building at cold climate

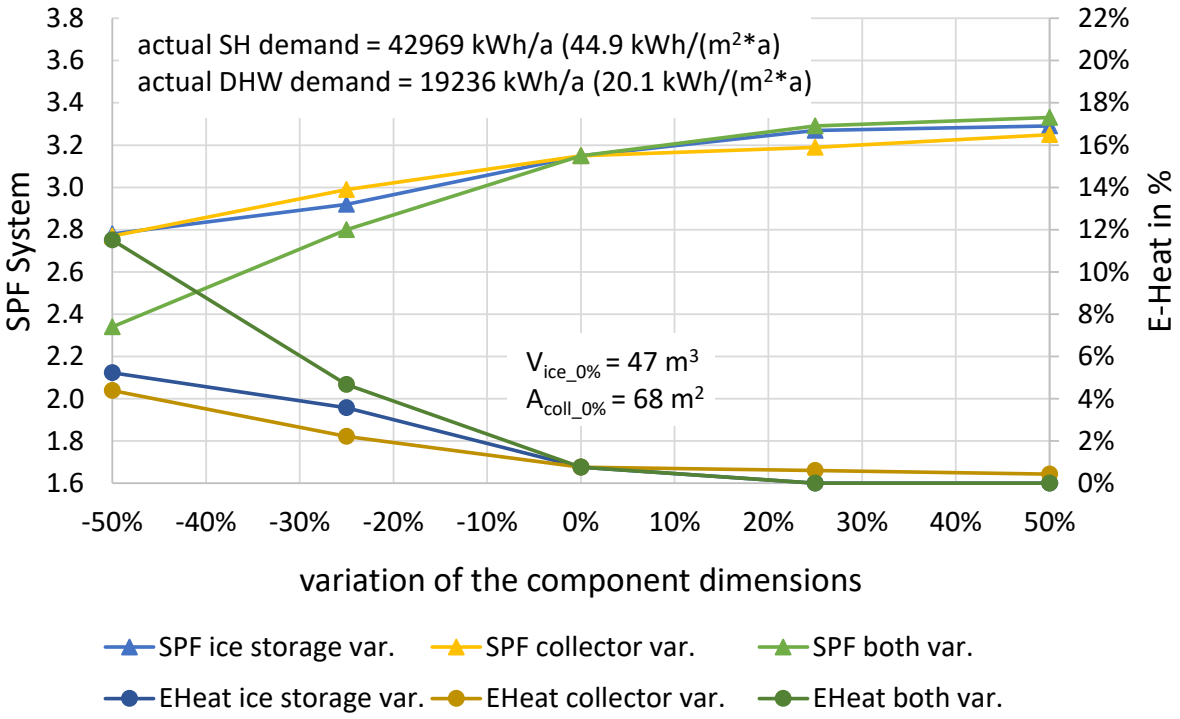

Figure A- 7: Sensitivity analysis of the $Q_{\_heat\_ideal}$ = 50 kWh/(m²*a) building at standard climate

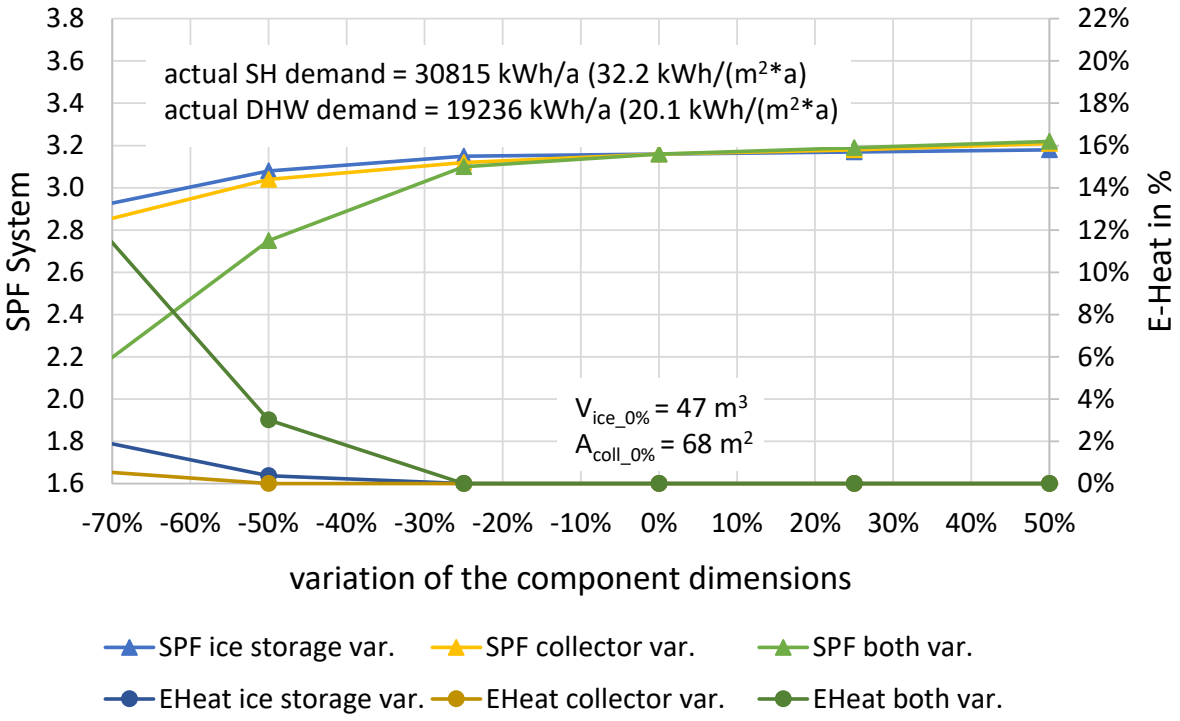

Figure A- 8: Sensitivity analysis of the $Q_{\_heat\_ideal}$ = 50 kWh/(m²*a) building at warm climate

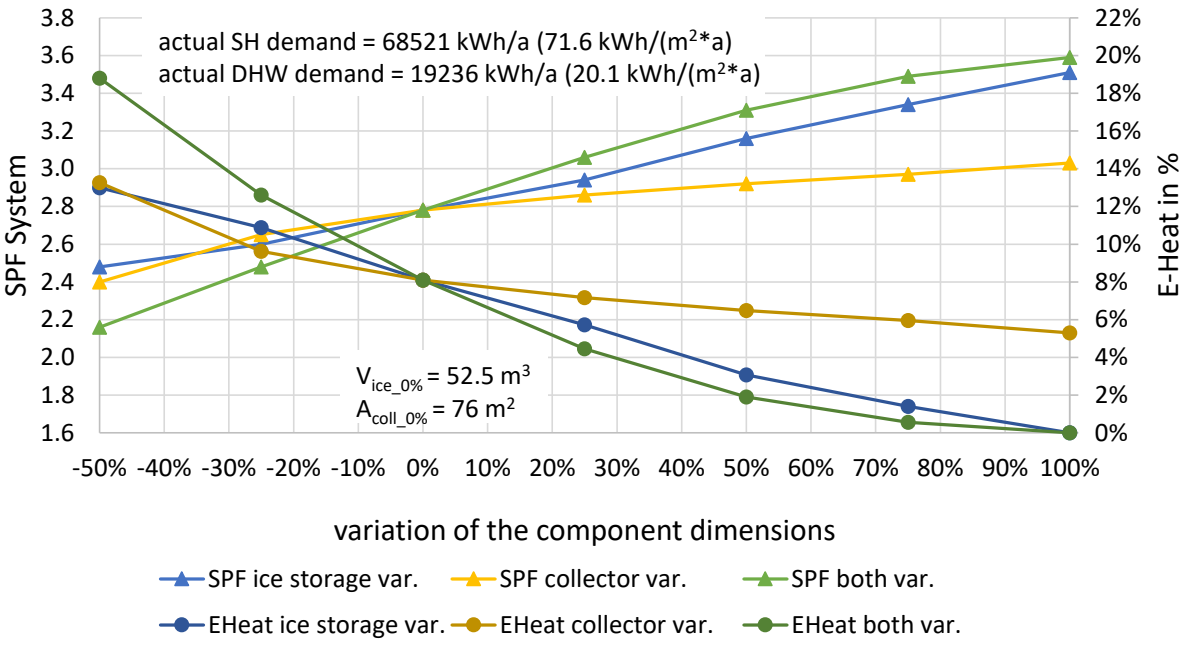

Figure A- 9: Sensitivity analysis of the $Q_{\_heat\_ideal}$ = 64 kWh/(m²*a) building at cold climate

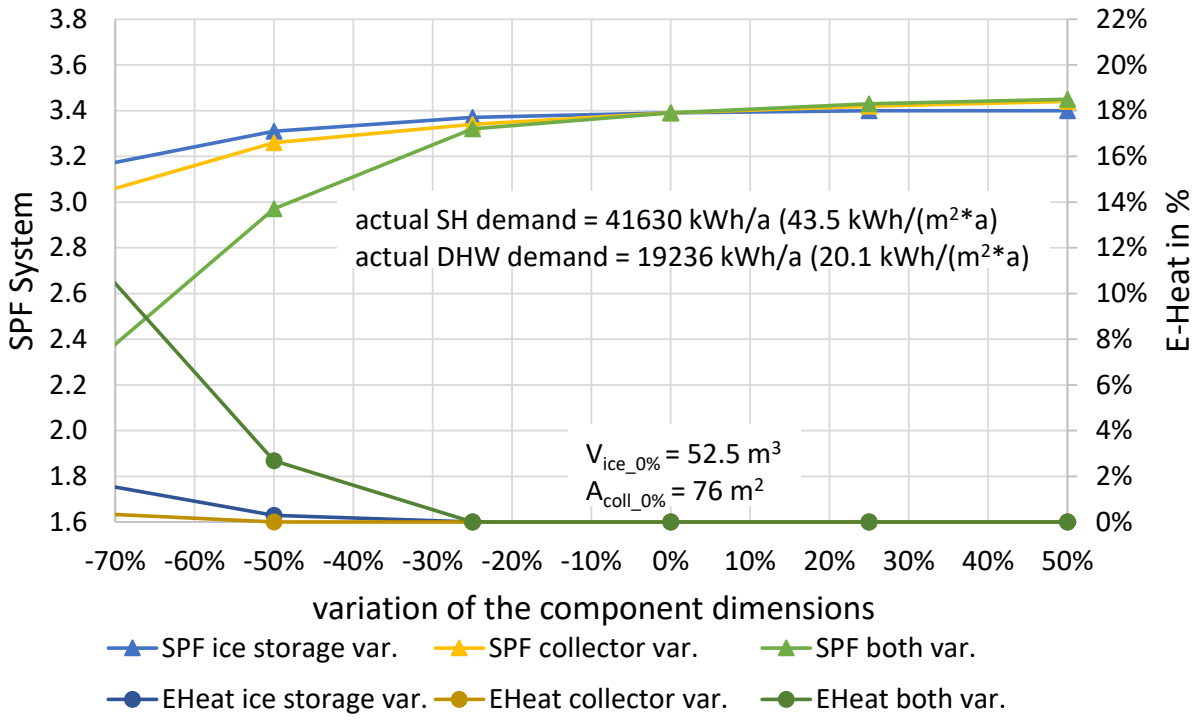

Figure A- 10: Sensitivity analysis of the $Q_{\_heat\_ideal}$ = 64 kWh/(m²*a) building at warm climate

A.2 Design guidelines

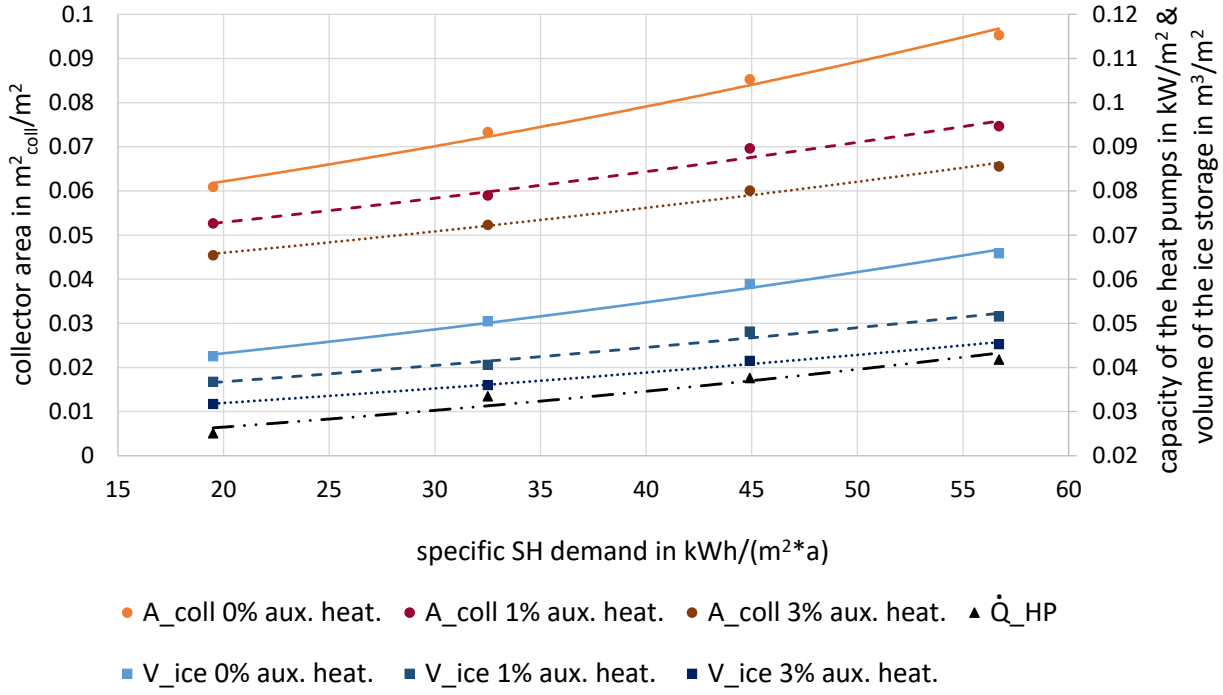

Figure A- 11: Design guideline for the standard climate data including 20.1 kWh/(m²*a) specific DHW demand without reading example

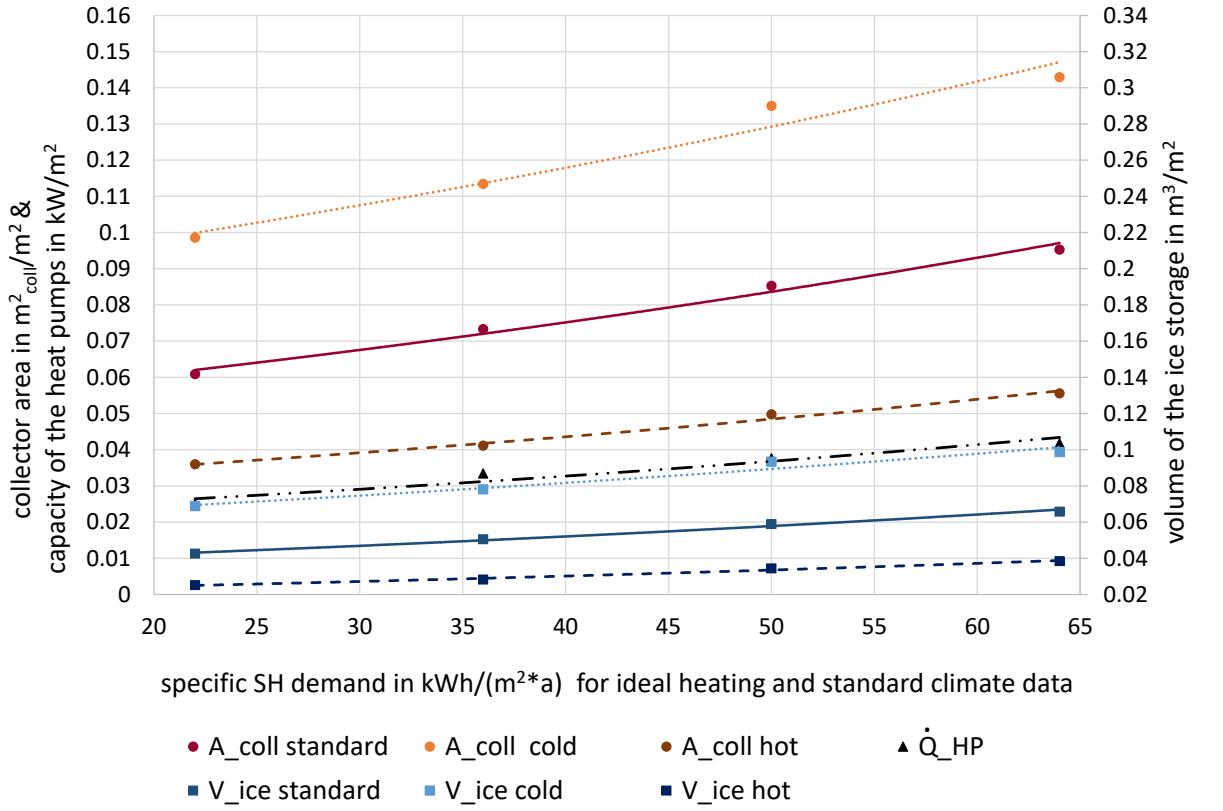

Figure A- 12: Comparison of the designs for 0 % auxiliary heating and for different climate data including 20.1 kWh/(m²*a) specific DHW demand

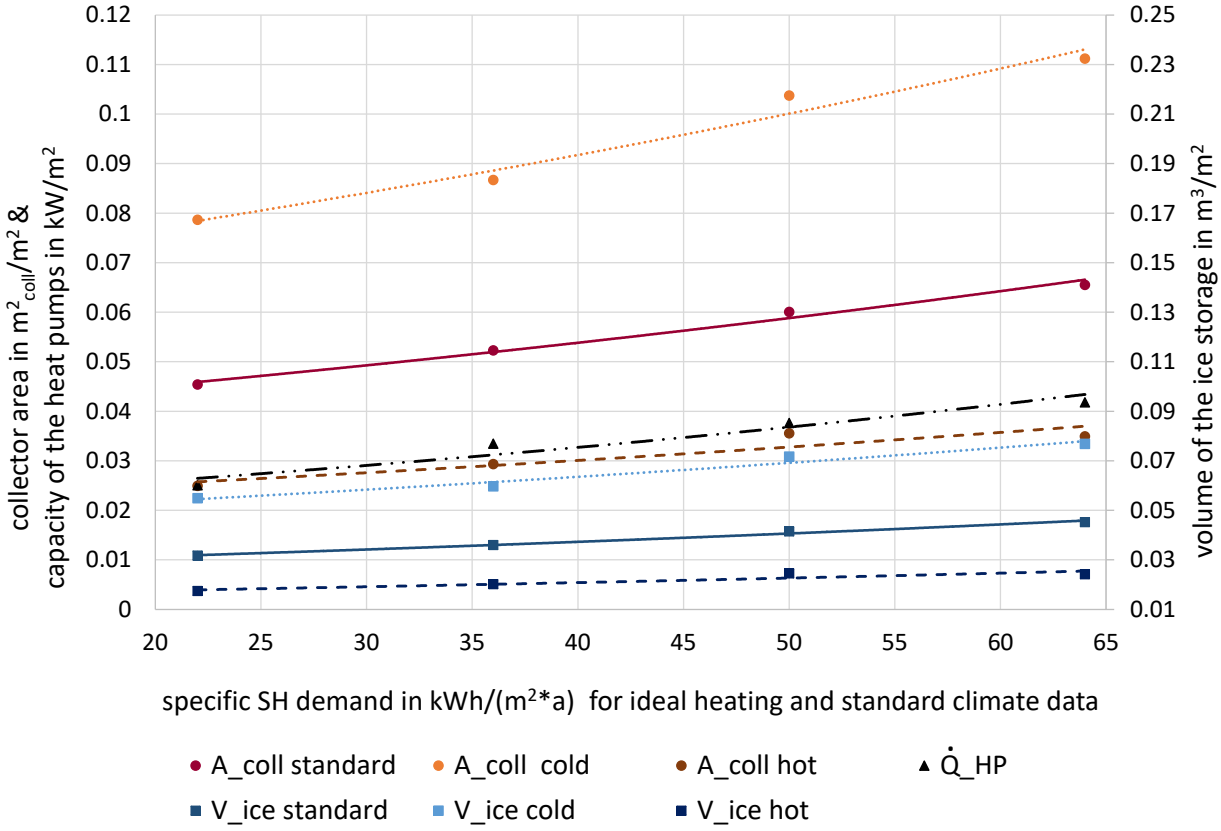

Figure A- 13: Comparison of the designs for 3 % auxiliary heating and for different climate data including 20.1 kWh/(m²*a) specific DHW demand

A.3 Parameter of the validated TRNSYS model

Table A- 1: Parameter of the validated ice storage model (type 843)

Nr.	Paramter	Value	Unit
1	V_store	10.5	m^3
2	h_store	2.3	m
3	nr_pipes	10	-
4	d_cyl	14.7	cm
5	d_pipe	32	mm
6	t_pipe	3	mm
7	lambda_pipe	0.25	W/(m*K)
8	t_ins	10	cm
9	lambda_ins	2.3	W/(m*K)
10	cp_brine	3.816	kJ/(kg*K)
11	rho_brine	1016	kg/m^3
12	T_init	1	°C
13	n_radial	5	-
14	n_axial	15	-
15	n_out_radial	5	-
16	n_out_axial	5	-

Table A- 2: Parameter of the validated ground model (type 708)

Nr.	Paramter	Value	Unit
1	storage height	2.3	m
2	storage volume	10.5	m^3
3	no. of storage fluid nodes	1	-
4	no. of storage zones, storage bottom to storage top	1	-
5	rel. height of storage zone	1	Fraction
6	heat loss coefficient storage fluid to outer storage surface, storage zone	450	W/K
7	heat loss coefficient storage fluid to outer storage surface, storage top	300	W/K
8	heat loss coefficient storage fluid to outer storage surface, storage bottom	200	W/K
9	heat transfer coefficient cistern surface and storage top to cistern cavity	2.1	$W/(m^2*K)$
10	height of cistern ground coverage	0.42	m
11	cistern wall thickness	0.12	m
12	height of cistern cavity	0.6	m
13	no. of vert. ground layers, ground surface to cistern bottom	1	-
14	height of ground layer 1	3.56	m
15	no. of vert. ground layer, cistern bottom to lower boundary	1	-
16	height of ground layer 2	10	m
17	backfill of cistern excavation differs from surrounding ground?	0	-
18	width of ground layer adjacent to cistern resp. cistern backfill	10	m
19	simulation mode	1	-
20	logical unit no. of start temperature file	1	-
21	average thermal conductivity, backfill / ground layers	12.5	W/(m*K)
22	average density, backfill / ground layers	1450	kg/m^3
23	average specific heat, backfill / ground layers	880	J/(kg*K)
24	yearly average of ambient temperature	9.78	C
25	amplitude of monthly averages of ambient temperature	10.29	Δ C
26	month no. with maximum monthly average of ambient temperature	7	-
27	day no. at simulation start	13	-
28	surface boundary mode	1	-
29	no. of time steps the temperature field will be stored	1	-
30	timestep	1	h

Table A- 3: Parameter of the validated solar collector model (type 203)

Nr.	Paramter	Value	Unit
1	kmode	2	-
2	wenn kmode > 2: pvmode	1	-
3	ukmode	1	-
4	uimode	1	-
5	Kollektorfläche	29	m^2
6	Kollektorneigungswinkel	15	°
7	Kollektorazimutwinkel	27	°
8	Konversionsfaktor	0.75	-
9	Windabhängigkeit des Konversionsfaktors	0.01	s/m
10	Wärmeverlustkoeffizient	42.5	$W/(m^2*K)$
11	Windabhängigkeit des Wärmeverlustkoeff.	3.59	s/m
12	Absorptionsgrad des Absorbers	0.95	-
13	Quotient aus Emissions- und Absorptionsgrad des Absorbers	0.85	-
14	effektive Wärmekapazität des Kollektors	40	$kJ/(m^2*K)$
15	spezifische Wärmekapazität des Arbeitsmittels	3.816	kJ/(kg*K)
16	Einfallswinkelkorrekturfaktor für Diffusstrahlung (Absorber)	0.99	-
17	logical unit no. der Einfallwinkelkorrekturfaktor-Datei (Absorber)	30	-
18	wenn kmode > 2: thermischer Leitwert der PV-Modulabdeckung (Glas + Folie)		$W/(m^2*K)$
19	wenn kmode > 2: Emissionsgrad der PV-Modulabdeckung		-
20	wenn kmode > 2: Transmissionsgrad der PV-Modulabdeckung		-
21	wenn kmode > 2: Einfallswinkelkorrekturfaktor für Diffusstrahlung (PV-Modul)		-
22	logical unit no. der Einfallwinkelkorrekturfaktor-Datei (PV-Modul)		-
23	wenn kmode > 2: Modulwirkungsgrad bei Standard-Testbedingungen (STC)		-
24	wenn kmode > 2: Kurzschlussstrom des PV-Moduls		A
25	wenn kmode > 2: MPP-Strom des PV-Moduls		A
26	wenn kmode > 2: Leerlaufspannung des PV-Moduls		V
27	wenn kmode > 2: MPP-Spannung des PV-Moduls		V
28	wenn kmode > 2: Leistungs-Temperaturkoeffizient des PV-Moduls		%/K
29	wenn kmode > 1: Relaxationsfaktor des Lösungsalgorithmus	0.5	-

A.4 Scheme of the system in Weiz

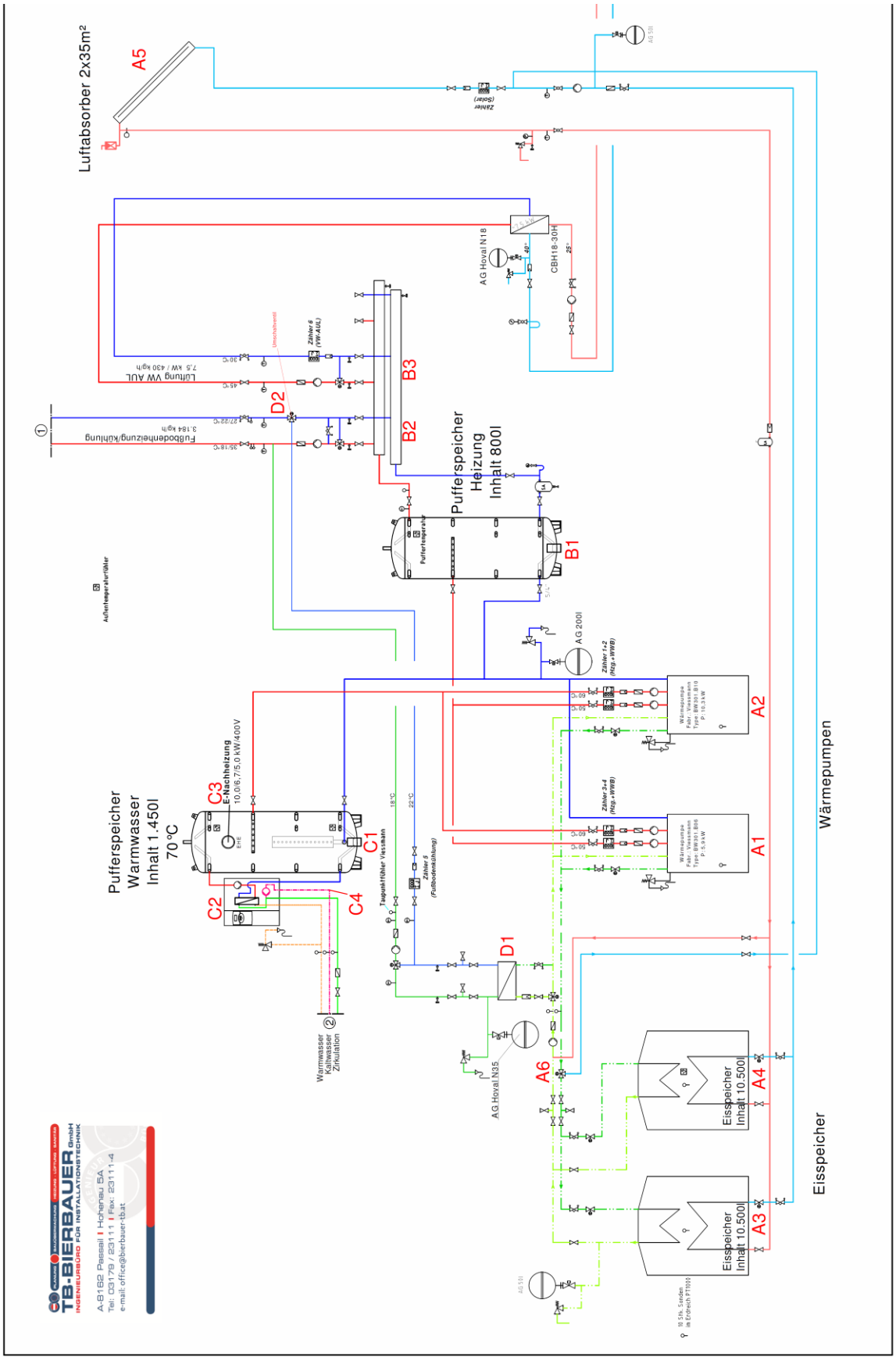

Figure A- 14: Measurement scheme (TB Bierbauer GmbH, 2015)

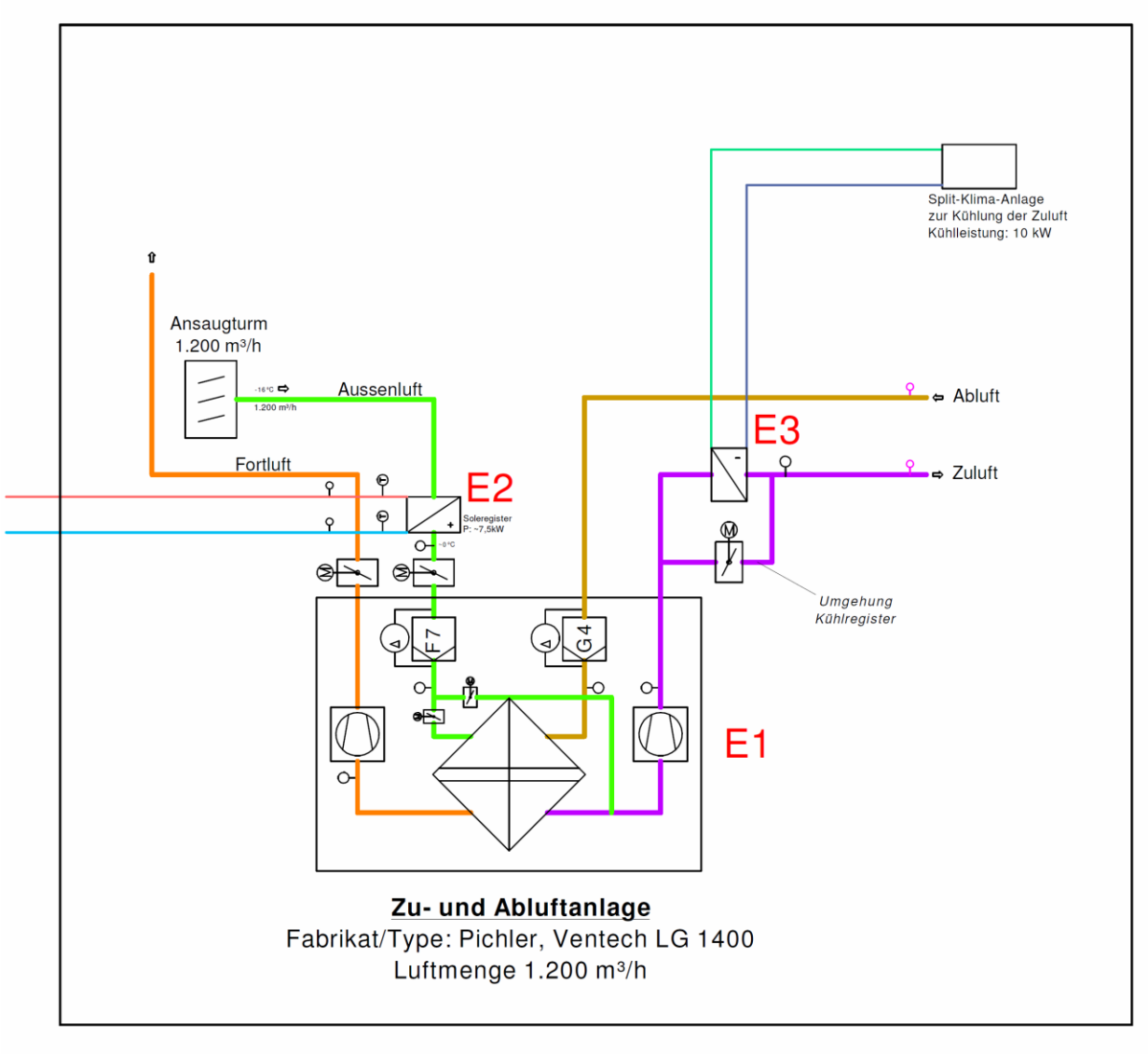

Figure A- 15: Ventilation system (TB Bierbauer GmbH, 2015)

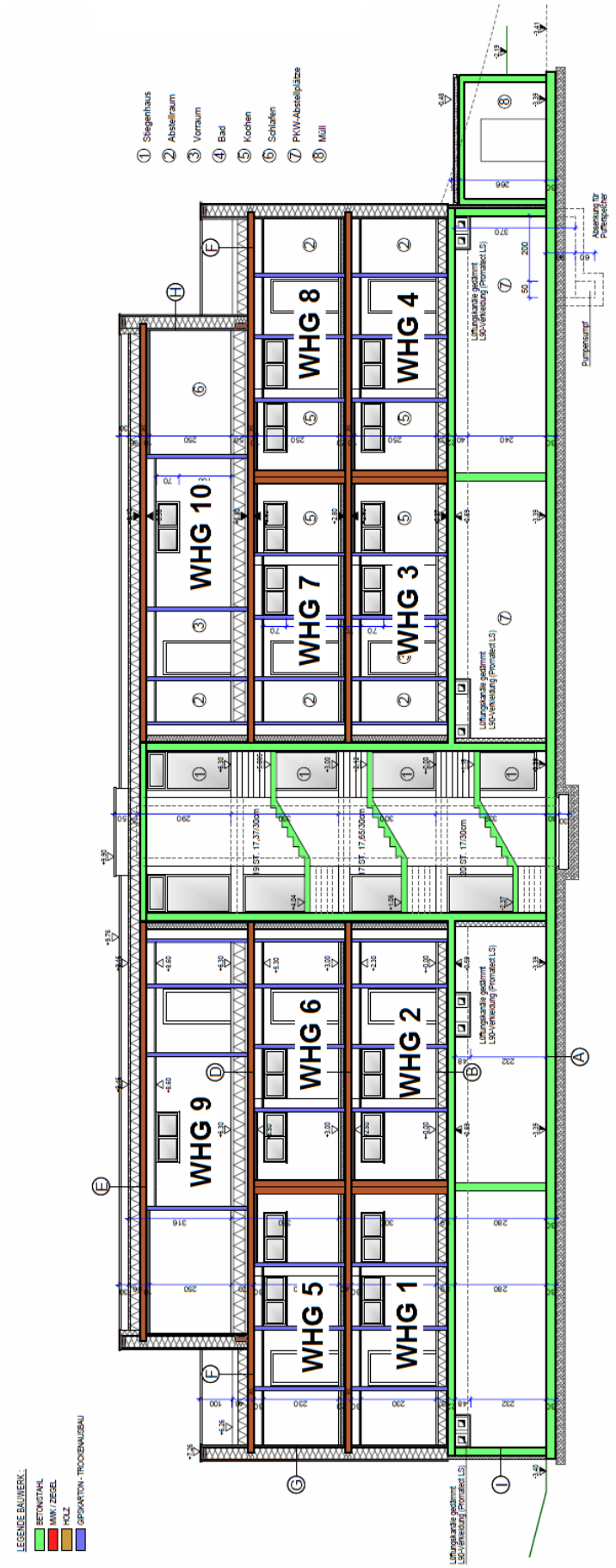

Figure A- 16: Scheme of the building in Weiz (Planungsbüro Wolfgang Enthaler GmbH, 2012)